Processing and Properties of Polycrystalline Nd:YAG Ceramics

A THESIS SUBMITTED IN PARTIAL FULFILMENT

OF THE REQUIREMENT FOR THE DEGREE OF

Master of Technology (Research)

in

Ceramic Engineering

By

K. SARATH CHANDRA

(614CR3002)

Under the Supervision of

Prof. Debasish Sarkar

Department of Ceramic Engineering
National Institute of Technology
Rourkela
March 2017

Ceramic Engineering
National Institute of Technology Rourkela

Dr. Debasish Sarkar

Associate Professor
Department of Ceramic Engineering
National Institute of Technology Rourkela

March 27, 2017

Supervisor's Certificate

This is to certify that the work presented in this dissertation entitled "*Processing and Properties of Polycrystalline Nd:YAG Ceramics*" by "*K. Sarath Chandra"*, Roll Number 614CR3002, is a record of original research carried out by him under my supervision and guidance in partial fulfilment of the requirements of the degree of *Master of Technology (Research)* in *Ceramic Engineering*. Neither this dissertation nor any part of it has been submitted for any degree or diploma to any institute or university in India or abroad.

Debasish Sarkar

Declaration of Originality

I, *K. Sarath Chandra*, Roll Number: 614CR3002, hereby declare that this dissertation entitled "*Processing and Properties of Polycrystalline Nd:YAG Ceramics*" represents my original work carried out as a postgraduate student of NIT Rourkela and, to the best of my knowledge, it contains no material previously published or written by another person, nor any material presented for the award of any other degree or diploma of NIT Rourkela or any other institution. Any contribution made to this research by others, with whom I have worked at NIT Rourkela or elsewhere, is explicitly acknowledged in the dissertation. Works of other authors cited in this dissertation have been duly acknowledged under the section "Bibliography". I have also submitted my original research records to the scrutiny committee for evaluation of my dissertation.

I am fully aware that in case of any non-compliance detected in future, the Senate of NIT Rourkela may withdraw the degree awarded to me on the basis of the present dissertation.

March 27, 2017

NIT Rourkela *K. Sarath Chandra*

ABSTRACT

Polycrystalline Neodymium doped Yttrium Aluminum Garnet (Nd:YAG) ceramics are potential solid state laser gain media with consist of optical transparency and combination of thermal and mechanical properties. The most common scattering sites in the polycrystalline ceramics are residual porosity, grain boundary thickness, and grain boundary with second phases that reduce the laser performance. In order to develop such a material, the present work demonstrates the systematic study on the nanoscale powder synthesis, coarsening of nanoparticles, pressureless sintering in presence of additives (SiO_2) and dopant (Nd), and eventually measure the mechanical, thermal, and optical properties to some extent.

In this respect, YAG nanopowders with ~40 nm average particle size was prepared via co-precipitation synthesis and characterized to establish their purity, crystallinity, and morphology. The nanoparticles were calcined in the temperature range of 900°C-1500°C with an equal interval of 100°C for 1, 6, and 12 h. at the peak temperatures to optimize the coarsening phenomenon of pure YAG nanoparticles for further consolidation and sintering study. Silica (SiO_2) was added in different proportions in the range of 0-2000 ppm to the optimum coarsened pure YAG (~0.7 μm) particles in order to understand its influence on the densification behaviour and sintered microstructure. Pressureless sintering at 1700°C for 2 h. comprises the uniform grain size (~3.9 μm) and high relative density (~97.2%) in the presence of optimum concentration of 1000 ppm SiO_2 compared to without SiO_2 (~ 96.1%). Despite SiO_2 optimization, Nd was doped in different proportions in the range of 0-2 at.% to the optimum coarsened

YAG powders containing 1000 ppm SiO_2 in order to fabricate highly dense Nd:YAG ceramics with fine and homogeneous microstructure. Interestingly, a reversible phase transition of garnet (YAG) to perovskite (YAP) composition noticed at an Nd concentration beyond 1.5 at.%. Nd:YAG ceramics with a high relative density (~99.2%) and grain size (~5.3 μm) were obtained at an optimum concentration of 1.5 at.% Nd. The mechanical properties of the Nd doped YAG ceramics that include Vickers hardness and flexural strength were measured as 13.1 GPa and 202 MPa, respectively. The thermal properties in specific average linear thermal expansion coefficient from 30°C to 1000°C was 9.124 x 10^{-6} /°C and thermal shock resistance parameters R_1 and R_2 at 1000°C were 51°C and 548 W/m, respectively. The in-line transmittance was ~20% in the visible region. Apart from the achieved properties, one can envisage further transparency increment in the perspective of SSL application of Nd:YAG.

Keywords: Nd:YAG; gain media; transparency; calcination; density; microstructure.

Table of Contents

List of Figures

List of Tables

Chapter 1

Introduction

1.1 Motivation

The first flash pumped Solid State Laser (SSL) using naturally occurring ruby as the host material was demonstrated by Maiman in 1960 [1]. In the past six decades, lasers have changed the face of scientific research in areas like light detection and ranging (LIDAR), femtosecond material processing, Raman spectroscopy, medical practice like arterial plaque elimination, dental drilling, and national defense [2-3]. The unique ability of solid state lasers of being tailored to specific applications have increased their demand for emerging industrial and medical needs. Solid state lasers have a clear advantage over other types of lasers because of the following credits: (i) high design possibility renders it to use a variety of gain media (ii) possibility to operate either in continuous wave or pulse mode, and (iii) high power output (>10 kW) [4-5].

Glass and crystalline materials are the two different types of existing solid state laser (SSL) gain media. The superior thermo-mechanical properties combined with the fabrication feasibility of crystalline materials relative to the glass gain media make them suitable choice for high energy applications. In recent years, solid state laser designs based on $Nd_{3x}Y_{3-3x}Al_5O_{12}$ (Nd:YAG) gain media have received greater attention in the field of high power laser applications due to high output power (100-400 kW) combined with superior fluorescent, optical, and thermo-mechanical properties [6-8].

Czochralski grown Nd:YAG single crystals have been widely accepted in laser technology for the last four decades, but there still exists some problems which limits its further application, such as low rare earth ion doping concentration, small crystal dimension, expensive fabrication and difficulty in fabricating plate or stick crystal with large cross-sections. In recent years, polycrystalline Nd:YAG ceramics have attracted much potential

over Czochralski single crystal technology due to several advantages interms of chemistry and processing such as (a) high rare earth ion doping concentration without concentration quenching, (b) greater dopant homogenity, (c) access to more dopants, (d) allowable to add functional elements (Q-switches) to the laser gain media to aid the thermal management, (e) enhanced thermo-mechanical properties, (f) possibility to fabricate big sized laser devices with near net shapes, and (g) lower processing temperatures, times, and possibilities for increased scalability [9-12].

The primary requisite characteristic of a laser host material is its optical transparency. Polycrystalline ceramics have various sites to scatter light (Fig. 1.1) that include residual porosity (inter or intra-granular), grain boundaries, secondary phase particles, and grain to grain birefringence (especially in optically anisotropic systems).

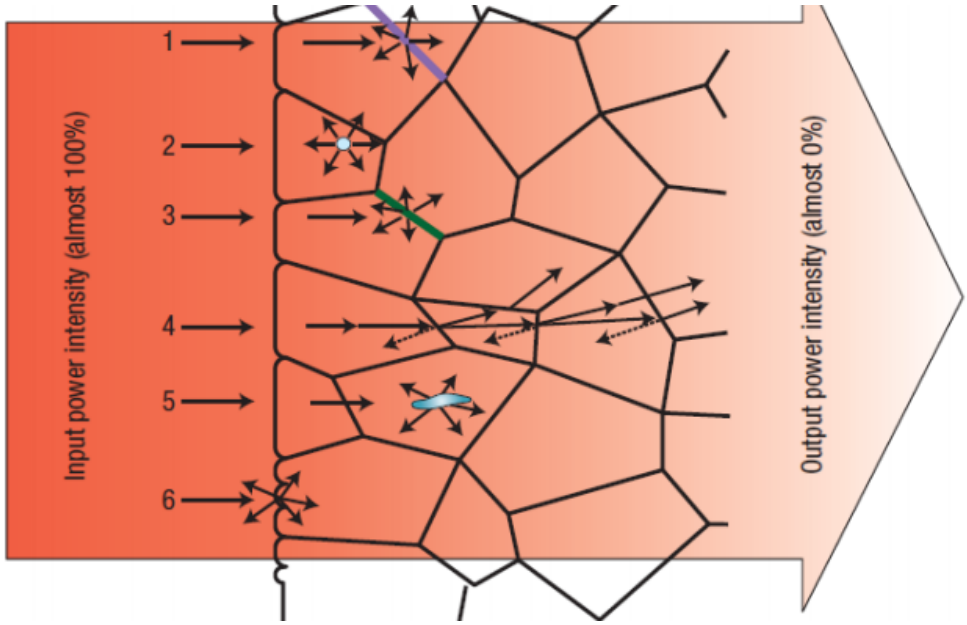

Figure 1.1: Schematic representation of scattering sites in polycrystalline ceramics: 1. Grain boundaries, 2. Residual porosity (inter and intra-granular), 3. Grain boundaries with secondary phases, 4. Birefringence (especially in non-cubic crystal systems), 5. Second phase particles, and 6. Surface defects [13].

Among these, residual porosity is the most significant factor for transparency. Thus, a critical condition for achieving transparency in ceramics is sintering it to full density as maximum as possible. However, development of highly dense YAG based materials need careful control of every step from synthesis of powders to sintering [13-15].

Numerous literature have reported co-precipitation is a promising technique for the large scale production of YAG nanometric powders with good sinterability. In this field, co-precipitation-calcination is the common practice in order to develop fully dense materials. It is observed that there are no systematic studies available on the YAG particle coarsening mechanism under calcination and the influence of particle coarsening characteristics on green state, densification behaviour, and microstructural devlopment [16-18].

SiO_2 doping concentration is critical to sinter YAG and Nd:YAG ceramics to full density because of the sluggish diffusion of Nd^{+3} and Y^{+3} ions. It is observed that the function of silica as a sintering aid differs in densification behaviour and microstructural development of the solid state route (SSR) and sol-gel derived YAG powders [19-22]. Further, there are no substantial studies which have reported about the role of silica on the sintering behaviour of co-precipitated powders and their resultant influence on microstructure and properties of Nd:YAG ceramics. However, there are still very few comprehensive studies which are available on novel fabrication approaches to develop fully dense Nd:YAG ceramics and relating interplay among the key variables like powder processing, green state, densification behavior, and microstructural development in phase pure and doped systems under pressureless sintering.

1.2 Objectives

The major objective of this thesis is to develop highly dense polycrystalline Nd:YAG ceramics by a novel particle coarsening approach and their property evaluation to some extent. Some specific objectives include:

1. To prepare pure and nanometric YAG powders through co-precipitation technique and their relevant characterizations.
2. To optimize the nanoparticle coarsening and growth kinetics in order to achieve highly dense green and sintered YAG ceramics.
3. To study the sintering behavior and optimization of silica and Nd concentration in the perspective of fabricating highly dense Nd:YAG ceramics.
4. To evaluate the different mechanical, thermal and optical response of optimized Nd:YAG ceramics to some extent.

1.3 Scope of the Thesis

Chapter 1 presents a brief introduction to solid-state laser materials, evolution of polycrystalline Nd:YAG ceramics over single crystal technology, and issues on transparency. **Chapter 2** highlights a concise literature review regarding knowledge on Nd:YAG ceramics, fundamental processing issues like powder synthesis and coarsening. More emphasis has been given to the role of silica doping on microstructural evolution. **Chapter 3** reports YAG nanopowder synthesis via co-precipitation method. Further, the formation of sequent phase up to pure YAG powders mechanism is emphasized systematically. **Chapter 4** illustrates the optimization of particle size and their growth kinetics by nanoparticle coarsening to obtain highly dense green and sintered YAG ceramics. The microstructural evolution of sintered ceramics is described by interplay among the particle size, green state, and densification nature. **Chapter 5** deals with the fabrication of highly dense Nd:YAG ceramics by optimization of SiO_2 and Nd concentration. The role of silica in densification behavior and microstructural development of pure YAG and Nd:YAG ceramics is demonstrated. Further, different mechanical, thermal, and optical properties of the optimized Nd:YAG ceramics are evaluated. **Chapter 6** constitutes the concluding remarks and future scope of the work.

References

1. T. H. Maiman, Stimulated Optical Radiation in Ruby, Nature, 187 (1960) 493-494.
2. W.Koechner and M. Bass, Solid-State Lasers: A Graduate Text, Springer, 2003.
3. Committee on Directed Energy Technology for Countering Indirect Weapons, National Research Council, Review of Directed Energy Technology for Countering Rockets, Artillery, and Mortars (RAM), The National Academies Press, Washington, D.C., 2008.
4. J. Marmo, H. Injeyan, H. Komine, S. McNaught, J. Machan, and J. Sollee, in Fiber Lasers VI: Technology, Systems, and Applications, SPIE, San Jose, CA, USA, 2009.
5. M. D. Perry and G. Mourou, Terawatt to Petawatt Subpicosecond Lasers, Science, 264 (1994) 917-924.
6. M. Ciofini and A. Lapucci, Compact Scalable Diode-Pumped Nd: YAG Ceramic Slab Laser, Appl. Opt., 43 (2004) 6174–6179.
7. R. L. Byer, AFOSR Study: Basic Research Opportunities in Lasers,2009.
8. H. Yagi, T. Yanagitani, and K.-I. Ueda, Nd^{3+}:$Y_3Al_5O_{12}$ Laser Ceramics: Flashlamp Pumped Laser Operation with a UV Cut Filter, J. Alloys and Compounds, 421 (2006) 195-199.
9. A. Ikesue, I. Furusato, and K. Kamata, Fabrication Of Polycrystalline, Transparent YAG Ceramics By A Solid-State Reaction Method, J. Am. Ceram. Soc. 78 (1995) 225-228.
10. K. Ueda, J. F. Bisson, H. Yagi, K. Takaichi, A. Shirakawa, T. Yanagitani, and A. A. Kaminskii, Scalable Ceramic Lasers, Laser Physics, 15 (2005) 927–938.
11. J. Lu, M. Prabhu, J. Song, C. Li, J. Xu, K. Ueda, A. A. Kaminskii, H. Yagi and T.Yanagitani, Optical Properties and Highly Efficient Laser Oscillation of Nd:YAG Ceramics, Appl. Phys. B, 71 (2000) 469-473.
12. J. Lu, J. Song, M. Prabhu, J. Xu, K. Ueda, H. Yagi, T. Yanagitani and A. Kudryashov, High-Power Nd:$Y_3Al_5O_{12}$ Ceramic Laser, Jpn. J. Appl. Phys., 39 (2000) 1048-1050.
13. A. K. Ikesue, Y. L. Aung, V. Lupei, Ceramic Lasers, 1st ed., Cambridge University Press, New York, 2013.
14. J. R. Lu, K. Ueda, H. Yagi, T. Yanagitani, Y. Akiyama and A. A. Kaminskii, Neodymium Doped Yttrium Aluminum Garnet (Y3Al5O12) Nanocrystalline Ceramics – a New Generation of Solid State Laser and Optical Materials, J. Alloy. Compd., 341 (2002) 220-225.
15. A. Ikesue, T. Kinoshita, K. Kamata and K. Yoshida, Fabrication and Optical Properties of High-Performance Polycrystalline Nd:YAG Ceramics for Solid-State Lasers, J. Am. Ceram. Soc., 78 (1995) 1033-1040.
16. J. Vrolijk, J. Willems, R. Metselaar, Co-precipitation of yttrium and aluminium hydroxde for preparation of ytrium aluminium garnet, J. Eur. Ceram. Soc., 6 (1990) 47-53.D. J. Sordelet, M. Aknic, M. L. Panchula, Y Han, synthesis of yttrium aluminium garnet precursor powders by homogeneous precipitation, J. Eur. Ceram. Soc., 14 (1994) 123-130.
17. N. Matsushita, N. Tsuchiya, K. Nakatsuka, T. Yanagitani, Precipitation and calcination processes for yttrium aluminium garnet precursors synthesized by the urea method, J. Am. Ceram. Soc., 82 (1999) 1977-1984.
18. M. Li, Principles and synthesis of ceramic powder by means of wet chemical method, J. Chin.Ceram. Soc. 22 (1994) 85-91.
19. S. Kochawattana, A. Stevenson, S.-H. Lee, M. Ramirez, V. Gopalan, J. Dumm, V. K. Castillo, G. J. Quarles, and G. L. Messing, Sintering and Grain Growth in SiO2 Doped Nd:YAG, J. Eur.Ceram. Soc., 28 (2008) 1527-1534.
20. A. Maître, C. Sallé, R. Boulesteix, J.-F. Baumard, and Y. Rabinovitch, Effect of Silica on the Reactive Sintering of Polycrystalline Nd:YAG Ceramics, J. Am. Ceram. Soc., 91 (2008) 406-413.
21. R. Boulesteix, A. Maître, J.-F. Baumard, C. Sallé, and Y. Rabinovitch, Mechanism of the Liquid-Phase Sintering for Nd:YAG Ceramics, Opt. Mater., 31 (2009) 711-715.

22. R. Boulesteix, A. Maître, J.-F. Baumard, Y. Rabinovitch, C. Sallé, S. Weber, and M. Kilo, The Effect of Silica Doping on Neodymium Diffusion in Yttrium Aluminum Garnet Ceramics: Implications for Sintering Mechanisms, J. Eur. Ceram. Soc., 29 (2009) 2517-2526.

Chapter 2

Background

2.1 Laser Ceramics

The need for materials that combine optical transparency with superior thermo-mechanical properties has led to the development of oxide materials for window, dome, transparent armor, and laser applications. These oxide materials are known as ceramic lasers [1-2]. In recent years, polycrystalline ceramics have received much attention over conventional Czochralski grown single crystal technology due to following crucial factors: (i) high rare earth ion doping concentration without concentration quenching, (b) possibility to fabricate big sized laser devices with near net shapes, and (c) enhanced thermo-mechanical properties [3-5].

However, for laser host applications, ceramic materials must meet the following requirements [6-8]. They are

(i) The crystal structure of the material must be optically isotropic.

(ii) The material must have fully dense microstructure with no porosity and secondary phases.

(iii) Segregation at grain boundaries must be avoided and narrow grain boundaries are required.

(iv) The material must possess superior thermo-mechanical properties to sustain extreme thermal loading during operation.

The first polycrystalline laser ceramic MgO doped Al_2O_3 was demonstrated by Coble [9]. He showed that polycrystalline ceramics, though exhibit birefringence, can have a substantial light transmission at optical frequencies when they are sintered to full density. From his work results, claims are made that the fully sintered MgO doped Al_2O_3 have an optical transmittance of 40-50% in UV-Visible region. The decreased transparency value

clearly reflects the birefringence effect. Anderson of GE developed a new polycrystalline laser gain media known as 'Yttralox' which has in line transmittance greater than 70% at optical wavelengths. This material is especially developed to use in lamp envelopes, high temperature windows, and high temperature lenses but higher sintering temperature beyond 2000ºC limit its commercialization [10]. In another study, fully dense MgO transparent ceramics were developed at sintering temperatures substantially lower than 'Yttalox' [11].

After 1970, numerous patents were published on sintering and hot pressing of various polycrystalline oxides but the laser slope efficiency was substantially low compared to the single crystals. In 1995, Ikesue and his co-workers sintered 0.9 at% polycrystalline Nd:YAG ceramics to full density using SiO_2 as sintering aid. The laser slope efficiency of the obtained laser ceramic material was similar to the Czochralski grown single crystals [12]. The superior thermo-mechanical properties coupled with the high laser slope efficiency establish Nd:YAG as a potential laser gain media.

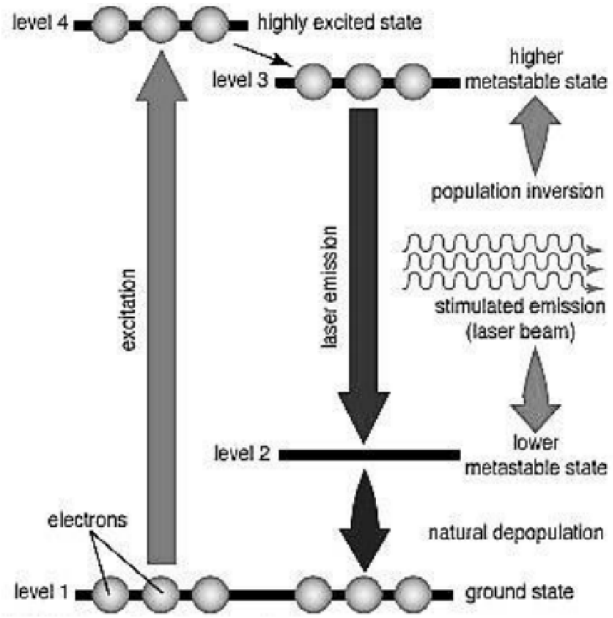

Figure 2.1: Working principle of four energy level solid-solid state laser [12].

The basic components of a Nd:YAG solid-state laser unit constitute an active lasing medium (Nd:YAG), Xenon flash lamp for laser pumping, fully and partially reflecting mirrors. The working principle (Fig. 2.1) of this solid-state laser comprises irradiation of the lasing medium by photons (wavelength ~532 nm) emerging out from the xenon flash lamp. This action triggers the Nd^{+3} ions to pump to a highest energy state (Level 4) that is

followed by a rapid non-radiative transition to a higher metastable state (Level 3). The lasing action is actuated by a radiative transmission between the higher (Level 3) and lower (Level 2) metastable states that generates the laser radiation (wavelength ~1064 nm).

2.2 YAG and Nd:YAG

Yttrium Aluminum Garnet ($Y_3Al_5O_{12}$) has a centro-symmetric cubic crystal structure (space group Ia3*d*) with 160 atoms per unit cell and lattice constant = 1.2001 nm [13-14]. The coordination of each cation site is shown schematically in Fig. 2.2.

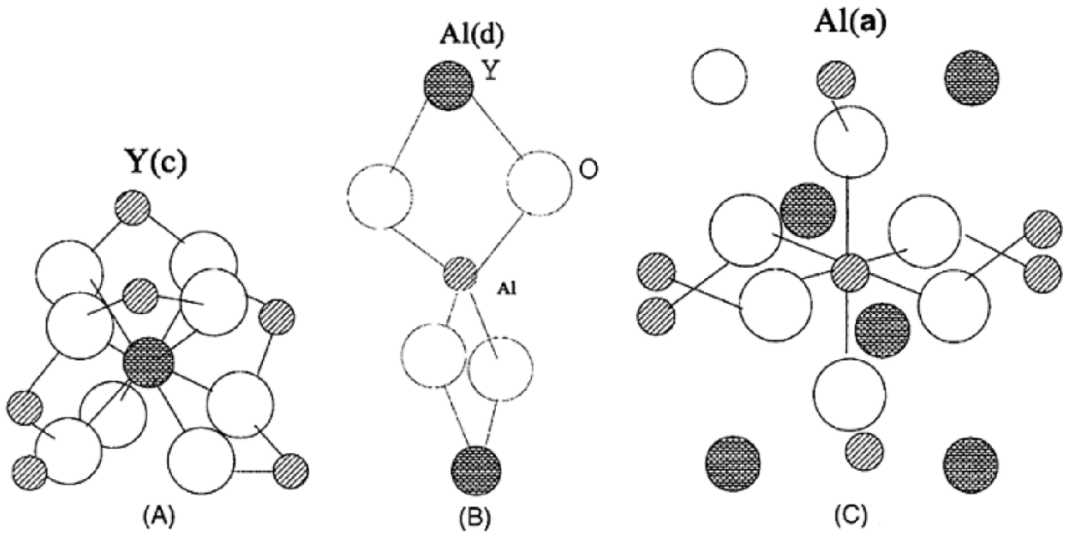

Figure 2.2: Schematic representation of atomic coordinations of YAG. (A) Y^{3+} dodecahedral site, (B) Al^{3+} tetrahedral site, and (C) Al^{3+} octahedral site.

YAG is unique because of the range of elements that can substitute into the structure. The dodecahedrally coordinated 24(*c*) site can accommodate the optically active ion like Nd^{+3} (0.1109 nm) for laser applications [15-16]. Trivalent Nd ion in Nd:YAG solid state laser ceramics has relatively higher importance compared to the other rare earth ions in the lanthanide group due to following credits [17, 18]:

(i) ability to exhibit a satisfactorily long fluorescence lifetime and narrow fluorescence line widths in crystals with ordered structures.

(ii) feasibility to perform lasing action under continuous wavelength mode (CW) and pulse mode.

2.3 Why Co-Precipitation?

The polycrystalline YAG based ceramics are usually produced by utilizing powders synthesized via two sources: (i) solid-state reaction (SSR) between the mixture of yttria (Y_2O_3) and alumina (Al_2O_3), which form YAG phase in situ during calcination [19-20], and (ii) wet chemical synthesized YAG powder [21-22]. Numerous works have reported that the wet chemical synthesis methods have several advantages over solid state route such as low crystallization temperature required to obtain pure YAG phase and easy control over morphology of the resulting powders. Among the many widely adopted wet chemical synthesis methods, co-precipitation is reported as a most promising technique for the large scale production of YAG nanometric powders due to the following essential factors: (a) simpler and more cost – effective way, (b) development of phase pure YAG nanopowder at low crystallization temperatures, (c) greater compositional homogeneity, and (d) possibility to prepare well sinterable YAG nanopowders [23-26].

The selection of source materials for yttrium and aluminum and the precipitant choice is crucial in the co-precipitation route to prepare the YAG nanometric powders. Because precursors have strong influence on the crystallization behavior of the resultant particles [27-28]. Palmero et al. have reported that complete crystallization of YAG occurs relatively at 1000ºC when yttrium chloride and aluminum chloride precipitated in presence of ammonium bi carbonate (AHC) precipitant [29]. In another study, J. Li et al. demonstrated the necessity of high crystallization temperature (~1000ºC) to obtain pure YAG phase in presence of ammonium aluminum dodecahydrate precursor [30]. However, numerous literature works have reported that lower crystallization temperature (~900ºC) of YAG is recognized when yttrium nitrate and aluminum nitrate are used as starting precursors and AHC as precipitant [23,27]. In the available literature, low temperature synthesis of YAG nanopowders through co-precipitation has not been emphasized that will be explored here.

2.4 Particle Coarsening

Particle coarsening involves growth of particles either by oriented particle attachment or Ostwald's ripening under a heat treatment known as calcination. Co-precipitation followed by calcination is a common practice in the field of laser ceramics in order to obtain highly dense materials (>99%) [31-33].

In a recent work, Fedyk et al, fabricated YAG ceramics with densities greater than 99 % by high pressure sintering (6 GPa and 450ºC) of ~50 nanometer sized YAG particles [34]. However, pressureless sintering of ~100 nm YAG particles densified to ~92% of the theoretical value with a grain size of ~3 µm at 1600ºC after particle calcination at 1200ºC [35]. In another study, D. L. Mandujano et al. reported that the YAG particles with an average size of 600 nm are densified to ~95% of the theoretical value with a grain size of ~4 µm at 1600ºC under pressureless sintering whereas the particles were calcined at 1500ºC [36].

However, there are no systematic investigations reported on the optimization of particle size and growth kinetics of YAG nanoparticles during calcination. Moreover, the interplay among particle morphology, green state, and densification behavior in the perspective of microstructural development has not been fully studied.

2.5 The role of SiO_2 in YAG and Nd:YAG ceramics

An optimum amount of SiO_2 doping is essntial to sinter YAG and Nd:YAG ceramics to achieve full density because of the slower diffusion kinetics of trivalent Nd and Y ions [37]. Kochawattana et al. studied densification and grain growth kinetics in 0-0.28 wt.% SiO_2 doped YAG and Nd:YAG ceramics. They found that average grain size increased with the increase of SiO_2 content [38]. These observations are well in agreement with the results obtained by Ikesue et al. [39]. However, in contrary, another study reported that decreased average grain size is observed with the increase of silica content [40-41]. In consideration of the earlier works, it is clear that the state of knowledge regarding the optimization and role of SiO_2 on densification is another scope for the sintered microstructural development of particle coarsened YAG and Nd:YAG ceramics.

2.6 Summary

The superior thermo-mechanical properties coupled with high rare earth ion doping concentration without concentration quenching and ease of fabrication qualified polycrystalline laser ceramics as potential materials over conventional Czochralski grown single crystals. The critical condition encountered in the fabrication of laser ceramics is sintering it to full density because residual porosity is the most significant optical defect for transparency. Co-precipitation – calcination is the widely used practice in order to develop fully dense YAG based laser materials. Calcination involves coarsening of particles, however, there are no systematic investigations reported on optimization of particle size and growth kinetics of YAG nanoparticles in order to fabricate highly dense materials with fine grained microstructure. Furthermore, SiO_2 doping is critical to sinter the YAG based ceramics to full density but the role of silica in densification and grain growth behavior of YAG and Nd:YAG systems are limited.

References

1. C. B. Hitz, Understanding Laser Technology, PennWell Publishing Company, Oklahoma, 1991.
2. T. H. Maiman, Stimulated Optical Radiation in Ruby, Nature, 187 (1960) 493-494.
3. M. mortier and D. Vivien, Ceramic and Glass-Ceramic Laser, Ann. Chim. Sci.Mat. 28, (2003) 21-33.
4. A. Ikesue, Polycrystalline Nd:YAG Ceramics Lasers, Opt. Mater., 19, (2002) 183-187.
5. J. Lu, M. Prabhu, J. Song, C. Li, J. Xu, K. Ueda, A. A. Kaminskii, H. Yagi and T. Yanagitani, Optical Properties and Highly Efficient Laser Oscillation of Nd:YAG Ceramics, Appl. Phys. B, 71 (2000) 469-473.
6. W.Koechner, Solid-State Laser Engineering, Springer-Verlag Berlin Heidelberg, Germany, 1999.
7. J. Peelen and R. Metselaar, Light-Scattering by Pores in Polycrystalline Materials - Transmission Properties of Alumina, J. Appl. Phys., 45 (1974) 216-220.
8. R. Apetz and M. P. B. Bruggen, Transparent Alumina: A Light-Scattering Model, J. Am.Ceram. Soc., 86 (2003) 480-486.
9. R.L. Coble, U.S. Patent No. 3,026,210 (1962).
10. R.C.Anderson, U.S. Patent No. 3545987 (1970).
11. M.W. Benecke, N.E. Olson, and J.A. Pask, Effect of LiF on Hot-Pressing of MgO, J. Am.Ceram. Soc., 50 (1967) 365-368.
12. A. K. Ikesue, Y. L. Aung, V. Lupei, Ceramic Lasers, 1st ed., Cambridge University Press, New York, 2013.
13. R. D. Shannon and C. T. Prewitt, Effective Ionic Radii in Oxides and Fluorides, Acta Cryst.B, 25 (1969) 925-946.
14. M. M. Kuklja and R. Pandey, Atomistic Modeling of Native Point Defects in Yttrium Aluminum Garnet Crystals, J. Am. Ceram. Soc., 82 (1999) 2881-2886.
15. C. Shawley, Optical and Defect Studies of Wide Band Gap Materials, Washington State University, 2008.
16. W. Koechner and M. Bass, Solid-State Lasers: A Graduate Text, Springer, 2003.
17. J. Saikawa, Y. Sato, T. Taira, and A. Ikesue, Passive Mode Locking of a Mixed Garnet Yb: Y3ScAl4O12 Ceramic Laser, Appl. Phys. Lett., 85 (2004) 5845-5847.
18. S. Kochawattana, Phase Formation and Sintering of YAG Ceramics, The Pennsylvania State University, 2008.
19. A. Ikesue, I Furussato, K. Kamata, Fabrication of polycrystalline, transparent YAG ceramics by a solid-state reaction method, J. Am. Ceram. Soc., 78 (1995) 225-228.
20. J. Li, Y.S. Wu, Y. B. Pan, Fabrication, microstructure and properties of highly transparent Nd:YAG laser ceramics, Opt. Mater., 31 (2008) 6-17.
21. T. Yanagitani, H. Yagi, A. Ichikawa, Production of yttrium aluminum garnet fine powder, Jpn Patent 10-101333 (1998).
22. T. Yanagitani, H. Yagi, M. Imagawa, Production of powdery starting material for yttrium aluminum garnet, Jpn Patent 10-101334 (1998).
23. J. Vrolijk, J. Willems, R. Metselaar, Co-precipitation of yttrium and aluminium hydroxde for preparation of ytrium aluminium garnet, J. Eur. Ceram. Soc., 6 (1990) 47-53.
24. D. J. Sordelet, M. Aknic, M. L. Panchula, Y Han, synthesis of yttrium aluminium garnet precursor powders by homogeneous precipitation, J. Eur. Ceram. Soc., 14 (1994) 123-130.
25. N. Matsushita, N. Tsuchiya, K. Nakatsuka, T. Yanagitani, Precipitation and calcination processes for yttrium aluminium garnet precursors synthesized by the urea method, J. Am. Ceram. Soc., 82 (1999) 1977-1984.
26. M. Li, Principles and synthesis of ceramic powder by means of wet chemical method, J. Chin. Ceram. Soc. 22 (1994) 85-91.

27. J. G. Li, T. Ikegami, J. H. Lee, T. Mori, Y. Yajima, Co-precipitation synthesis and sintering of yttrium aluminum garnet (YAG) powders: The effect of precipitant, J. Eur. Ceram. Soc., 20 (2000) 2395-2405.
28. M. Z. Napierala, M. M. Bucko, K. Haberko, The effect of non-stoichiometry on microstructure and selected properties of YAG polycrystals, Ceram. Int., 38 (2012) 2589-2592.
29. P. Palmero, R. Traverso, Co-precipitation of YAG Powders for Transparent materials: Effect of the synthesis parameters on processing and microstructure, Materials, 7 (2014) 7145-7156.
30. J. Li, T. Ikegami, J. H. Lee, T. Mori, Low temperature fabrication of transparent yttrium aluminium garnet (YAG) ceramics without additives, J. Am. Ceram. Soc., 83 (2000) 961-63.
31. P. Palmero, R. Traverso, Co-precipitation of YAG Powders for Transparent materials: Effect of the synthesis parameters on processing and microstructure, Materials, 7 (2014) 7145-7156.
32. G. Xu, X. Zhang, W. He, H. Liu, H. Li, R. I. Boughton, Preparation of highly dispersed YAG nano-sized powder by co-precipitation method. Materials Letters 60 (2006) 962-965.
33. P. L. Chen, I. W. Chen, Sintering of fine oxide powders. 1. Microstructural evolution. J. Am.Ceram. Soc., 79 (1996) 3129-3141.
34. R. Fedyk, D. Hreniak, W. Lojkowski, W. Strek, H. Matysiak, E. Grzanka, S. Gierlotka, P. Mazur, Method of preparation and structural properties of transparent YAG nanoceramics. Opt. Mater., 29 (2007) 1252–1257.
35. Y. L. Kopylov, V. B. Kravchenko, A. A. Komarov, Z. M. Lebedeva, V. V. Shemet., Nd:Y_2O_3 nanopowders for laser ceramics. Opt. Mater., 29 (2007) 1236-1239.
36. D. L. Mandujano, J. Z. Medina, R. M. Estrella, J. M. Saldaña, Synthesis and mechanical characterization by nano indentation of polycrystalline YAG with Eu and Nd additions. Ceram. Int., 39 (2013) 3141–3149.
37. R. Boulesteix, A. Maître, J.-F. Baumard, C. Sallé, and Y. Rabinovitch, Mechanism of the Liquid-Phase Sintering for Nd:YAG Ceramics, Opt. Mater., 31 (2009) 711-715.
38. S. Kochawattana, A. Stevenson, S. H. Lee, M. Ramirez, V. Gopalan, J. Dumm, V. K. Castillo, G. J. Quarles, G. L. Messing., Sintering and grain growth in SiO_2 doped Nd:YAG. J. Eur. Ceram. Soc., 28 (2008) 1527 – 1534.
39. A. Ikesue and K. Kamata, Role of Si on Nd Solid-Solution of YAG Ceramics, J. Jpn.Ceram. Soc.,103 (1995) 489-493.
40. A. Maître, C. Sallé, R. Boulesteix, J.-F. Baumard, and Y. Rabinovitch, Effect of Silica on the Reactive Sintering of Polycrystalline Nd:YAG Ceramics, J. Am. Ceram. Soc., 91 (2008) 406-413.
41. R. Boulesteix, A. Maître, J.-F. Baumard, Y. Rabinovitch, C. Sallé, S. Weber, and M. Kilo, The Effect of Silica Doping on Neodymium Diffusion in Yttrium Aluminum Garnet Ceramics: Implications for Sintering Mechanisms, J. Eur. Ceram. Soc., 29 (2009) 2517- 2526.

Chapter 3

Co-Precipitation Synthesis of YAG Nanoparticles

3.1 Introduction

Yttrium Aluminum Garnet (YAG:$Y_3Al_5O_{12}$) has been well established as a solid state laser (SSL) gain media, owing to its relatively stable lattice structure over a wide temperature range, large thermal conductivity, high melting point, good chemical resistance, and isotropic optical properties [1-2]. YAG single crystal has been widely accepted in laser technology for the last four decades, but some problems still which continues to exist limits its further application, such as low rare earth ion doping concentration, small crystal dimension, expensive fabrication and difficulty in fabricating plate or stick crystal with large cross-sections [3-4]. In comparison with the single crystal technology, polycrystalline YAG based ceramics prepared from YAG nanometric particles offer several advantages such as (a) high rare earth ion doping concentration without concentration quenching, (b) possibility to fabricate large sized laser devices with near net shapes, and (c) enhanced thermo-mechanical properties which qualifies it as a promising substitute for conventional YAG single crystals [5-6]. The microstructural features of the polycrystalline YAG ceramics are remarkably influenced by characteristics of the starting precursor powders [7-8].

In recent studies, many efforts have been made to synthesize large scale YAG nanopowders to fabricate polycrystalline YAG ceramics for high power solid state laser (SSL) applications [9-10]. Owing to such a wide and diverse application potential for YAG based materials, development of a rapid synthesis technique for the large scale production of well sinterable YAG nanopowders is highly desirable.

Usually, the polycrystalline YAG based ceramics are produced by utilizing powders synthesized via two sources: (i) solid-state reaction (SSR) between the mixture of yttria (Y_2O_3) and alumina (Al_2O_3), which form YAG phase in situ during calcination [11-12], and (ii) wet chemical synthesized YAG powder [13-15]. Zhang WX et al. reported that SSR approach is a relatively simpler to fabricate polycrystalline YAG based ceramics and a range of compositions can be easily implemented [16]. However, numerous works have reported that the SSR method has few unavoidable disadvantages, such as high calcination temperature to obtain pure YAG phase and difficulty is encountered to control the microstructure, grain size or shape of the resulting powders [17-18]. In this respect, several wet chemical synthesis methods have been developed to reduce the crystallization temperature of YAG, by allowing the reactant cations (Y, Al) to mix intimately in the atomic level which develops greater cation homogeneity in the precursor [19-21]. The wet chemical methods such as sol-gel processing [22], hydrothermal synthesis [23], glyco thermal method [24], co-precipitation [25-26], spray pyrolysis [27], microemulsion [28], and metal-organic preceramic processing [29] are common practice in order to synthesize the YAG nanoparticles.

Unfortunately, most of these solution based techniques suffer some intrinsic disadvantages such as, complex and time consuming procedures and the difficulty to obtain precursors with greater cation homogeneity [30-32]. In comparison with these methods, most of the literature have reported co-precipitation as a promising technique for the large scale production of YAG nanometric powders due to the following essential factors: (a) simpler and more cost – effective way, (b) development of phase pure YAG nanopowder at low crystallization temperatures, (c) greater compositional homogeneity, and (d) possibility to prepare well sinterable YAG nanopowders [33-36].

The selection of source materials for yttrium and aluminium and the precipitant choice is crucial in the co-precipitation route to prepare the YAG nanometric powders. These factors have a strong influence on the physio-chemical characteristics of the precursor as well as on the sinterability of resultant YAG nano powders [25, 37]. Most of the literature have reported that yttrium nitrate and aluminium nitrate are the most common sources of yttrium and aluminium, respectively, to synthesize well sinterable YAG nanometric powders [38-40].

The most common precipitants employed for the production of YAG nanosized powders are ammonium bicarbonate, AHC [25], and ammonia water, AW [40]. In all the cases, ammonium hydrogen carbonate (AHC) has proven to be an excellent precipitant for the large scale production of less agglomerated and well sinterable YAG powders [39, 41-44]. J. G. Li et al. have reported that soft agglomerated YAG nanopowder with a particle size of 52 nm was prepared by co-precipitation technique, using AHC as precipitant. These powders are sintered to full density (>99.9%) without any sintering aids which reflects the well sinterability of the synthesized co-precipitated powder [25]. The results reported by J. G. Li et al. are found to be in agreement with the other investigations [40, 42-44].

Despite the clear importance behind the large scale production of well sinterable YAG nanopowders for high power SSL applications, numerous literature works have reported that co-precipitation is the widely adopted synthesis route. In this chapter, we report YAG nanopowder synthesis via co-precipitation method. Further, the formation of sequent phase up to pure YAG powders mechanism in solid state route as well as the wet chemical synthesis route is demonstrated.

3.2 Experimental

3.2.1 Powder Synthesis

Yttrium nitrate $Y(NO_3)_3.6H_2O$ (99.9% pure, analytical grade, SD Fine chemicals) and Aluminium nitrate $Al(NO_3)_3.9H_2O$ (99.9% pure, analytical grade, SD Fine chemicals) were used as starting materials without further purification to prepare YAG nano powders. Ammonium bicarbonate NH_4HCO_3, named AHC, (99% pure, Analytical grade, SD Fine chemicals) was taken as the precipitant. Separately, 0.15 M aqueous solutions of two nitrates were prepared by the addition of yttrium nitrate and aluminium nitrate to the distilled water with constant stirring by a magnetic stirrer. Similarly, high concentration 1.5 M AHC solution was prepared to ensure the complete precipitation during reverse strike mixing. The initial pH of the solution was about 8.3.

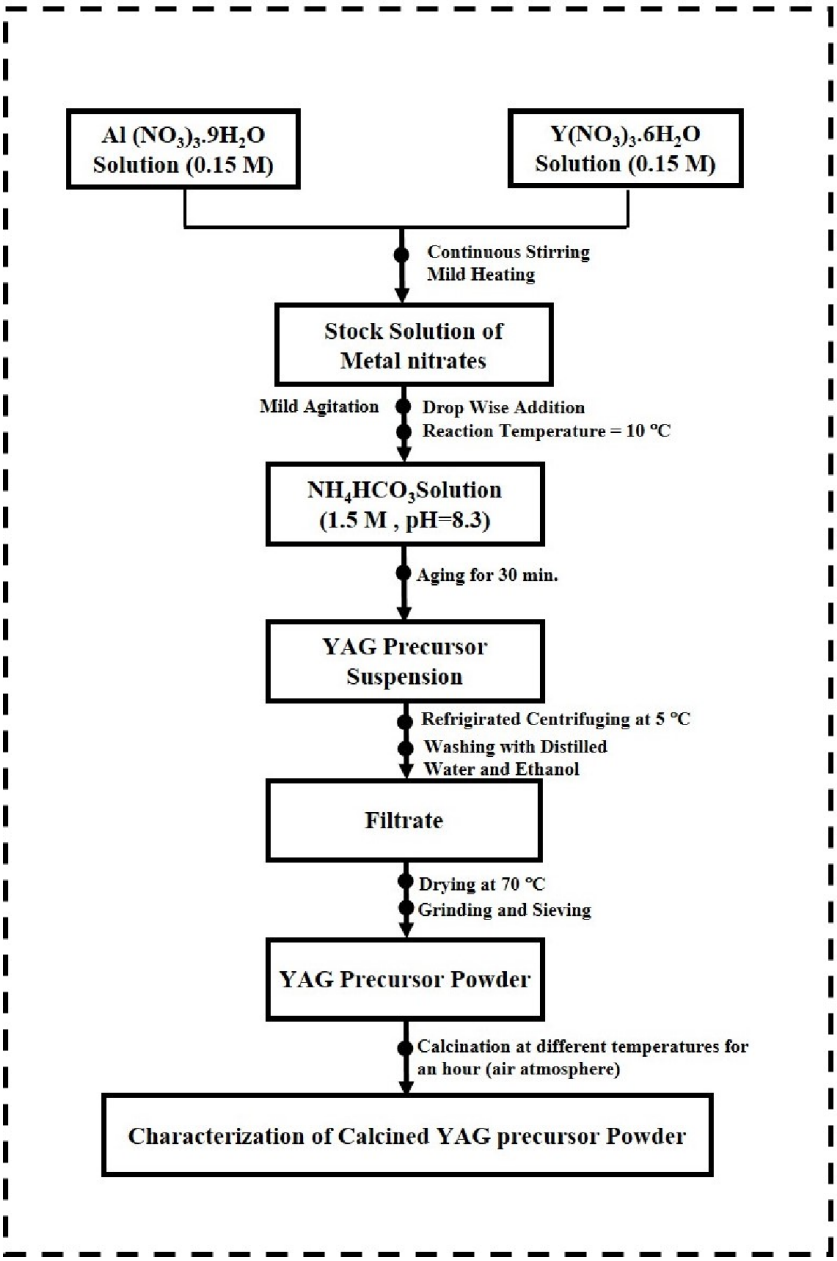

Figure 3.1: Nanosized YAG crystalline powders produced by the Co-precipitation method, employing AHC as precipitant.

The stock solution of the metal nitrates was slowly added through burette to the precipitant solution (Reverse strike technique) under mild agitation. The final pH value of the suspension was found to be 7.8. The process methodology is represented in Fig. 3.1. The precipitate was obtained at 10°C in an ice bath and kept for 30 min to complete the reaction. The precipitate was then separated by centrifuging at 5°C, washed four times with distilled water, rinsed with ethanol, and dried at 70°C in an oven. The soft

agglomerated powder was slightly ground and sieved to get fine powder. The resultant YAG precursor powder was then calcined at different temperatures for an hour in air atmosphere to form garnet phase.

3.2.2 Physico-Chemical Characterizations

Thermal analysis technique was employed to investigate the decomposition behaviour of YAG precursor powders prepared through co-precipitation synthesis technique. The phase structure, crystallite size, average particle size and morphology of the calcined precursor powders were systematically analysed by using XRD, FESEM, and TEM, respectively.

3.2.2.1 Thermal Analysis (DSC-TG)

Thermal analysis refers to a group of techniques which continuously measure the physical or chemical changes in a given system as a function of temperature. These techniques provide basic information including reaction kinetics, decomposition behaviour, phase transition, and formation of products etc., from the synthesized precursor powders. Thermo Gravimetric (TG) and Differential Scanning Calorimetry (DSC) of the dried YAG precursor powder was performed on a DSC-TG analyser (Netzsch, STA 449C, Germany) up to 1100°C at a heating rate of 10°C/min in dynamic atmosphere of air. In thermo gravimetric analysis (TGA), the sample was heated at a controlled rate to record the weight loss as a function of temperature. Every material either absorbs or evolves thermal energy of characteristic range when it undergoes certain physico-chemical changes. In DSC, the temperature difference between the test specimen and inert reference material (α-alumina) is recorded as a function of temperature whilst the sample and reference materials are subjected to a controlled heating program and represented by either as an exothermic or endothermic peak in the DSC plot. An exothermic reaction (liberation of heat) includes oxidation, crystallization etc., results an upward peak, whereas an endothermic reaction (absorption of heat) like melting, decomposition etc., gives a downward peak in the DSC plot.

3.2.2.2 Phase Evolution by X-ray Diffraction and Crystallite Size Measurement

X-ray diffraction is a rapid analytical tool which is primarily performed to study the phase evolution and characterization of materials based on their diffraction pattern. In this, X-rays are being scattered by atoms whilst the monochromatic x-ray radiation interacts with the examining material. The X-ray diffraction pattern is generated from the constructive interference of the resultant scattered X-rays. The diffraction of X-rays follows the principle of Bragg's law (Fig. 3.2), can therefore be mathematically written as

$$n\lambda = 2d\,sin\theta \qquad \ldots\ldots\ (3.1)$$

Where,

n= order of reflection

λ= wavelength of the X-ray radiation (°A)

d = inter planar spacing (°A)

θ= Bragg's angle (degrees).

In this expression, the wavelength of X-ray radiation is related to the diffraction angle and interplanar spacing in a crystalline material. The powdered specimen is being scanned through a range of twice theta (2θ) angles to obtain all the possible diffraction directions of the lattice due to its random orientation with respect to x-rays. Every mineral has a set of characteristic d-spacings that allows to identify them by converting the evolved diffraction peaks to d-spacings. X-ray diffraction (Rigaku (Japan) Ultima-IV X-Ray Diffractometer) measurements were performed at room temperature using nickel filtered CuKα radiation (1.5418 °A) as a source to investigate the phase, crystal structure, crystallinity, and crystallite size of the YAG nanopowders prepared via different synthesis techniques. The operating conditions for diffractometer were 35 kV and 30 A. The scattering angle (2θ) for all data ranged from 20° to 50° with 0.05° step size at a scanning rate of 20° per minute. The obtained experimental XRD results were analysed with the standard X-ray powder diffraction database (JCPDS – Joint Committee on Powder Diffraction Standards) to investigate the phase purity.

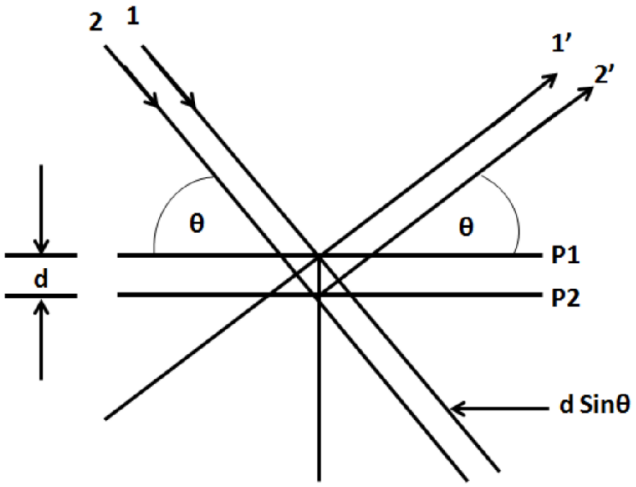

Figure 3.2: Schematic representation of constructive interference in Bragg's Law [45].

Crystallite Size Measurement

The size of a coherently diffracting domain can be referred as crystallite size. Scherrer's formula is used to calculate the crystallite size [45], can be written as

$$t = \frac{0.9\lambda}{BCos\alpha} \qquad \ldots\ldots (3.2)$$

Where,

t = average crystallite size (°A)

λ= wavelength of X-rays (°A)

α = Bragg's angle (degree)

B = Full width at half maximum (radians).

The instrumental broadening was subtracted from the peak width prior to the calculation of crystallite size by using the following formula.

$$B^2 = B^2_{observed} - B^2_{instrument} \qquad \ldots (3.3)$$

Where,

$B_{observed}$ = measured full width at half maximum from peak values

$B_{instrument}$ = instrumental broadening.

The average crystallite size of the synthesized YAG nano powder was calculated through Scherer's equation.

3.2.2.3 Field Emission Scanning Electron Microscopy (FESEM)

This microscopic technique is used to analyse the surface characteristics of materials. In this technique, a beam of accelerated electrons is used as a source of illumination instead of light. The electrons are discharged from a field emission source under huge electrical field gradient known as primary electrons. A focused electron beam is produced through deflecting these electrons by electronic lenses. Interaction of the electrons with the atoms in the specimen, excites them and secondary electrons are emitted (Fig. 3.3).
Surface features of the examining specimen are related to the nature of these secondary electrons. The resultant secondary electrons have been caught by the detector and produces an electronic signal. Amplification of this signal generates a scanned image containing required surface characteristics of the material. The Energy Dispersive X-ray Spectroscopy (EDX), an analytical technique that allows us to analyse the elements in the specimen in a qualitative and quantitative fashion. In this, X-rays of specific energies are released due to the interaction of high energy electronic beam with the atoms of various elements present in the material. The unique atomic structure of every element ensures X-rays to distinguish them in a distinctive way. The morphological analysis of the precursor and calcined YAG nano powders were observed by the field emission scanning electron microscope (FESEM, NOVA NANOSEM FEI 450, Netherland).

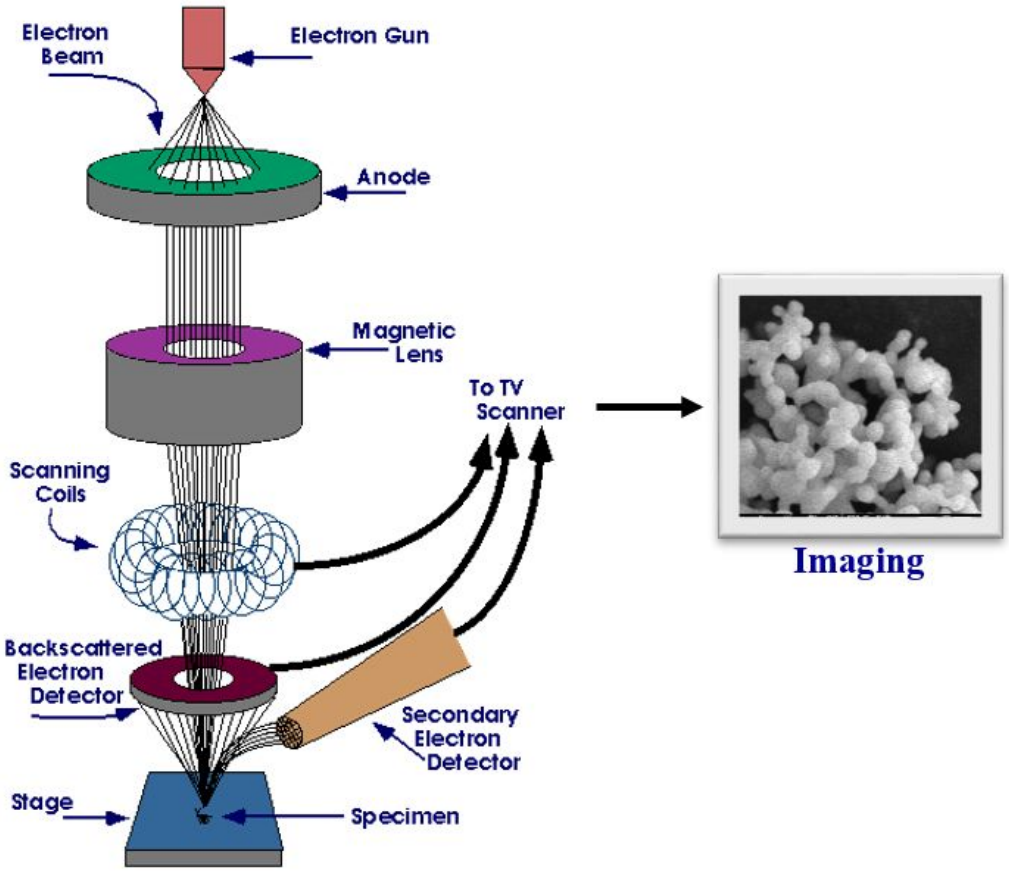

Figure 3.3: Working principle of Field Emission-Scanning Electron Microscopy [46].

The samples for FESEM analysis were prepared by mounting the powders onto a carbon tape attached SEM stub and sputter coated with a thin layer of gold for 2 minutes to render them conductive prior to the observation.

3.2.2.4 Transmission Electron Microscopy (TEM)

Transmission electron microscopy (TEM) is a microscopic technique which is widely used to investigate the structure, morphology and composition of the materials. In this technique, electrons are being scattered while a high energy electronic beam interacts with the ultra-thin section of the material as it passes through it. These scattered electrons

are allowed to focus by a sophisticated system of electromagnetic lenses to develop a diffraction pattern or an image according to the mode of the operation (Fig. 3.4).

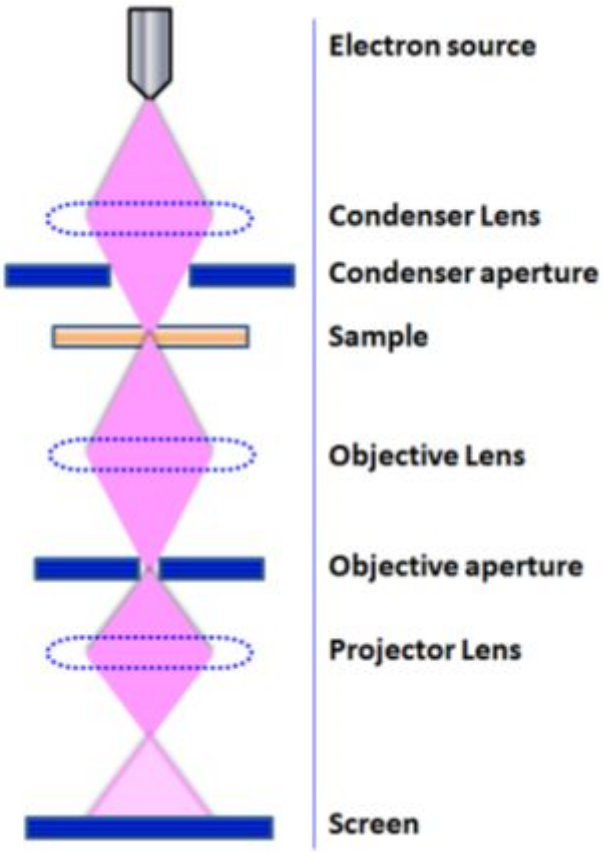

Figure 3.4: Working principle of Transmission Electron Microscopy [46].

The electron diffraction pattern displays the information to investigate the crystal structure and chemical composition of precipitants, contaminants and distinct phases etc. TEM, HRTEM, and SAED pattern, techniques were performed to study the average particle size, morphology, crystal structure, crystallographic parameters like d-spacing and degree of crystallinity of the YAG nano powder synthesized via co-precipitation process, respectively. The samples for TEM observations were prepared by ultrasonic dispersion of powder sample in ethanol. A thoroughly dispersed YAG solution was dripped onto a carbon coated copper grid and then dried at room temperature. The bright field transmission electron microscopy (TEM, JEOL JEM-2100) was performed to observe the powder morphology.

3.3 Results

3.3.1 Thermal Analysis

The recorded DSC-TG traces of the co-precipitated precursor shows one endothermic and two exothermic peaks up to 1000°C with an overall weight loss to nearly ~ 50% in Fig.3.5.

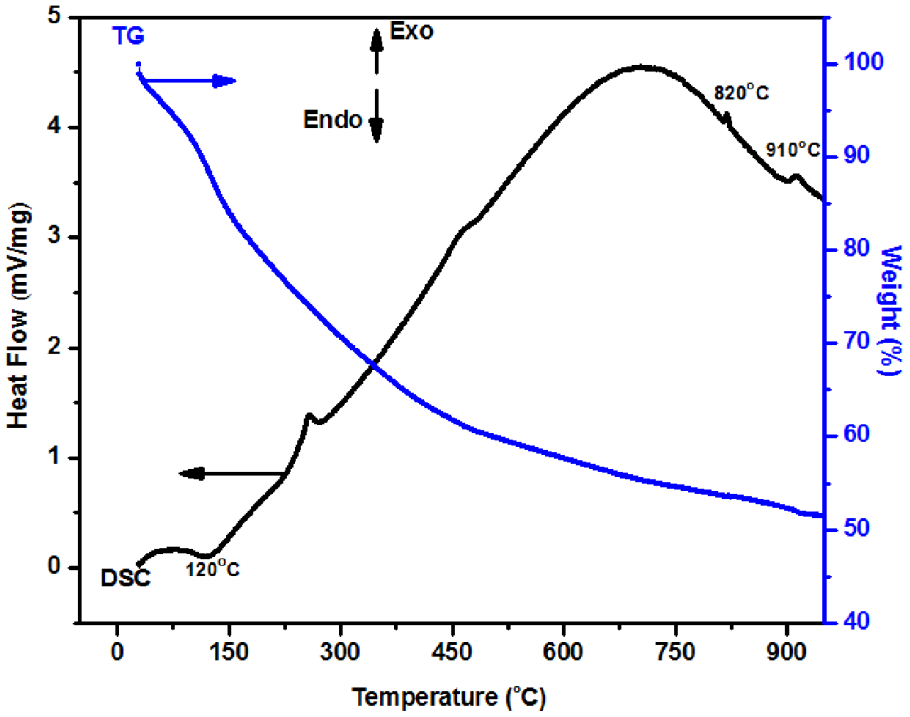

Figure 3.5: DSC-TG curves of the co-precipitated YAG precursor exhibits an exothermic peak at about 910°C which is attributed to the crystallization of YAG phase and mass loss of 48%.

It has been observed that the mass loss of the precursor at a temperature below 400°C is mainly due to release of molecular water, ammonia, and the partial decomposition of carbonate species while the transition occurred at a temperature above 400 °C (range: 400 – 600 °C) is primarily attributed to the complete decomposition of carbonate matter.The relatively diffuse endotherm at ~120 °C is assigned to the removal of physically absorbed water. The exotherms located at 820°C and 910°C are ascribed to the crystallization of YAP and YAG compositions. These thermal alteration behaviors are further confirmed by the XRD pattern at different steps in later section.

3.3.2 Phase Analysis

XRD spectra of the as synthesized precursor via co-precipitation and the resultant powders produced by calcining the precursor at 600, 750, 850 and 900°C for an hour in air atmoshpere is presented in the Fig. 3.6.

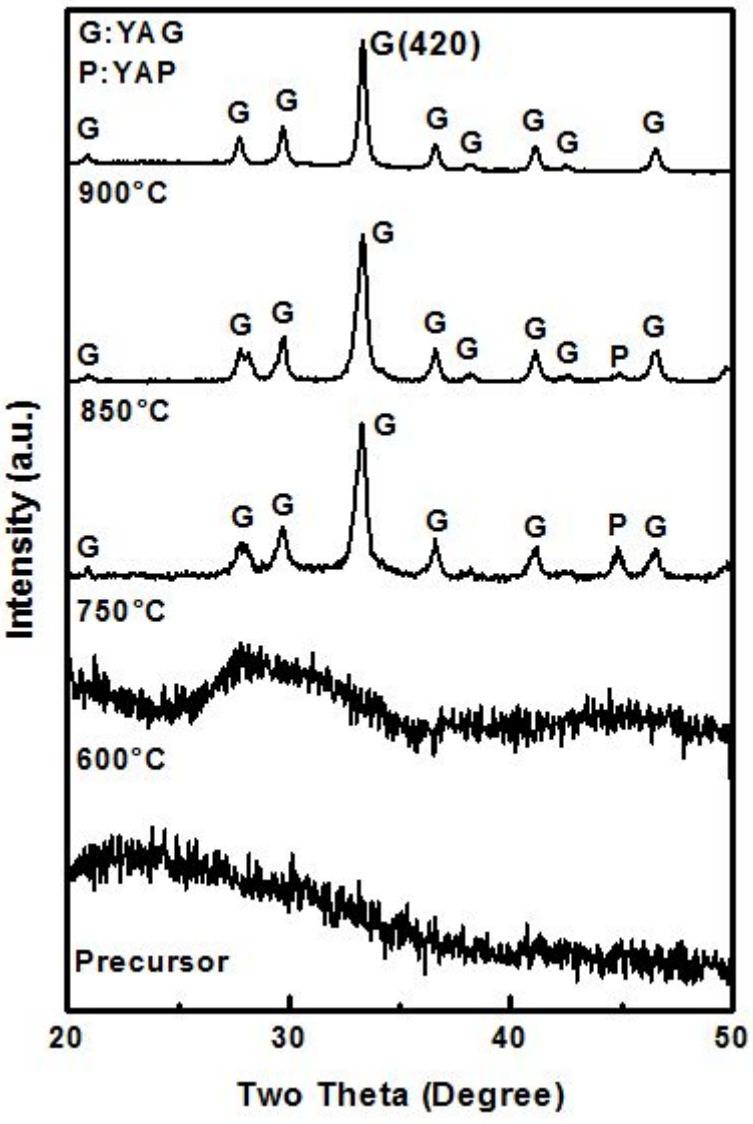

Figure 3.6: The composite XRD spectra of the YAG precursor and the samples calcined for an hour in air at different temperatures: precursor, 600°C, 750°C, 850°C and 900°C. Pure garnet phase is obtained at 900°C and dramatic reduction in the intensity of YAP in between 750°C and 850°C can be observed.

The precursor and the powders calcined at 600°C are found to be completely amorphous to the X-rays. However, the XRD pattern of the precursor heat treated at 750°C shows partial crystallization of the precursor to stable garnet structure (YAG, JCPDS 79-1891) with perovskite (YAP, JCPDS 74-1334) as intermediate phase. Upon subsequent calcination of the precursor to 850°C, no further phase change is exhibited but refinement in peak shape and intensity is being noticed. However, the precursor powders calcined at 900°C represents strong cubic – YAG diffraction peaks without the presence of any intermediate phases. In this, crystallization of YAG composition has occurred at a lower temperature of 900°C compared to the Marlot's work [39] which can be ascribed to the greater chemical homogenity of cations due to employment of reverse strike chemical preciptiation over normal strike method. The mean crystallite size of the YAG nanopowder obtained at 900°C is found to be ~24 nm.

The phase structures of the powders obtained by calcining the precursor at different temperatures are summarized in Table 3.1. When multiphase coexistance occurs, the phases detected at the particular temperature are sequenced according to their relative content that can be determined from their respective diffraction peak intensities.

Table 3.1: The phase compositions of co-precipitated powders obtained at different calcination temperatures (P:YAP, G:YAG)

Al-Source, Y-Source, Precipitant	600°C	750°C	850°C	900°C
Al $(NO_3)_3.9H_2O$, Y $(NO_3)_3.6H_2O$, AHC	-	G, P	G, P	G

3.3.3 Morphology

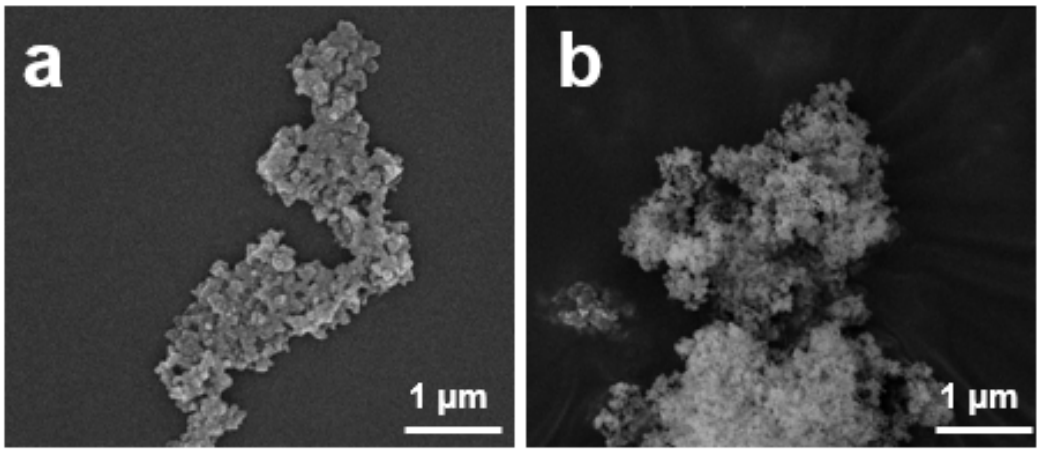

Figure 3.7: FESEM morphologies of the (a) co-precipitated precursor and (b) the resultant YAG nanopowder obtained at 900°C.

Fig. 3.7 shows the FESEM morphologies of the co-precipitated YAG precursor and the calcined YAG nanopowders obtained at 900°C. The morphology of the precursor (Fig. 3.7a) is mainly composed of nanometric primary particles. However, the morphology of YAG nanopowders (Fig. 3.7b) obtained at 900°C displays relatively discrete and nearly spherical shaped particles with an average size of ~40 nm at a higher magnification.

Based on the above produced thermal analysis (DSC-TG), phase evolution (XRD), and morphological study (FESEM) of the co-precipitated precursor, the following conclusions have been drawn:

(i) Thermal alteration behaviour by DSC-TG is in well agreement with the phase evolution study by XRD.

(ii) Low crystallization temperatures (about 900°C) are needed to obtain phase pure YAG nanopowders

(iii) Morphology of the YAG nanopowder obtained at 900°C reflects the key features of a well sinterable nature through which highly dense polycrystalline YAG ceramics can be fabricated with near to pore-free microstructure.

(iv) Greater yield, cost-effective and reproducible powders.

3.4 Discussions

As known to us diffusion of ions plays an important role in the solid-state reactions (SSR) [47]. A sintering model, illustrating the formation of YAG phase in solid state route via sequent phase transitions i.e. Yttrium Aluminum Monoclinc (YAM: $Y_4Al_2O_9$) →Yttrium Aluminium Pervoskite (YAP: $YAlO_3$) → Yttrium Aluminum Garnet (YAG: $Y_3Al_5O_{12}$) is presented in Fig. 3.8. The reactions reported in the Fig. 3.8 are given below.

$$2\ Y_2O_3 + Al_2O_3 \rightarrow Y_4Al_2O_9 \quad \text{..... (A1)}$$

$$Y_4Al_2O_9 + Al_2O_3 \rightarrow 4\ YAlO_3 \quad \text{..... (A2)}$$

$$3\ YAlO_3 + Al_2O_3 \rightarrow Y_3Al_5O_{12} \quad \text{..... (A3)}$$

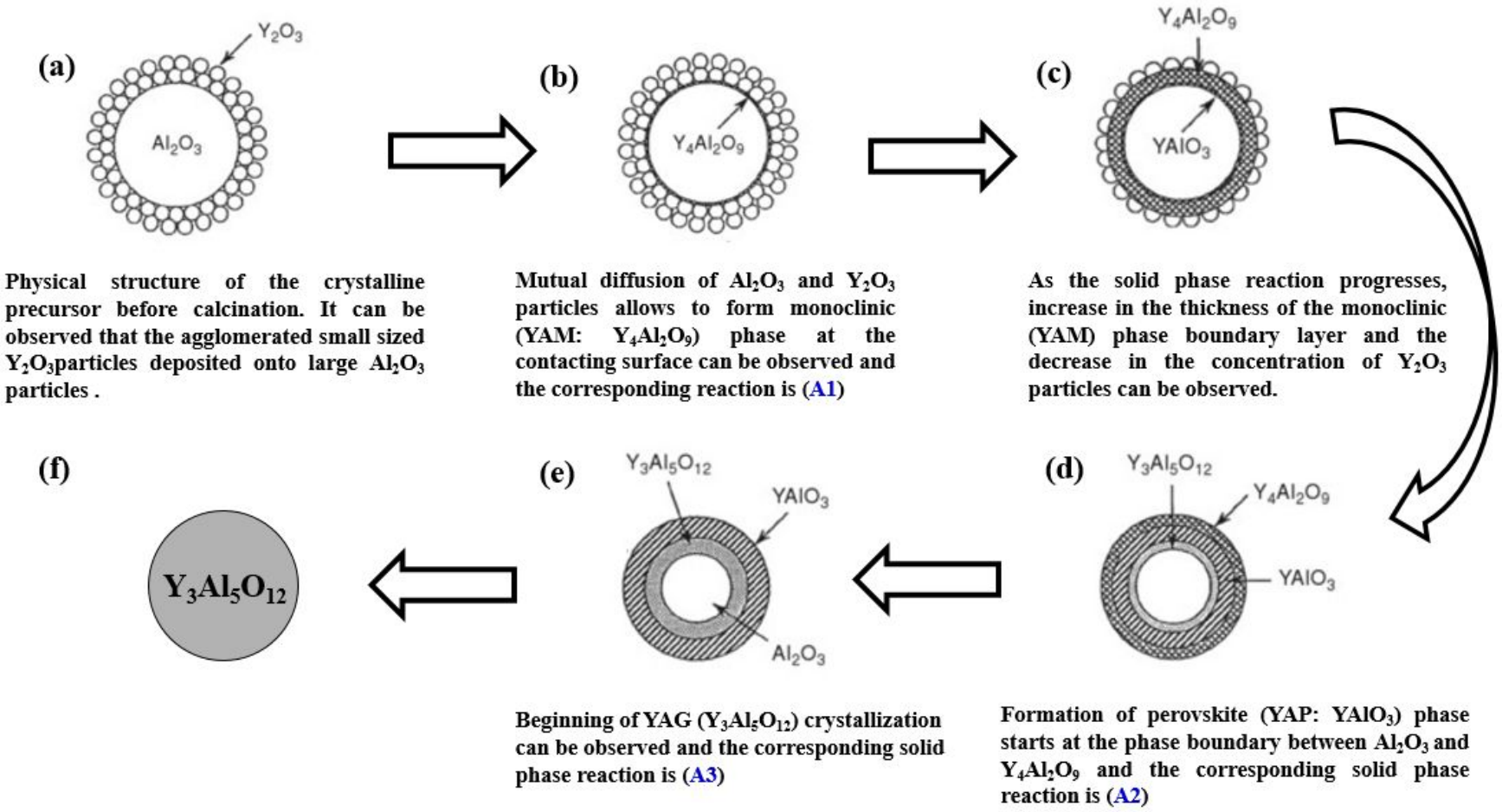

Figure 3.8: A sketch illustrating the sequent phase transitions involved in the synthesis of YAG via solid state route [47].

Numerous literature works have clearly reported that the solid state reaction products obtained at 1100°C is still a mixture of YAG, YAP, YAM, α-Al_2O_3 and cubic Y_2O_3**.** The presence of intermediate phases after being calcined at 1100°C, is primarily due to the lengthening of diffusion distance caused by the following factors: (i) simultaneous growth of α-Al_2O_3 and cubic Y_2O_3 particles during calcination (ii) decrease in the homogeneity of oxide mixtures, presumably due to the presence of oversized Y_2O_3 particles [47].

In solution-based techniques, the phase transition phenomenon of precursor to YAG powders is not actually a solid state reaction between alumina and yttria; however, this transformation for the co-precipitation synthesis on the basis of obtained experimental results can be correlated and demonstrated in a systematic manner. Fig. 3.9 schematically illustrates a plausible pathway for the crystallization of amorphous precursor prepared by co-precipitation process into YAG phase. Herein, the crystallization path is developed according to the experimental results provided by DSC-TG (Fig. 3.5), XRD (Fig. 3.6) of the co-precipitated powders. The facts behind the experimental observations during crystallization are clearly explained with the help of Ostwald's theory, 'The Rule of Stages' [48-50]. As shown in Fig. 3.9, the usual chemical composition of precursor prior to calcination is of hydrated ammonium yttrium aluminum carbonate type [25, 42]. Calcination of such a precursor to 600°C results in the formation of an amorphous Y-Al-O system by releasing the decomposable matter (carbonates, ammonia, and water) as evidenced from the DSC-TG and XRD plots. Subsequent calcination to 750°C causes crystallization of Y-Al-O system into two different crystalline phases YAP and YAG. When the calcination temperature rises to 850°C a significant growth in YAG phase and reduction in YAP content can be observed. With the further increase of calcination temperature to 900°C the YAP phase completely disappears and the system is fully transformed to YAG.

Careful examination of Fig. 3.6, reveals that the rise in the peak intensity of YAG and fall in the intensity of YAP in the powders calcined at 850°C compared to 750°C suggests that the existing conditions are favourable for the growth of YAG phase than YAP. This phenomenon follows the Ostwald's rule of stages whereas an amorphous precursor of highest free energy transforms to a most stable crystalline state of lowest

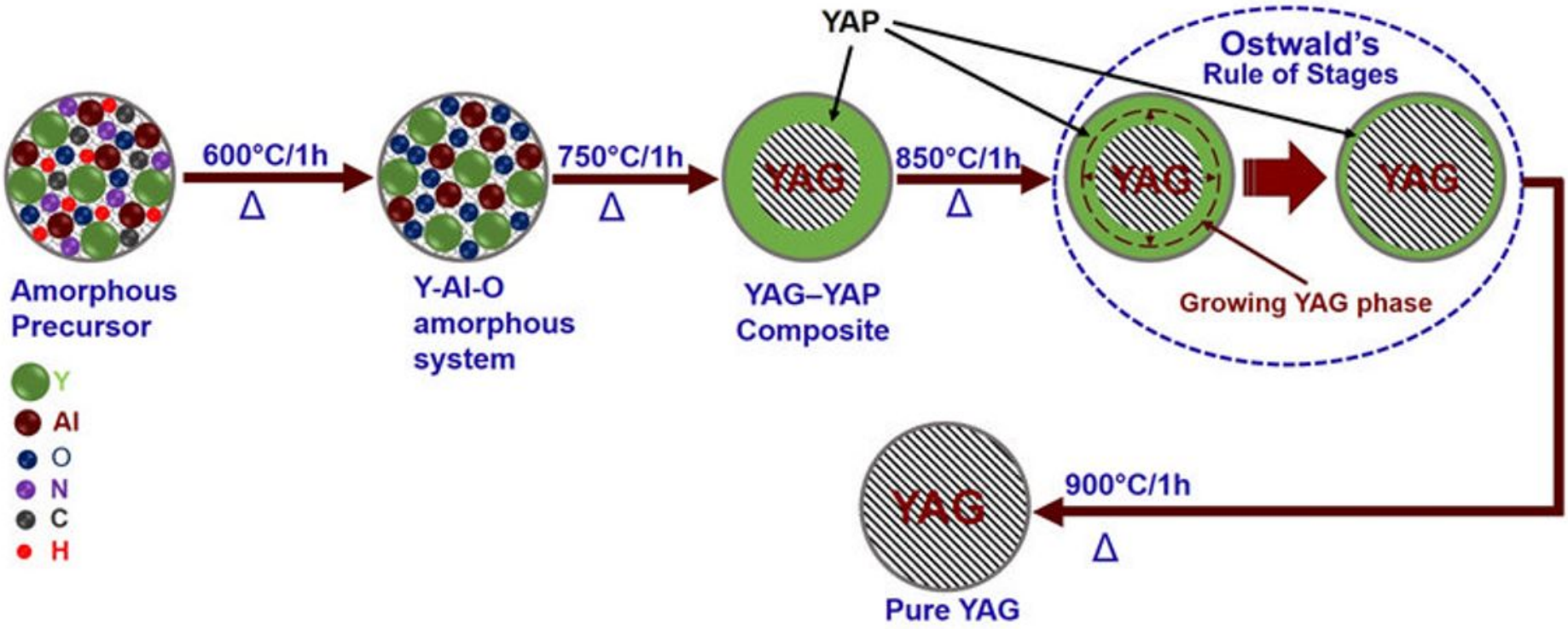

Figure 3.9: Schematic representation of the crystallization path for the formation of YAG nanopowder according to the obtained experimental data.

free energy via metastable intermediate crystalline phases. This experimental evidence discloses a fact that the system tends to transform towards YAG, establishes that YAG is a thermodynamically stable crystalline phase than YAP. In reference to the DSC observations (Fig. 3.5), higher crystallization temperature of YAG (910°C) than YAP (820°C) also confirms that YAG is the most thermodynamically stable crystalline phase. TEM analysis further enables to illustrate the aforesaid hypothesis.

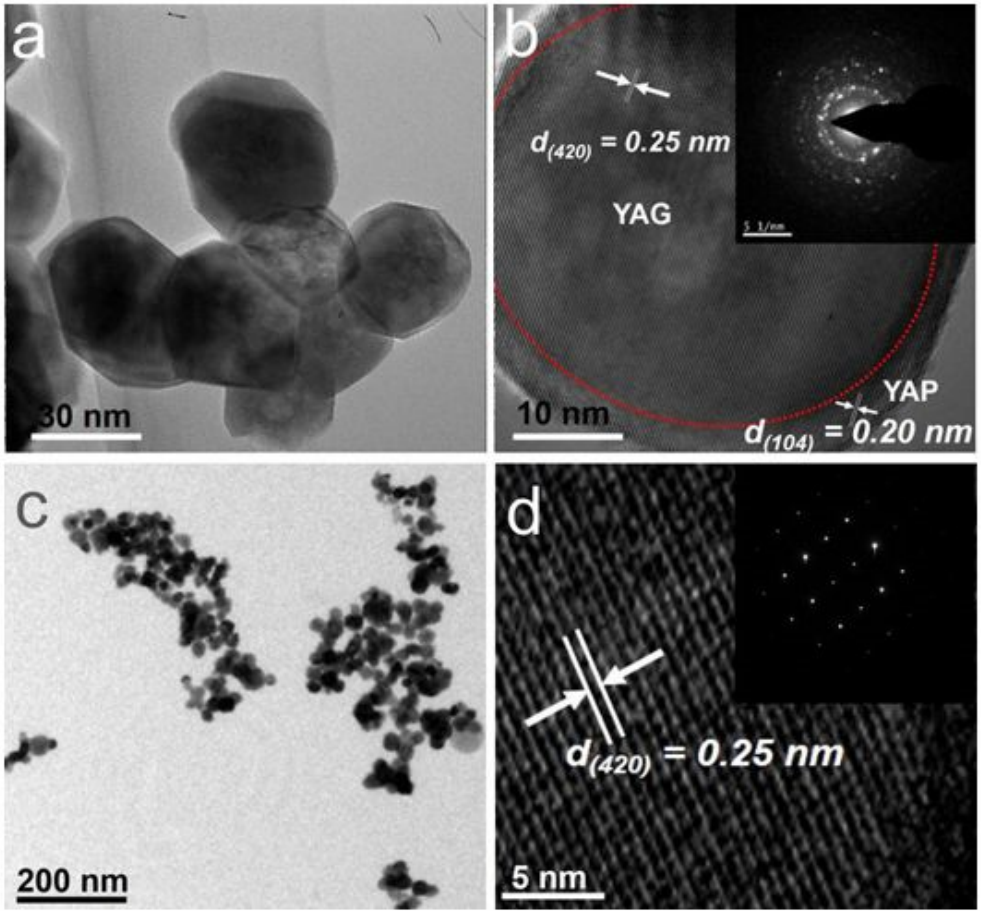

Figure 3.10: (a) TEM, (b) HRTEM image of the co-precipitated powders calcined at 850°C; (c) TEM, and (d) HRTEM image of the co-precipitated powders calcined at 900°C. Inset of (b) and (d) show their corresponding SAED patterns. The increase in crystallinity of YAG from 850°C to 900°C is further confirmed by SAED pattern.

TEM characterizations of the optimized process powders calcined at different temperatures is presented in Fig. 3.10. TEM image (Fig. 3.10a) clearly distinguishes that the powders obtained at 850°C, are quasi spherical in shape and average particle size is about 35 nm. High resolution TEM image (Fig. 3.10b) observations suggest

that the coexistence of YAP and YAG phases in the powders obtained at 850°C. The interplanar spacings of about 0.2 nm and 0.25 nm correspond to the (104) plane of hexagonal YAP and (420) plane of cubic YAG, respectively. The coexistence of YAP and YAG are further confirmed by the SAED pattern (inset). TEM morphology and high resolution images of the powders obtained at 900°C are presented in Fig. 3.10c and 3.10d. TEM morphology (Fig.3.10c) clearly indicates that the particles are remarkably less agglomerated, nearly spherical in shape, fairly uniform and have an average particle size of ~ 40 nm. The d-spacing calculated from the HRTEM image (Fig.3.10d) is found to be 0.25 nm which corresponds to the (420) plane of cubic YAG. SAED pattern (inset) further confirms that YAG is the only phase present at this temperature.

Based on the above stated experimental observations and corresponding theoretical arguments it can be concluded that the amorphous precursor prepared via co-precipitated synthesis is completely transformed into the most thermodynamically stable crystalline phase YAG via a metastable intermediate crystalline phase YAP.

3.5 Conclusions

YAG nanopowders were successfully synthesized in a large scale with greater yield and reproducible nature by co-precipitation of $Al(NO_3)_3.9H_2O$, $Y(NO_3)_3.6H_2O$, NH_4HCO_3 at pH ~ 8 and calcination temperature of 900 °C with the following characteristics: (i) free flowing pure and high crystalline ~40 nm YAG particles. (ii) typical morphology with relatively discrete, fine and almost spherical particles to develop highly dense polycrystalline YAG ceramics with pore-free microstructure. (iii) amorphous to crystalline YAG transformation via a metastable intermediate YAP phase follows the Ostwald's 'Rule of Stages'.

References

1. T. Taira, Ceramic YAG lasers, Comptes Rendus Physique 8 (2007) 138-152.
2. A. Ikesue, Y. L. Aung, Ceramic laser materials, Nature photonics 2 (2008) 721-727.
3. A. Ikesue, T.Kinoshita, Fabrication and optical properties of high performance polycrystalline Nd:YAG ceramics for solid-state lasers, J. Am. Ceram. Soc., 78 (1995) 1033-1040.
4. N. Uehara, K. Ueda, Ultra-stabilized by laser-diode pumped Nd:YAG lasers, Rev. Lasers Eng., 21 (1993) 590-600.
5. G. With De, H. J. A. Van Dijk, Translucent $Y_3Al_5O_{12}$ ceramics, Mater. Res. Bull., 19 (1984) 1669-1674.
6. M. Sekita, H. Haneda, T. Yanagitani, S. Shirasaki, Induced emission cros section of Nd:$Y_3Al_5O_{12}$ ceramics, J. Appl. Phys., 67 (1990) 453-458.
7. N. Frage, V. Kasiyan, A. Rothman, M.P. Dariel , Effect of the spark plasma sintering parameters and LiF doping on the mechanical properties and the transparency of polycrystalline Nd-YAG, Ceram. Int., 38 (2012) 5513-5519.
8. A. Krell, J. Klimke, T. Hutzler, Transparent compact ceramics: Inherent physical issues, Opt. Mater., 41 (2013) 20-54.
9. Y. Zhang, H. Yu, Synthesis of YAG powders by the co-precipitaton method, Ceram. Int., 35 (2009) 2077-2081.
10. R. Manalert, M. N. Rahaman, Sol-gel processing and sintering of yttrium aluminum garnet (YAG) powders, J. Mater. Sci., 31 (1996) 3453-3458.
11. A. Ikesue, I Furussato, K. Kamata, Fabrication of polycrystalline, transparent YAG ceramics by a solid-state reaction method, J. Am. Ceram. Soc., 78 (1995) 225-228.
12. J. Li, Y.S. Wu, Y. B. Pan, Fabrication, microstructure and properties of highly transparent Nd:YAG laser ceramics, Opt. Mater., 31 (2008) 6-17.
13. T. Yanagitani, H. Yagi, A. Ichikawa, Production of yttrium aluminum garnet fine powder, Jpn Patent 10-101333 (1998).
14. T. Yanagitani, H. Yagi, M. Imagawa, Production of powdery starting material for yttrium aluminum garnet, Jpn Patent 10-101334 (1998)
15. T. Yanagitani, H. Yagi, H. Yamazaki, Production of fine powder of yttrium aluminum garnet. Jpn Patent 10-101411 (1998).
16. W. X. Zhang, Y. B. Pan, J. Zhou, Diode-pumped Tm:YAG ceramic laser, J. Am. Ceram. Soc., 92 (2007) 2434-2437.
17. J. Y. Pastor, J. Llorca, A. Martin, Fracture toughness and strength of Al_2O_3-$Y_3Al_5O_{12}$ and Al_2O_3-$Y_3Al_5O_{12}$ –ZrO_2 directionally solidified eutectic oxides up to 1900 K, J. Eur. Ceram. Soc., 28 (2008) 2345-2351.
18. M. Medraj, R. Hammond, M. A. Parvez, R. A. L. Drew, W. T. Thompson, High temperature neutron diffraction study of the Al_2O_3-Y_2O_3 system, J. Eur. Ceram. Soc., 26 (2006) 3515-3524.
19. G. De With and H. J. A. Van Dijik, Translucent $Y_3Al_5O_{12}$ ceramics, Mater. Res. Bull., 19 (1984) 1669-1674.
20. K. M. Kinsman, J. Mc Kittrick, E. Sluzky, Phase development and luminescence in chromium – doped yttrium aluminum garnet (YAG:Cr) phosphors, J. Am. Ceram. Soc., 77 (1994) 2866-2872.
21. L. E. Shea, J. Mc Kittrick, O. A. Lopez, and E. Sluzky, Synthesis of red emitting small particle size luminiscent oxides using an optimized combustion process, J. Am. Ceram. Soc., 79 (1996) 3257-3265.
22. A. Boukerika, L. Guerbous, N. Brihi, Ce-doped YAG phsphors prepared via sol-gel method: Effect of some modular parameters, J. Alloy Compd., 614 (2014) 383-388.

23. B. Huang, Y. Ma, S. Qian, Luminiscent properties of low-temperature-hydrothermally-synthesized and post-treated YAG:Ce (5%) phsophors, Opt. Mater., 36 (2014) 1561-1565.
24. M. Inoue, Glycothermal synthesis of metal oxides, J. Phys. Condens. Matter., 16 (2004) S1291-1303.
25. J. G. Li, T. Ikegami, J. H. Lee, T. Mori, Y. Yajima, Co-precipitation synthesis and sintering of yttrium aluminum garnet (YAG) powders: The effect of precipitant, J. Eur. Ceram. Soc., 20 (2000) 2395-2405.
26. P. Palmero, C. Esnouf, L. Montanaro, G. Fantozzi, Influence of the co-precipitaton temperature on phase evolution in yttirium – aluminium oxide materials, J. Eur. Ceram. Soc., 25 (2005) 1565-1573.
27. J. Li, Y. Pan, F. Qiu, Y. Wu, Nanostructured Nd:YAG powders via gel combustion: the influence of citrate-to-nitrate ratio, Ceram. Int., 34 (2008) 141-149.
28. C. H. Lu, C. H. Hang, B. M. Cheng, Synthesis and luminiscene properties of micro-emulsion derived $Y_3Al_5O_{12}$: Eu^{+3} phosphors, J. Alloy Compd.,473 (2009) 376-381.
29. Y. Liu, Synthesis of yttrium aluminium garnet using isobutyrate precursors, J. Am. Ceram. Soc., 79 (1996) 385-389.
30. P. F. S. Pereira, J. M. A. Caiut, E. J. Nassar, Microwave synthesis of YAG:Eu by sol-gel methodology, J. Lumin., 126 (2007) 378-382.
31. Y. Hakuta, T. Haganuma, K. Arai, Continous production of phsophor YAG:Tb nanopartciles by hydrothermal synthesis in super critical water, Mater. Res. Bull., 38 (2003) 1257-1265.
32. S. Aasland, P. F. McMillan, Density-drivenliquid-liquid phase separation in the system Al_2O_3-Y_2O_3 , Nature, 369 (1994) 633-636.
33. J. Vrolijk, J. Willems, R. Metselaar, Co-precipitation of yttrium and aluminium hydroxde for preparation of ytrium aluminium garnet, J. Eur. Ceram. Soc., 6 (1990) 47-53.
34. D. J. Sordelet, M. Aknic, M. L. Panchula, Y Han, synthesis of yttrium aluminium garnet precursor powders by homogeneous precipitation, J. Eur. Ceram. Soc., 14 (1994) 123-130.
35. N. Matsushita, N. Tsuchiya, K. Nakatsuka, T. Yanagitani, Precipitation and calcination processes for yttrium aluminium garnet precursors synthesized by the urea method, J. Am. Ceram. Soc., 82 (1999) 1977-1984.
36. M. Li, Principles and synthesis of ceramic powder by means of wet chemical method, J. Chin. Ceram. Soc. 22 (1994) 85-91.
37. M. Z. Napierala, M. M. Bucko, K. Haberko, The effect of non-stoichiometry on microstructure and selected properties of YAG polycrystals, Ceram. Int., 38 (2012) 2589-2592.
38. M. Zeng, Y. Ma, Y. Wang, C. Pei, The effect of precipitant on co-precipitation synthesis of yttrium aluminium garnet powders, Ceram. Int., 38 (2012) 6951-6956.
39. C. Marlot, E. Barraud, S. L. Gallet, M. Eichhorn, F. Bernard, Synthesis of YAG nanopowder by the co-precipitation method: Influence of pH and study of the reaction mechanisms, J. Solid State. Chem., 19 (2012) 114-120.
40. P. Palmero, R. Traverso, Co-precipitation of YAG Powders for Transparent materials: Effect of the synthesis parameters on processing and microstructure, Materials, 7 (2014) 7145-7156.
41. Y. Zhang, H. Yu, Synthesis of YAG powders by the co-precipitation method, Ceram. Int., 35 (2009) 2077-2081.
42. J. Li, F. Chen, W. Liu, W. Zhang, L. Wang, Co-precipitation synthesis route to yttrium aluminum garnet (YAG) transparent ceramics, J. Eur. Ceram. Soc., 32 (2012) 2971-2979.
43. J. Li, T. Ikegami, J. H. Lee, T. Mori, Low temperature fabrication of transparent yttrium aluminium garnet (YAG) ceramics without additives, J. Am. Ceram. Soc., 83 (2000) 961-63.

44. Y. Sang, Y. Lv, H. Qin, H. Liu, X. Zhang, J. Wang, X. Sun, R. I. Boughton, Chemical composition evolution of YAG co-precipitate determined by pH during aging period and its effect on precursor properties, Ceram. Int., 38 (2012) 1635-1641.
45. H.P. Klug, L.E. Alexander, Crystallite Size Determination from Line Broadening, Wiley, New York, 1954.
46. Ian M. Watt, The Principles and Practice of Electron Microscopy, 2nd ed., Cambridge University Press, New York, 1997.
47. A. K. Ikesue, Y. L. Aung, V. Lupei, Ceramic Lasers, 1st ed., Cambridge University Press, New York, 2013.
48. S. Y. Chung, Y. M. Kim, J. G. Kim, Y. J. Kim, Multiphase transformation and Ostwald's rule of stages during crystallization of a metal phosphate, *Nature Physics* 5 (2009) 68-73.
49. T. H. Zhang, X. Y. Liu, How Does a Transient Amorphous Precursor Template Crystallization, J. Am. Chem. Soc. 129 (2007) 13520-13526.
50. W. Ostwald, Studien uber die Bildung und Umwandlung feter Korper. Z. Phys. Chem. 22 (1897) 289-330.

Chapter 4

Nanoparticle Coarsening Effect on Sintered Density and Microstructure of YAG

4.1 Introduction

Yttrium aluminum garnet (YAG, $Y_3Al_5O_{12}$) is one phase of the yttria-alumina composite with centro-symmetric cubic crystalline structure. The superior thermo-mechanical properties like low thermal expansion coefficient and high thermal shock resistance etc. coupled with a variety of good optical properties established YAG as a potential gain media for solid state laser (SSL) applications. Czochralski grown YAG single crystals are the most widely used solid state laser gain media for the last four decades. Recently, polycrystalline YAG ceramics which are commercially prepared from the synthesized powders have attained both industrial as well as technological interest and become a promising substitute for conventional single crystal technology, ascribed to several potential benefits that include: (i) low price, ease of manufacture, and mass production, (ii) possibility to make large sized monoliths with high doping concentrations, (iii) enhanced thermo-mechanical properties etc. [1]

Optical transparency is the primary requisite characteristic of a laser gain media. The most common scattering sites in ceramic materials that include residual porosity (either inter or intra granular), grain boundary thickness, grain boundary with secondary phases, and birefringence. Of these, residual porosity is the most significant factor for transparency. Thus, a limiting condition to obtain transparency in ceramics is sintering to full density, i.e., eliminating all of the residual porosity in the material. Moreover, fabrication of highly dense YAG based materials need careful control of every step from synthesis of powders to sintering. Furthermore, there are

few comprehensive studies which have reported novel processing approaches in order to fabricate highly dense YAG ceramics [2].

Commercially, the polycrystalline YAG ceramics are produced by utilizing powders synthesized via two sources: (i) solid state reaction (SSR) and (ii) wet chemical synthesis. Numerous research reports demonstrated that SSR approach constitutes few unavoidable disadvantages such as high calcination temperature to obtain pure YAG phase, difficulty to control particle size and morphology of the resulting powders. In this respect, several wet chemical synthesis methods have been developed to reduce the crystallization temperature of YAG, by allowing the reactant cations (Y, Al) to mix intimately in the atomic level, which develops greater cation homogeneity in the precursor. The wet chemical methods include sol-gel processing, hydrothermal synthesis, glyco thermal method, co-precipitation, spray pyrolysis, microemulsion, and metal-organic preceramic processing are common practice in order to synthesize the YAG nanoparticles. Among these, co-precipitation is a promising technique for YAG nanoparticle synthesis because of greater possibility to prepare phase pure powder with good sinterability at low calcination temperatures, simple synthesis process, and more cost-effective [3-4].

Numerous literature works on YAG nanopowder synthesis demonstrated that calcination of the co-precipitated YAG powders is a common practice in this field to develop highly dense microstructure with minimal porosity by controlling the particle coarsening characteristics that mostly include the average particle size. J. Su et al. synthesized 40-100 nm sized YAG nanoparticles by calcining the co-precipitated precursor in the range of 800°C - 1000°C in air atmosphere [5]. In another study, ~500 nm sized YAG particles were developed by calcination at 1200°C in air [6]. It can be inferred from the above literature, the increase in the average size of the YAG nanoparticles with increasing particle calcination temperature suggests the growth or coarsening of particles under calcination. However, no substantial investigations have been reported on the particle coarsening kinetic behaviour as a function of calcination temperature and time.

The fundamentals of sintering science clearly elucidate that the average particle size, particle packing and density in the green state are the key factors that exert significant

influence on the evaluation of sintered density and microstructural development by controlling the sintering potential as well as densification rate. The predicted expression for the dependence of densification rate ($\in_p$) on the average particle size (G) for any stage of sintering can be expressed in the following general form [7].

$$\in_p = \frac{HD\Omega\emptyset^{(m+1)/2}}{G^m kT}(P_a + \Sigma) \qquad \ldots\ldots. (4.1)$$

where H is the numerical constant, D is the diffusion coefficient, Ω is the atomic volume of the rate controlling species, ϕ is the stress intensification factor, m is the particle size exponent, P_a is the externally applied pressure, Σ is the sintering stress, k is the Boltzmann constant, and T is the absolute temperature.

Zhou et al. studied the densification behaviour of CeO_2 powder with three different particle sizes in order to obtain highly dense sintered compacts. They have reported that the densification rate increases with the decrease of average particle size [8]. This observation supports the predicted expression (4.1) which states that the densification rate ($\in_p$) varies inversely with the average particle size (G) of the powder compact. In another study, Rahaman et al. agreed with the results of Zhou et al. and suggested that besides the average particle size, particle packing in the green body and green density have significant influence on the densification rate and subsequent sintering behaviour [9]. The observations of Rahaman et al. are good in agreement with the other relevant works.

In the field of YAG based ceramics, literature works strictly report the details including the average particle size obtained at the particular calcination conditions, sintered density, grain size, and often microstructural development with respect to sintering profile. J. G. Li et al. synthesized YAG nanopowders with an average particle size of 220 nm by calcination at 1300°C and these powders were densified to 81% of the theoretical density under atmospheric sintering at 1500°C [10]. In another study, 93.5% dense YAG ceramics were developed by sintering of calcined YAG nanoparticles with an average particle size of ~53 nm in air atmosphere and the particle calcination temperature was 1100°C [11]. R. Chaim et al. reported that spark

plasma sintering of the soft agglomerated YAG nanoparticles with an average particle size of ~50 nm are sintered to 90% relative density with a grain size of 600 nm under temperature and pressure of 1300°C and 100 MPa [12]. J. Li et al. have fabricated pure YAG ceramics over 99% relative density with a rain size of 8.5 µm by vacuum sintering of calcined YAG nanoparticles with an average particle size of 500 nm at 1730°C for 10 h. and the particle calcination conditions were 1200°C for 3 h [6]. In considerations of the above reported works, it is clear that there are no comprehensive studies available on the evaluation of sintered density and microstructural development in YAG ceramics as a function of particle calcination temperature, average particle size, and green state.

In this chapter, we report YAG nanoparticle coarsening behaviour and their kinetics as a function of particle calcination temperature and time by performing an extensive calcination study in the temperature range of 900°C - 1550°C for 1, 6, and 12h. in order to understand the substantial particle growth behaviour since particle growth is significant under longer calcination periods only. Further, we demonstrate how to optimize the average particle size of the coarsened powder in order to develop YAG ceramics of high dense microstructure with minimal porosity by investigating the combined effects of particle calcination temperature, average particle size, and green state on sintered density and microstructural evaluation. In addition, a qualitative hypothetical mechanism is discussed for YAG nano particle coarsening via Ostwald's ripening.

4.2 Experimental

4.2.1 Powder Synthesis and Coarsening

Phase pure YAG nanometric powders were synthesized according to the optimized process (Process 2) as described in the previous chapter. FESEM morphology of the as synthesized YAG nanopowder was presented in Fig. 4.1. The morphology clearly indicates that the particles are remarkably less agglomerated, nearly spherical in shape, fairly uniform and have an average particle size of ~40 nm.

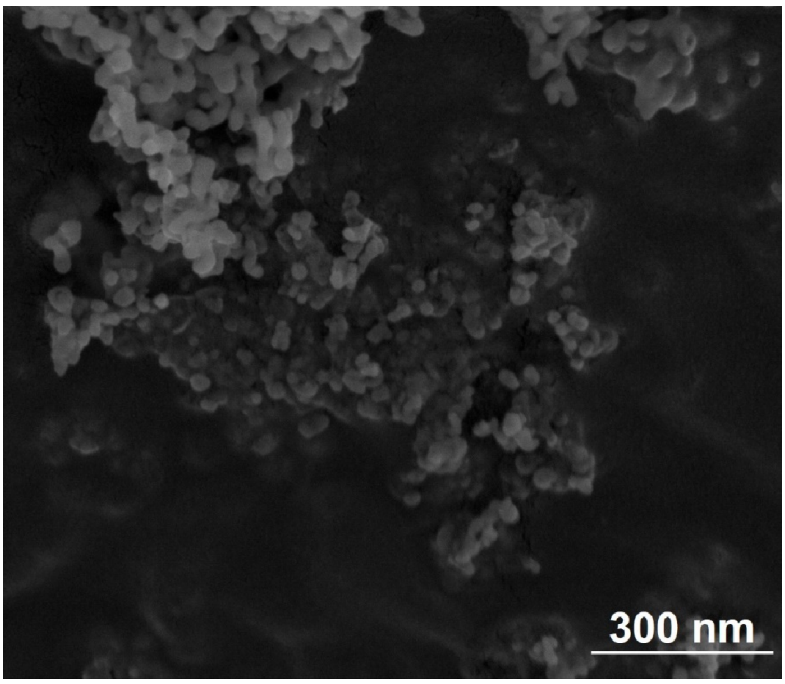

Figure 4.1: FESEM morphology of the as synthesized ~40 nm YAG nanopowder. This powder was recalcined at a temperature ranging from 900°C-1550°C for 1, 6 and 12 h. to perform the particle coarsening study.

The entire particle coarsening phenomenon was studied from the as synthesized ~ 40 nm YAG powder, by recalcining at a certain pre–determined time and temperature combination cycles, ranging from 900°C-1550°C for 1,6, and 12 h. A wide range of time – temperature profile has been selected in order to understand the particle coarsening behaviour.

4.2.2 Green Forming and Sintering

Green discs were prepared by thoroughly mixing the calcined YAG nanopowders with a binder (PVA, 3wt%) in an agate mortar followed by uniaxially pressing the mix at 400 MPa. Further, the powder compacts were sintered at a temperature of 1700 °C for 2 h. in an electrically heated furnace with Molybdenum disilicide ($MoSi_2$, also known as Kanthal Super) heating elements in the air atmosphere. The typical sintering profile has been illustrated in the Fig. 4.2. The heating rate of 5 °C per minute was maintained up to 1000 °C, 2 °C per minute was in between 1000 – 1500 °C and 1 °C per minute was in the range of 1500 – 1700 °C. Here in, isothermal sintering temperature for the densification study was chosen as 1700°C followed by

annealing at 1650°C in order to relieve the thermal stresses and modify the microstructural features that can be attributed to improvement in thermo-mechanical properties of YAG ceramics.

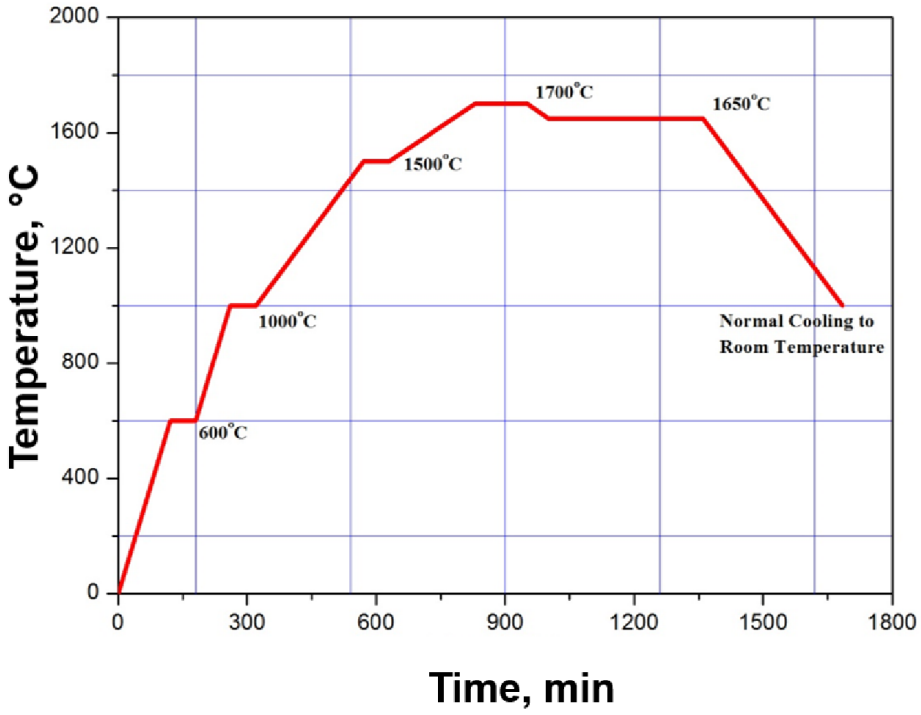

Figure 4.2: Sketch of a typical sintering cycle for YAG ceramics

4.2.3 Physical Characteristics of the Green and Sintered YAG Compacts

4.2.3A Green Density

Green density of YAG pellets was calculated from its geometric dimensions and weight by using following expressions:

$$Green\ Density\ = \frac{W_g}{V_g} = \frac{W_G}{\pi R^2 H} \qquad \ldots\ldots\ldots \quad (4.2)$$

$$\%\ Relative\ Green\ Density\ = \frac{Green\ Density}{Theoretical\ Density}\ X\ 100 \qquad \ldots\ldots (4.3)$$

Where,

W_G = Weight of the green disc (g)

V_G = Volume of the green disc (cc)

R = Radius of the green disc (cm)

H = Thickness of the green disc (cm)

Theoretical density of YAG = 4.55 g/cc [12]

4.2.3B Bulk Density and Apparent Porosity

The bulk density and apparent porosity of the sintered YAG samples were determined by using Archimedes' principle. The specimens were dried at a temperature of 110 °C for 2 h. to make the open pores free of moisture, weighed in the dried condition and noted as dry weight (D). The specimens were then soaked in boiling water for 2 h. until all the open pores were completely filled with water. After cooling, the suspended weights (S) and soaked weights (W) of the saturated specimens were measured. Bulk density and Apparent porosity of the sintered specimens were calculated from the following expressions.

$$Bulk\ Density = \frac{D}{(W-S)}\ X\ 100 \qquad \ldots\ldots\ldots \quad (4.4)$$

$$\%\ Apparent\ Porosity = \frac{(W-D)}{(W-S)}\ X\ 100 \qquad \ldots\ldots\ldots \quad (4.5)$$

$$\text{Relative Density (\%)} = \frac{\text{Bulk Density}}{\text{Theoretical Density}}\ X\ 100 \qquad \ldots\ldots\ldots \quad (4.6)$$

Where,

D = Dry weight of the specimens (g)

S = Suspended weight of the specimens (g)

W = Soaked weight of the specimens (g)

Theoretical density of YAG is 4.55 g/cc.

4.2.3C Shrinkage

Linear shrinkage ($\Delta D/D_o$) and Volume shrinkage ($\Delta V/V_o$) of the sintered compacts were determined from their physical dimensions to evaluate the shrinkage behaviour, and the corresponding expressions are stated below.

(i) Linear Shrinkage $\% LS = \frac{\Delta D}{D_o} X\ 100$ ..... (4.7)

(ii) Volume Shrinkage $\% VS = \frac{\Delta V}{V_o} X\ 100$ ..... (4.8)

Where, $\Delta D = D - D_o$; $\Delta V = V - V_o$;

D_o = Diameter of the green specimen (cm)

D = Diameter of the sintered specimen (cm)

V_o = Volume of the green specimen ($\pi D_o^2 H_o/4$, cm^3)

V = Volume of the sintered specimen ($\pi D^2 H/4$, cm^3)

H_o = Thickness of the green specimen (cm)

H = Thickness of the sintered specimen (cm).

4.2.4 Microstructure and Grain Phenomenon

Morphology of the coarsened powders, nature of particle packing in the unpolished green specimens obtained by compaction of coarsened powders, and microstructural characteristics of the sintered specimens were evaluated by the field emission scanning electron microscope (FESEM, NOVA NANOSEM FEI 450, Netherland). For microstructural characterization, the sintered specimens were ground sequentially on SiC abrasive pads having grit sizes of 800, 1000 and 1200 μm. These samples were then polished with 1 μm diamond paste to get a mirror finish. Further, the polished specimens were cleaned with acetone and thermally etched at 1550 °C for 30 minutes to reveal grain boundaries. The average grain size was measured from several hundred grains.

4.3 Results

4.3.1 Particle Coarsening and Green state

Figure 4.3 shows the coarsening behaviour of ~40 nm YAG particles which are calcined in the temperature regime of 900°C-1550°C for 1, 6, and 12 h. The particle coarsening or growth behaviour based on the slope of the curve in this regime can be classified into three different stages.

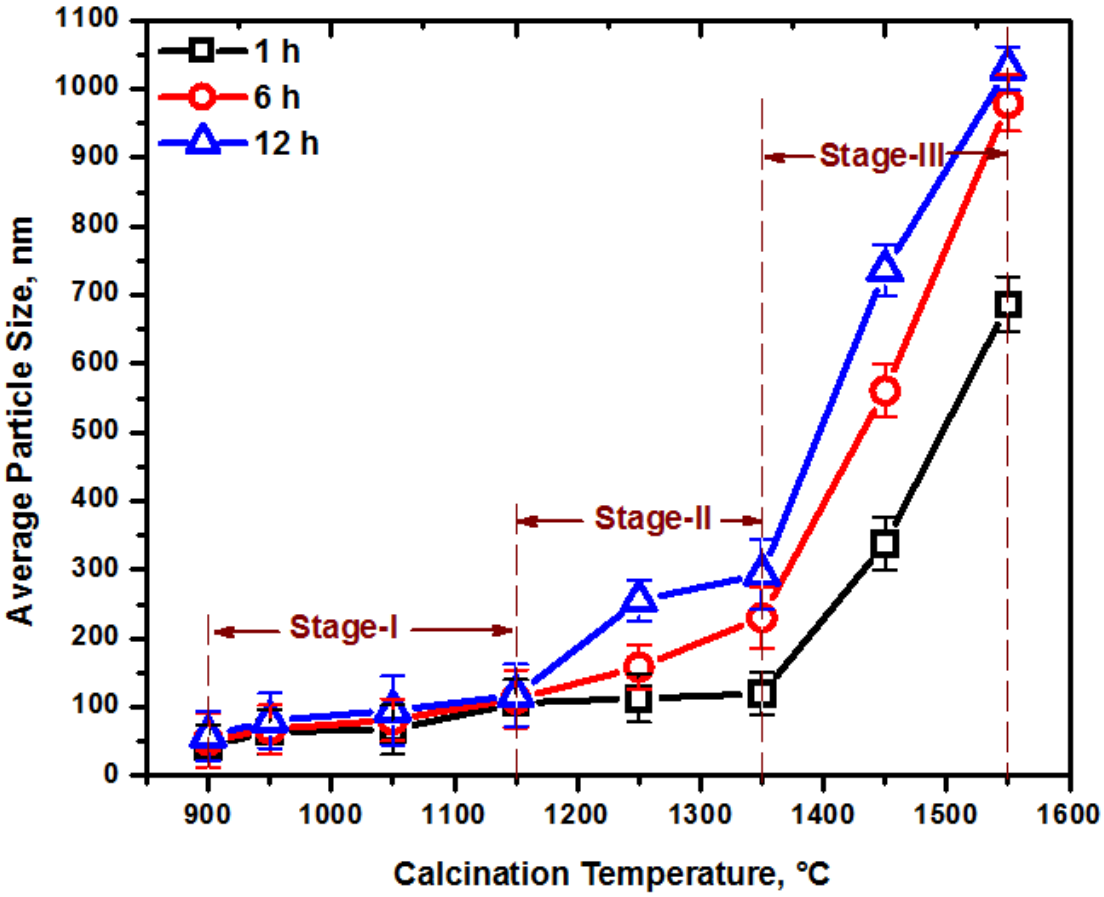

Figure 4.3: Influence of calcination temperature and time on the particle size of YAG nanocrystalline powders. Standard deviation indicates the predominant overlapping of same particle size in low temperature range up to 1150 °C.

They are

(i) Stage I - negligible coarsening up to 1150°C

(ii) Stage II - nearly steady state coarsening in between 1150°C and 1350°C

(iii) Stage III - accelerated coarsening in between 1350°C and 1550°C

So that the average particle sizes are almost equal for the powders which are obtained at calcination temperatures below 1150°C irrespective of the calcination time. However, a significant increase in the average particle size (0.1-1.0 μm) of the calcined powders at temperatures in the range between 1150°C and 1550°C is evidenced. Moreover, it is clearly noticed that the average particle size increases with increasing time of calcination over the range of 1-12 h. in this temperature profile. This observation signifies that calcination time have a remarkable effect on the particle growth relatively at higher calcination temperatures since particle growth kinetics are critically influenced by the temperature. The highest average particle size (~ 1μm) is obtained by the powders calcined at 1550°C for 12 h. in the entire study.

Figure 4.4 exhibits the morphology of YAG nanopowders obtained at different calcination temperatures between 900°C and 1550°C for 1, 6, and 12 h. respectively. It is clearly observed that at 900°C the garnet powders (Fig. 4.4a-c) constitute weakly agglomerated nano scaled particles with nearly spherical morphology and exhibit almost similar structure to that of the as synthesized powder (Fig. 4.1). The increase in calcination time at this temperature from 1 to 12 h doesn't have any profound effect on particle growth. With further increase of calcination temperature from 950°C-1150°C particles tend to grow by Ostwald ripening, however, the growth is observed to be insignificant in this regime (Fig. 4.4d-l). When the temperature is further raised to 1250°C (Fig. 4.4m-o) particle growth has become appreciable for all the time profiles, likely due to accelerated diffusion kinetics. Moreover, the growth process proceeds at a faster rate as further increase of temperature to 1350°C-1450°C (Fig. 4.4p-u) and particles develop an oblong morphology as the calcination time proceeds in this profile as similarly reported in earlier group of researchers [13]. Furthermore, a typical growth behaviour of particles is recognized for the powders calcined at 1550°C in the entire study. In reference to Fig. 4.4v-x, clearly demonstrates that the oblong shaped YAG particle tends to spheroidize themselves by reducing their contact surface area in order to attain the lowest possible free energy.

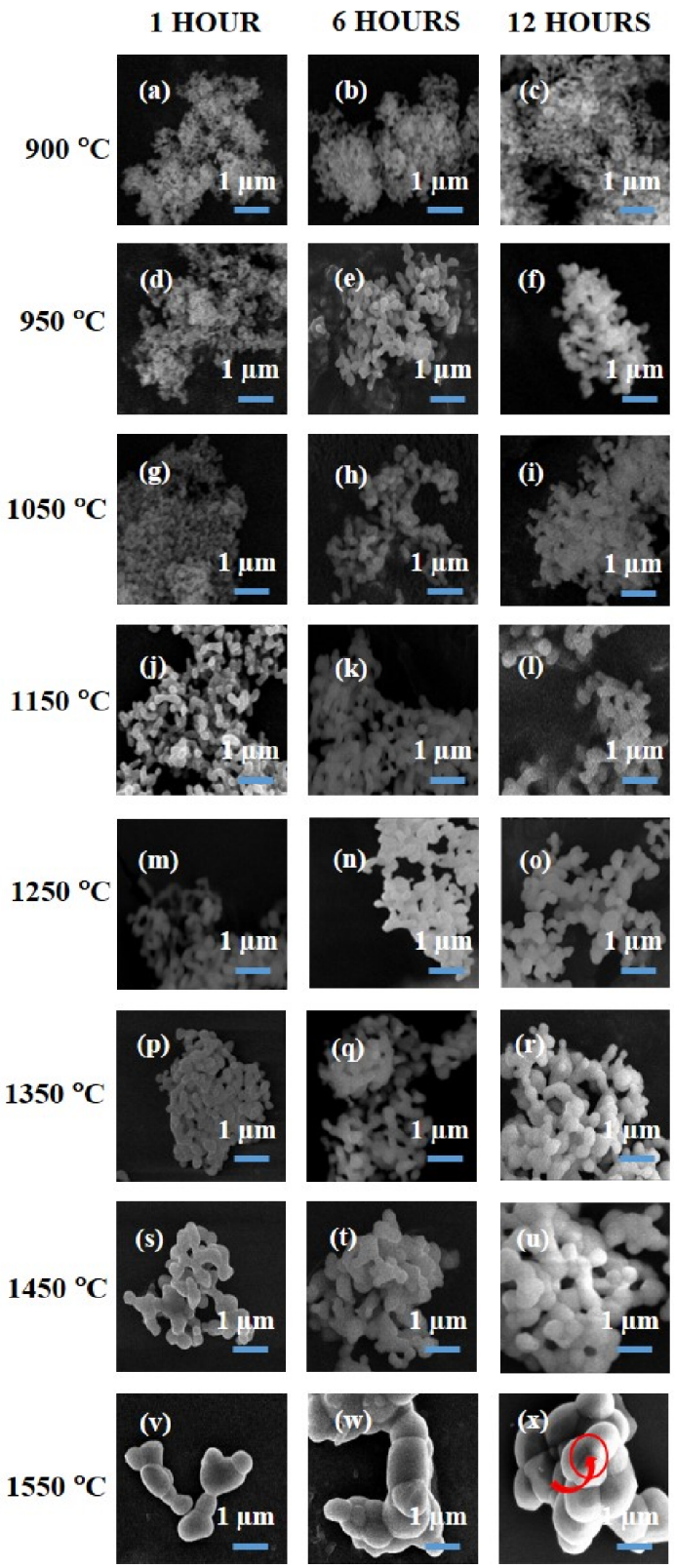

Figure 4.4: FESEM images representing the morphologies of YAG nano – powders calcined at different temperature and time profiles. A typical coarsening behaviour can be experienced for the 1550°C calcination profile.

The green specimens were prepared from the calcined particles and plotted their relative density as a function of calcination temperature (Fig. 4.5).

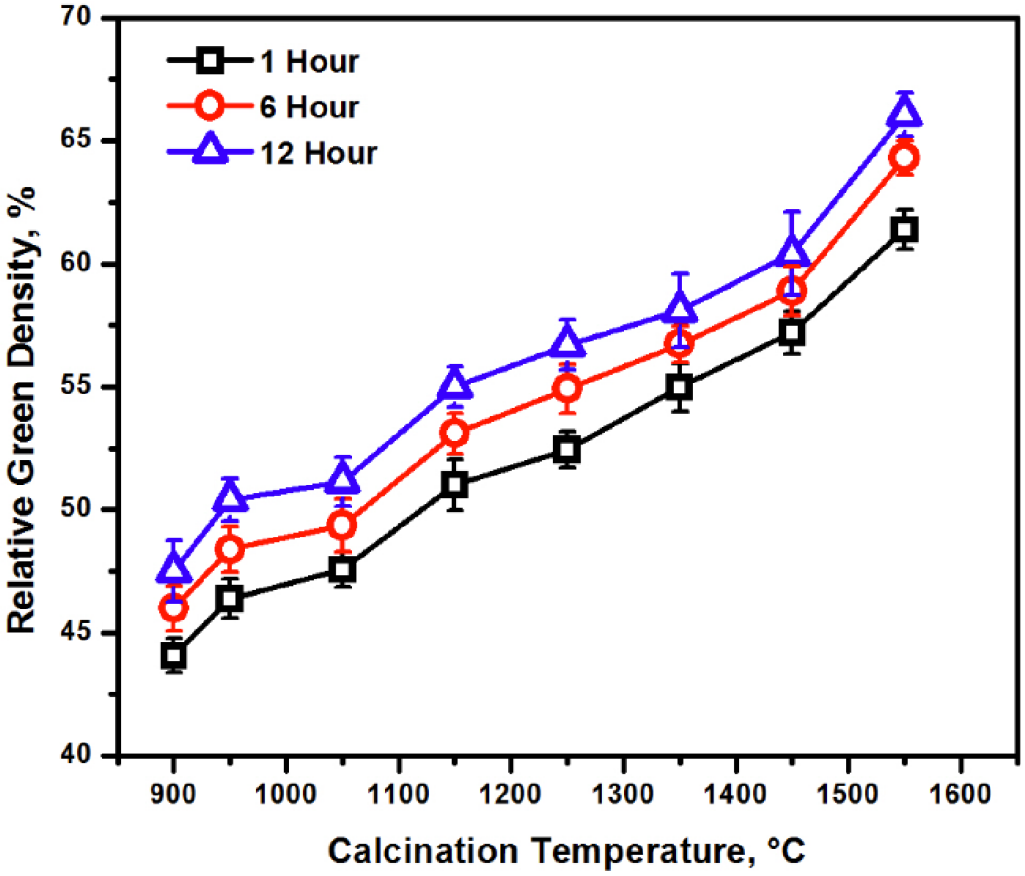

Figure 4.5: Relative density (%) of YAG green compacts as a function of calcination temperature and time. The increase in green density trend with respect to calcination profile exhibits the role of particle morphology on green state.

Herein, as-synthesized to calcined particle size varies in the range of 40-1000 nm as described in Fig. 4.4. A continuous increment in the green density is noticed with increasing temperature and time. This is due to the formation of densely packed structures in the green state with wider sized fractions actuated by the breaking down of agglomerated particles produced during calcination [14]. The powders which are calcined above 1150°C are compacted to a minimum of 50% green density and the highest (i.e. 66%) is obtained by the powders calcined at 1550°C for 12 h.

The YAG ceramics prepared from the as-synthesized powder calcined at 1350°C, 1450°C, and 1550°C for 12 h. constitute particle sizes and green densities of (~0.3 µm, ~55%), (~0.7 µm, ~60%), and (~1 µm, 66%), respectively. In order to

understand the influence of such particle size and green density, these three grades of YAG particles were considered for next sintering and densification study.

4.3.2 Sintering Behaviour of Coarsened Particles

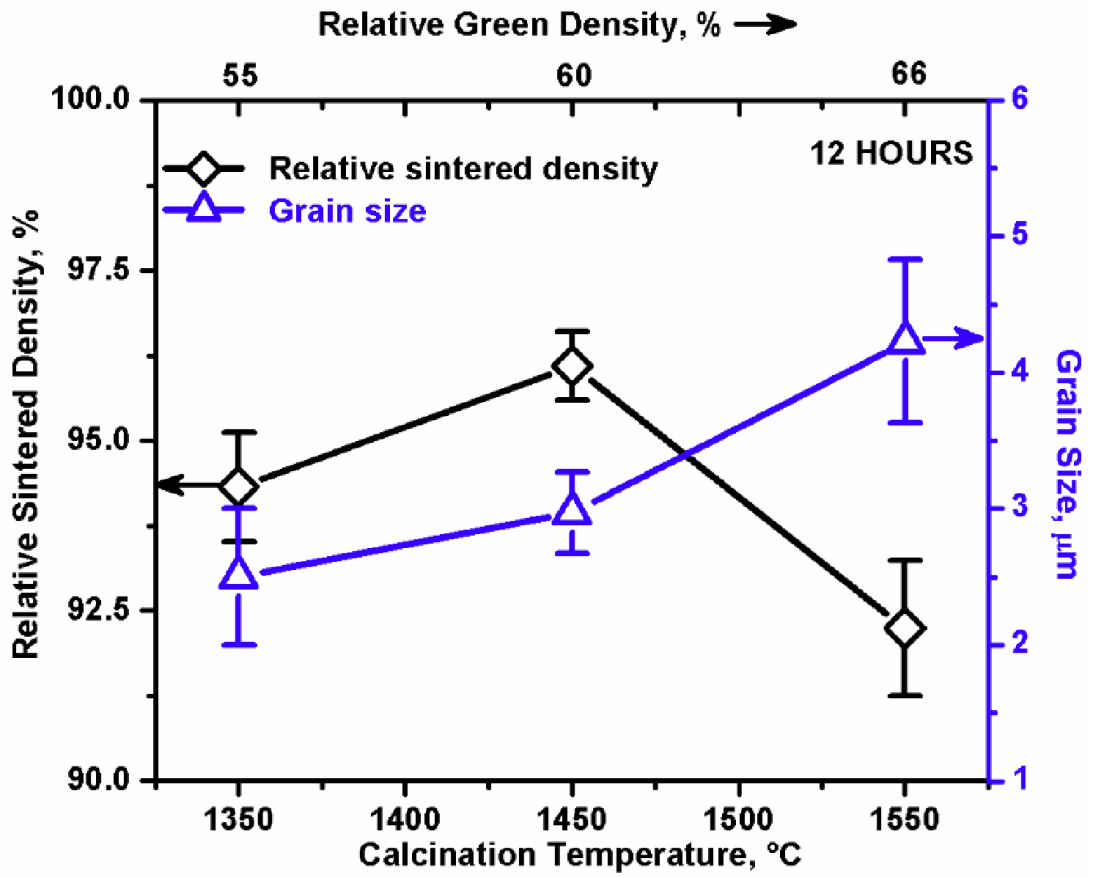

Figure 4.6: Densification behaviour and grain growth of pure YAG compacts sintered at 1700°C for 2 h. as a function of calcination temperature and time.

Fig. 4.6 shows the relative density and grain size of the selected YAG ceramics after sintering at 1700°C for 2 h. as a function of the calcination temperature. The sintered density increases rapidly from 94% to 96.1% with starting particle size of ~0.7 µm that obtained at 1450°C but it drops abruptly to 92% with further increase of calcination temperature to 1550°C with consist of particle size ~1.0 µm. But the grain growth trend increases with the increasing calcination temperature and the highest average grain size (i.e. ~4.2 µm) is obtained at 1550°C. However, the interplay among particle size, green state, and sintering behaviour of

the selected YAG ceramics is discussed in details at section 4.4. The sintered YAG ceramics fabricated from powders calcined at 1450°C for 12 h. have reached 96.1% relative density and ~ 3 micron grain size.

In order to explore the influence of average particle size and green density on the dimensional variation of selected green bodies during sintering at 1700°C for 2 h. the shrinkage data is plotted as a function of calcination temperature in Fig. 4.7.

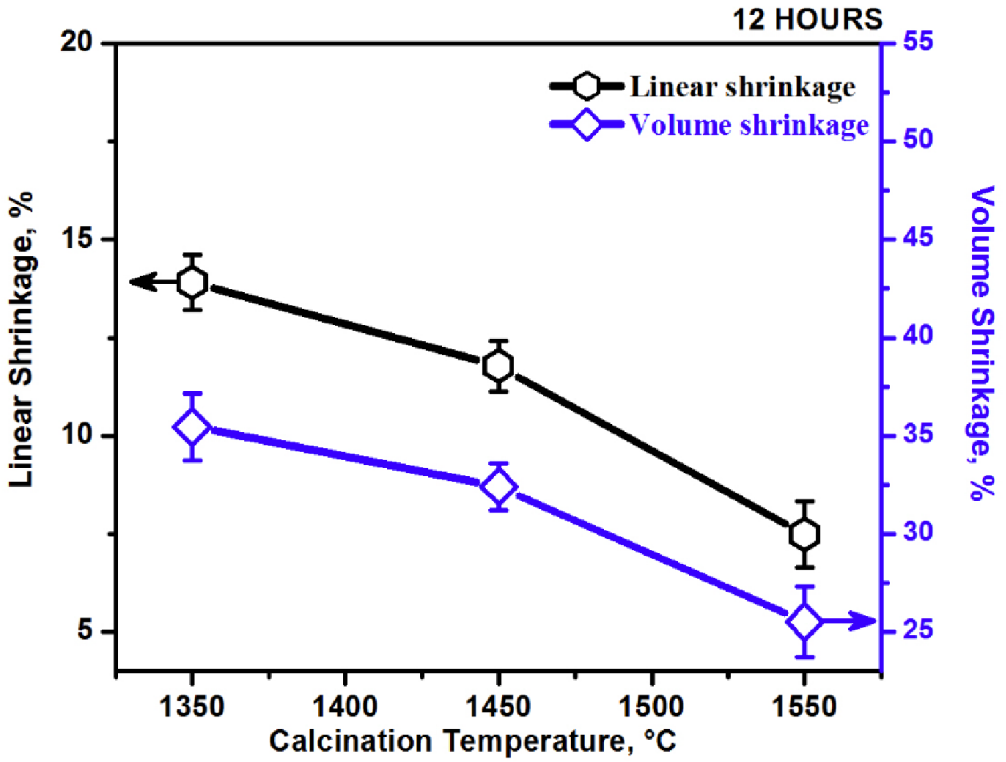

Figure 4.7: Variation in the linear and volume shrinkage of pure YAG specimens sintered at 1700ºC for 2 h. as a function of calcination temperature and time. Decrease in shrinkage plateau with respect to calcination temperature suggests the reduced particle diffusion kinetics.

The percent linear and volume shrinkages tend to decrease with increasing calcination temperature in the range of 1350°C-1550°C. The linear and volume shrinkages of sintered YAG ceramics prepared from powders calcined at 1450°C for 12 h. are found to be ~12%, and ~32%, respectively.

Fig. 4.8 shows the change of percent apparent porosity of selected YAG ceramics sintered at 1700°C for 2 h as a function of calcination temperature. It is observed that the percent open porosity after sintering tends to increase with the increase of

calcination temperature. The YAG ceramics fabricated from powders calcined at 1550°C for 12 h. have attained relatively larger open porosity (i.e. 3%).

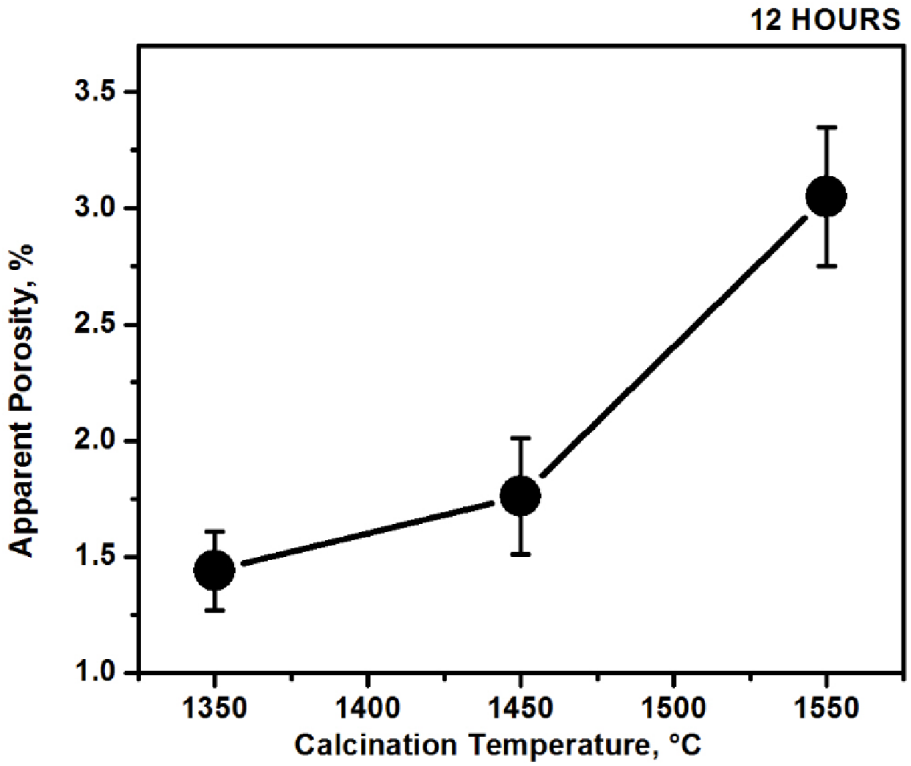

Figure 4.8: Apparent porosity of pure YAG compacts sintered at 1700 °C for 2 h. Deviation in the experimentally obtained porosity trend in reference to the theoretical studies demonstrate the distinct sintering behaviour of calcined particles.

Fig. 4.9 presents FESEM microstructures of the selected YAG ceramics sintered at 1700°C for 2 h. as a function of the calcination temperature. It is clearly observed that the development of distinct microstructures with the increase of calcination temperature although the increase in grain size is evidenced. The sintered microstructure (Fig. 4.11a) of YAG ceramics fabricated from powders calcined at 1350°C constitutes of finer sized grains with lots of pores distributed in non-uniform fashion. The average grain size in this sample is about ~2.5 micron. Subsequent increase of calcination temperature to 1450°C, the obtained sintered YAG yields a microstructure (Fig. 4.9b) of relatively dense packed grains with minimal porosity and the average grain size slightly increases to ~ 3 micron. With further increase of

calcination temperature to 1550°C, the resultant sintered microstructure (Fig. 4.11c) contains large and crack like voids between relatively denser regions, and the average grain size further increases to ~4.2 micron.

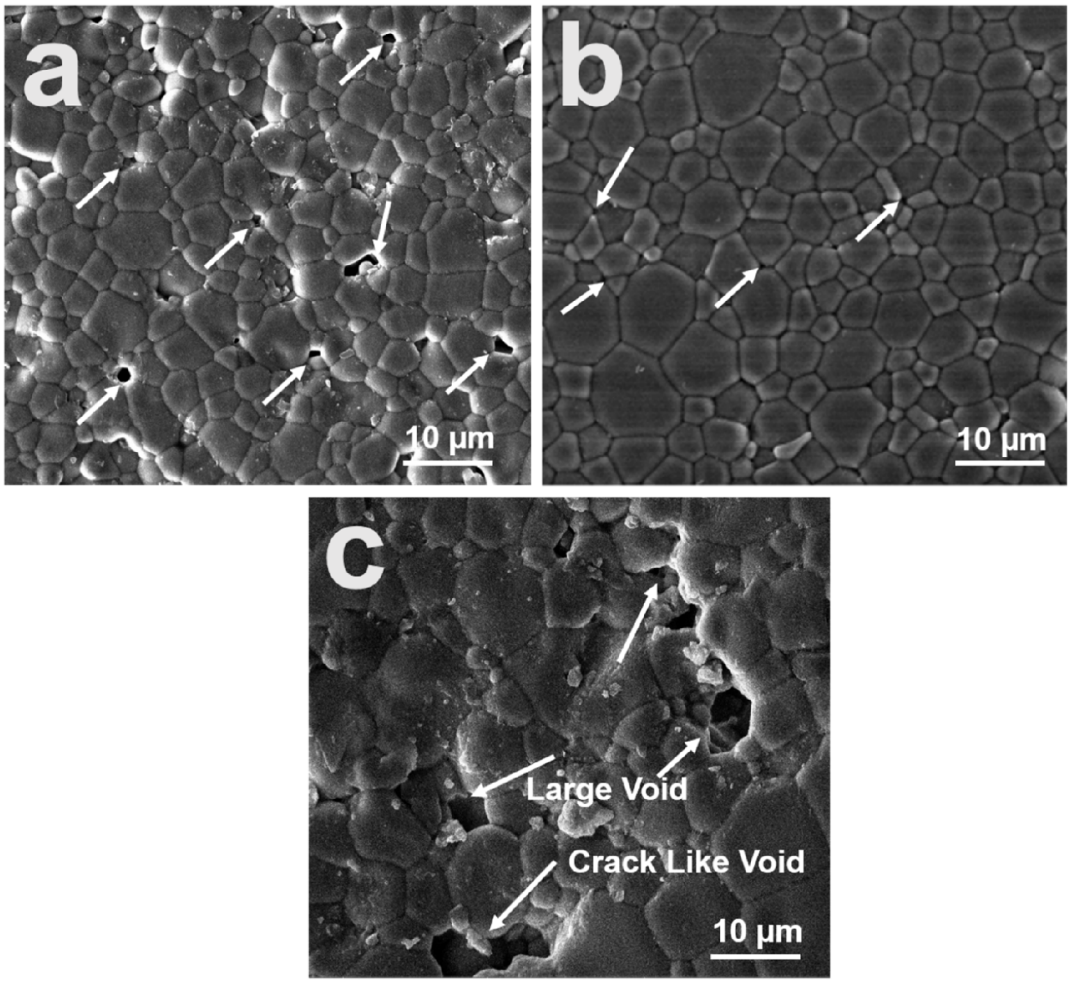

Figure 4.9: FESEM images indicating the microstructures of sintered YAG specimens (1700ºC for 2 h.) prepared from the YAG powders which were separately calcined for 12 h. at (a) 1350ºC, (b) 1450ºC, and (c) 1550ºC. Development of highly dense microstructure with minimal porosity and nearly uniform grain growth supports the good sinterability nature of powders calcined at 1450ºC.

4.4 Discussions

Calcination leads to particle coarsening that results in reduction in the total interfacial energy of the system. The coarsening process occurs via two primary mechanisms; known as 'Oriented attachment' and 'Ostwald's ripening' [15, 16]. The entire particle coarsening study is demonstrated by Ostwald's ripening mechanism that involves

coarsening of large particles at the expense of small particles in a particle system with different sizes and this process is driven by the chemical potential difference of atoms in large and small particles [16, 17]. Fig. 4.10 illustrates the qualitative mechanism for coarsening of particles of slightly different size in contact using a simple sphere – sphere model via Ostwald's ripening where the coarsening is assumed to be primarily controlled by the surface diffusion. The coarsening of YAG nanoparticles occurs via continuous operation of Ostwald's ripening mechanism under calcination and results in increase in the particle size with the increase of calcination temperature and time (Fig. 4.3).

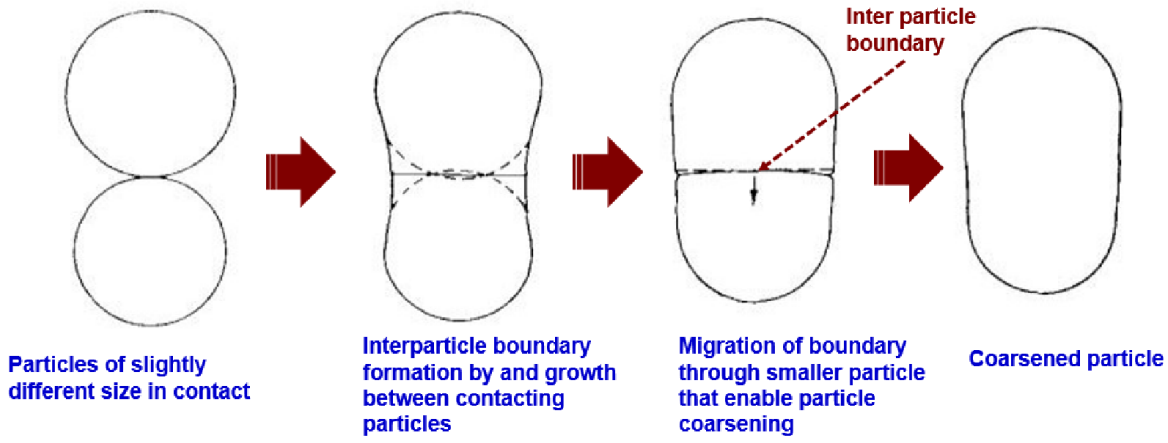

Figure 4.10: Qualitative mechanism for particle coarsening via Ostwald ripening demonstrated using a simple sphere – sphere model [17].

The fundamentals of sintering science clearly elucidate that the average particle size, particle packing and density in the green state are the key factors that exert significant influence on the evaluation of sintered density and microstructural development by controlling the sintering potential as well as densification rate [7].

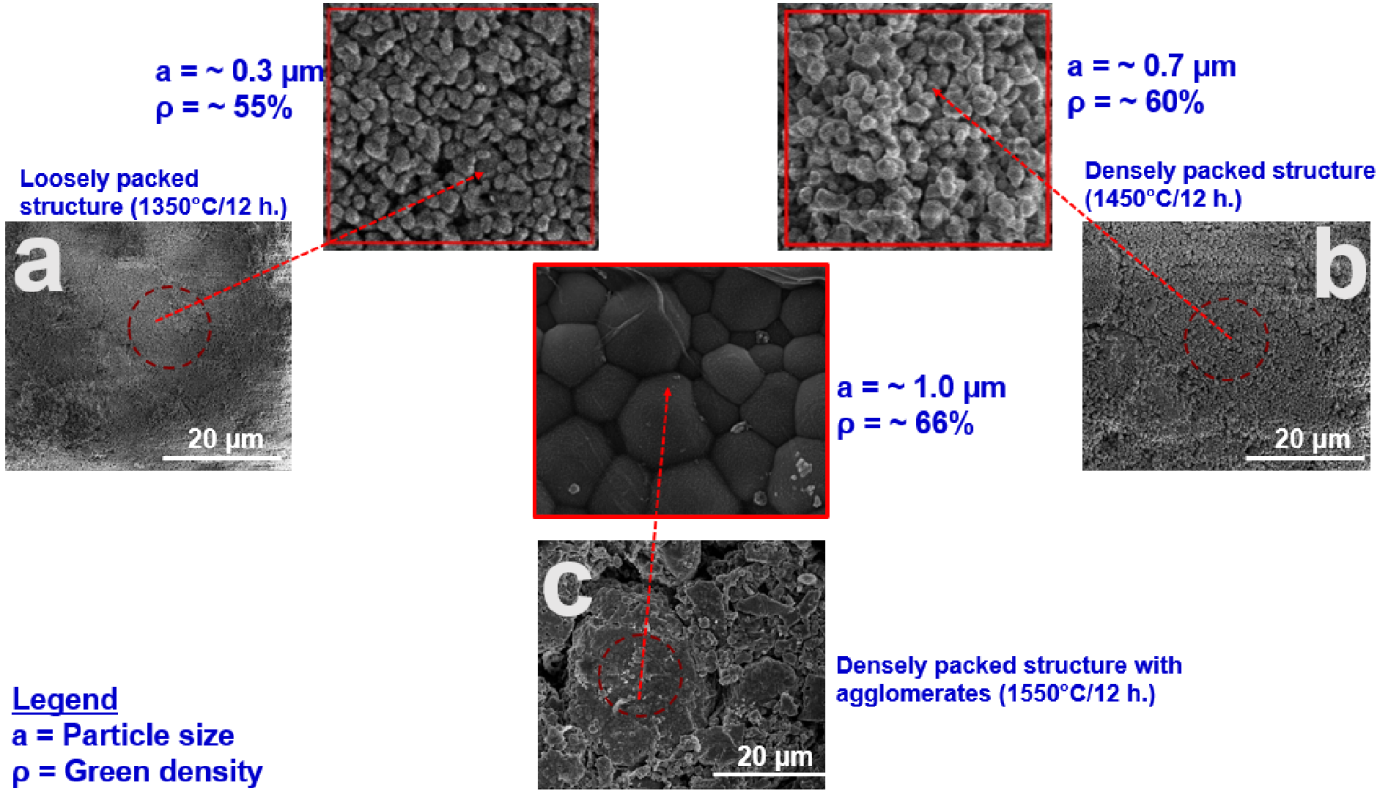

Figure 4.11: FESEM microstructures of the green bodies fabricated from the powders calcined at (a) 1350°C, (b) 1450°C, and (c) 1550°C for 12h.

The average particle size and green density of the selected YAG ceramics prepared from the powders calcined at 1350°C, 1450°C, and 1550°C for 12 h. are of (~0.3 µm, ~55%), (~0.7 µm, ~60%), and (~1 µm, ~66%), respectively. In accordance with the predicted expression (Eqn. 4.1), the powder compacts with finer particle size (~0.3 µm, 1350°C/12 h.) should have the highest densification rate, however, this system is densified to 94% of the theoretical density under sintering at 1700°C for 2 h. Based on the fundamental aspects of sintering kinetics [7], the compacts with highest green density (~ 66%, 1550°C/12 h.) supposed to have greater sintering potential (P) to attain highest sintered density that is actuated from the formation of more sintered necks and finer sized pores (r), however, this system (1550°C/12 h.) is densified to lowest sintered density (~92%). Interestingly, the powder compacts (1450°C/12 h.) with an average particle size (~0.7 µm) and green density (~ 60%) have attained the highest sintered density in the entire study emphasizing the significance of particle packing on the densification behaviour. Fig. 4.11 shows the FESEM green body microstructures of the selected YAG ceramics. The green microstructures of the specimens prepared from the powders calcined at 1350°C (Fig. 4.11a) and 1450°C (Fig. 4.11b) for 12 h. display loosely packed structure (~55%) of the finer sized particles (~0.3 µm) and densely packed structure (~60%) of the sub-micron sized particles (~0.7 µm). However, the green state of the specimens prepared from the powders calcined at 1550°C for 12 h. (Fig. 4.11c) exhibit densely packed structure (~66%) of coarser particles (~1.0 µm) besides hard agglomerates (inset). The presence of hard agglomerates in the green state (Fig. 4.11c, 1550°C/12 h.) reduce the sintering potential by triggering differential densification [18] results in lowest sintered density (~92%).

Based on the above experimental observations and theoretical arguments it can be clinched that the sintering of optimum coarsened particles (~0.7 µm) obtained under calcination of 1450°C for 12 h. develop highly dense microstructure (~96.1%) with fine grain size (~3 µm).

4.5 Conclusions

In consideration of the above stated experimental results the following conclusions have been drawn.

(i) Particle calcination temperature has a profound influence on the kinetics of coarsening, green state, and sintering behaviour of coarsened particles developed under calcination profile of 900°C-1550°C for 1, 6, and 12 h.

(ii) The average size of the YAG nanoparticles was found to be increased with increasing calcination temperature and time, but calcination time has profound effect on particle coarsening relatively at higher temperatures, since coarsening kinetics are critically influenced by the temperature.

(iii) The powders calcined at 1550°C for 12 h. exhibited lowest free energy state in the entire study that can be evidenced from the morphology and particle growth (~1 μm)

(iv) The green density of coarsened YAG nanoparticles was observed to be increased with the increase of calcination profile. This was primarily due to the formation of densely packed structures in the green state with wider sized fractions actuated by the breaking down of agglomerated powders produced by calcination.

(v) The presence of hard agglomerates in the green state (1550°C/12 h.) reduced the sintering potential by triggering differential densification that results in lowest sintered density.

(vi) Sintering of coarsened particles (~0.7 μm) obtained under calcination of 1450°C for 12 h. develop highly dense microstructure (~96.1%) with fine grain size (~3 μm) in the entire study which qualified the optimum particle size as ~0.7 μm.

References

1. T. Taira, Ceramic YAG lasers, Comptes Rendus Physique 8 (2007) 138-152
2. A. Ikesue, T.Kinoshita, Fabrication and optical properties of high performance polycrystalline Nd:YAG ceramics for solid-state lasers, J. Am. Ceram. Soc., 78 (1995) 1033-1040.
3. J. Vrolijk, J. Willems, R. Metselaar, Co-precipitation of yttrium and aluminium hydroxde for preparation of ytrium aluminium garnet, J. Eur. Ceram. Soc., 6 (1990) 47-53.
4. M. Zeng, Y. Ma, Y. Wang, C. Pei, The effect of precipitant on co-precipitation synthesis of yttrium aluminium garnet powders, Ceram. Int., 38 (2012) 6951-6956.
5. J. Su, Q. L. Zhang, C. J. Gu, D. L. Sun, Z. B. Wang, H. L. Qiu, A. H. Wang, S. T. Yin, Preparation and characterization of $Y_3Al_5\ O_{12}$ (YAG) nano-powder by co-precipitation method, Materials Research Bulletin, 40 (2005) 1279-1285.
6. J. Li, F. Chen, W. Liu, W. Zhang, L. Wang, Co-precipitation synthesis route to yttrium aluminum garnet (YAG) transparent ceramics, J. Eur. Ceram. Soc., 32 (2012) 2971-2979.
7. M. N. Rahaman, Ceramic processing and sintering, Marcel Dekker, New York, 1995.
8. Y. C. Zhou, M. N. Rahaman, Hydrothermal synthesis and sintering of ultra-fine CeO_2 powders, J. Mater. Res., 8 (1993) 1680-1686
9. M. N. Rahaman, Y. C. Zhou, Effect of dopants on the sintering of ulta-fine CeO_2 powder, J. Eur. Ceram. Soc., 15 (1995) 939-950.
10. J. G. Li, T. Ikegami, J. H. Lee, T. Mori, Y. Yajima, Co-precipitation synthesis and sintering of yttrium aluminum garnet (YAG) powders: The effect of precipitant, J. Eur. Ceram. Soc., 20 (2000) 2395-2405.
11. D. L. Mandujano, J. Z. Medina, R. M. Estrella, J. M. Saldaña, Synthesis and mechanical characterization by nano indentation of polycrystalline YAG with Eu and Nd additions. Ceram. Int., 39 (2013) 3141–3149.
12. R. Chaim, R. Marder-Jaeckel , J.Z. Shen., Transparent YAG ceramics by surface softening of nanoparticles in spark plasma sintering. Mater. Sci. Eng. A, 429 (2006) 74–78.
13. B. Liu, J. Li, R. Yavetskiy, M. Ivanov, Y. Zeng, T. Xie, H. Kou, S. Zhuo, Y. Pan, J. Guo, Fabrication of YAG transparent ceramics using carbonate precipitated yttria powder, J. Eur. Ceram. Soc., 35 (2015) 2379-2390.
14. R. Fedyk, D. Hreniak, W. Lojkowski, W. Strek, H. Matysiak, E. Grzanka, S. Gierlotka, P. Mazur, Method of preparation and structural properties of transparent YAG nanoceramics. Opt. Mater., 29 (2007) 1252–1257.
15. J. Qin, R. Yang, G. Liu, M. Li, Y. Shi, Grain growth and microstructural evolution of yttrium aluminum garnet nanocrystallites during calcination process, Mater. Res. Bull., 45 (2010) 1426-1432.
16. J. Pan, H. Le, S. Kucherenko, J. A. Yeomans, A model for the sintering of spherical particles of different sizes by solid state diffusion, Acta Mater., 46 (1998) 4671-4690.
17. C. Greskovich, K. W. Lay, Grain growth in very porous Al_2O_3 compacts. J. Am.Ceram. Soc., 55 (1972) 142.
18. F. F. Lange, Powder processing science and technology for increased reliability. J. Am. Ceram. Soc., 72 (1989) 3-15.

Chapter 5

Optimization and Properties of Silica Doped Nd:YAG Ceramics

5.1 Introduction

Yttrium aluminum garnet (YAG, $Y_3Al_5O_{12}$) is an oxide material and it has been established as a potential solid state laser gain media which can be attributed to its several attractive properties that include high temperature strength, large thermal conductivity, and optically isotropic nature [1-2]. To produce laser effect, the solid state laser materials are usually doped with rare earth ions such as Nd^{+3}, Eu^{+3}, and Yb^{+3}. Among these, Nd^{+3} ion has earned considerable interest due to a number of beneficial features such as: (i) charge compensation is not required because Nd^{+3} ion substitutes for Y^{+3} ion in the host lattice, (ii) They are known to exhibit narrow fluorescence line width and satisfactory long fluorescence life time in crystals with ordered structures, (iii) ability to generate lasing action under either continuous wave mode (CW) or pulse mode, and (iv) ability to exhibit high laser slope efficiency similar to single crystals [3-5]. So, Nd:YAG ceramics are the most studied materials for high energy laser applications.

Nd:YAG single crystals which are commercially fabricated by the conventional Czochralski melt grown method have been the most widely used solid state laser gain media for the last four decades [6-7]. Recently, polycrystalline Nd:YAG ceramics have qualified as a promising substitute for conventional single crystal technology which can be ascribed to the following prominent benefits that include: (i) high rare earth ion doping concentration without concentration quenching, (ii) possibility to fabricate big sized laser devices with the near net shapes, (iii) enhanced thermo-mechanical properties, and (iv) high laser power output [8-10]. Numerous studies reported that highly dense Nd:YAG ceramics are commercially fabricated via two different approaches. They are solid-state

reaction (SSR) and sintering of co-precipitated Nd:YAG powders[11-12]. However, there are no comprehensive studies are available on the fabrication of highly dense Nd:YAG ceramics via coarsening of co-precipitated particles followed by pressureless sintering.

Optical transparency is the prime requisite characteristic of a laser ceramic material. The most common scattering sites in the laser ceramics are residual porosity (either inter or intra granular), grain boundary thickness, grain boundary with secondary phases, and birefringence. Of these, residual porosity is the most significant factor for transparency. Thus, a limiting condition to obtain transparency in ceramics is sintering to full density, i.e., eliminating all of the residual porosity in the material. This limiting condition enables to use considerable additions of SiO_2 as a sintering aid in the form of tetraethyl orthosilicate (TEOS) and this has become common practice in this field to obtain fully dense YAG based ceramics at lower sintering temperatures [13-15].

S. Bhattacharya et al. studied the sintering behaviour in 0-2500 ppm SiO_2 doped YAG ceramics. They found that sintered density increases with increasing SiO_2 content and 93% dense silica doped YAG ceramics are obtained by pressureless sintering at 1650˚C [16]. B. Liu et al. and co-workers reported that 5000 ppm SiO_2 doped co-precipitated YAG powders are sintered to 95% relative density with a grain size of 2 μm under vacuum at 1600˚C [17]. M. Suraez et al. fabricated 1 at.% Nd:YAG ceramics with 93% density by pressureless sintering of co-precipitated powders at 1650˚C [18]. H. Yihua et al. developed 2000 ppm SiO_2 doped Nd:YAG ceramics with a relative density of 94% by solid-state reactive sintering at 1550˚C in oxygen atmosphere [19]. Nd:YAG ceramics doped with 5000 ppm SiO_2 are sintered to 97% density with a grain size of 5 μm under vacuum at 1750˚C [20]. J. Li et al. fabricated 1400 ppm SiO_2 doped 1.0at.% Nd:YAG ceramics with 97% density and grain size of 7 μm under vacuum sintering of solid-state powders at 1700˚C [21]. In another study, 1400 ppm SiO_2 doped YAG and 5 at.% Nd:YAG ceramics were prepared with a relative density of 95% and 98%, respectively, under vacuum sintering of solid-state powders at 1550˚C [22]. However, there are no literature works which have provided definite paths to optimize SiO_2 and Nd proportions in order to fabricate highly dense SiO_2 doped Nd:YAG ceramics.

Several research investigations have reported that a distinct behaviour of SiO_2 on densification and microstructural development is observed in YAG and Nd:YAG ceramics fabricated by different approaches. Kochatwana et al. studied densification and grain growth kinetics in 0-2800 ppm SiO_2 doped YAG and Nd:YAG ceramics fabricated via solid state reaction. They found that the grain size increases with the increase of SiO_2 proportion in both systems [23]. These observations are well in agreement with the results obtained by Ikesue et al [24]. However, in contrast, relevant research investigations reported that the grain size decreases with the increase of SiO_2 content in YAG based ceramics developed by sintering of sol-gel derived powders [25-26]. In consideration of the earlier investigations, it is obvious that the state of knowledge regarding the role of SiO_2 on densification and microstructural development of both YAG and Nd:YAG systems is not clear.

Besides the importance of microstructural features in connection to density aspects of Nd:YAG, the mechanical and thermal properties are very much crucial to ensure structural reliability under mechanical and thermal loads during lasing action. Therefore, it is imperative to measure the fundamental mechanical properties that include hardness and flexural strength that will control the overall mechanical reliability. The measurement of thermal properties that include thermal expansion coefficient and different thermal shock resistance parameters provide valuable information about fracture resistance of the laser material under thermal load caused by induced thermal gradients during lasing action [27-28].

In this chapter, a novel fabrication approach has been adopted to develop highly dense optimum SiO_2 doped Nd:YAG ceramics by careful optimization of SiO_2 and Nd concentration and pressureless sintering in detail. Further, we elucidate the role of SiO_2 in densification and microstructural development of both YAG and Nd:YAG systems. Furthermore, mechanical, thermal, and optical properties of the optimized Nd:YAG ceramics are determined and compared with the existing literature.

5.2 Experimental

5.2.1 Powder Source

The optimized YAG nanopowder with an average particle size of ~0.7 µm obtained under atmospheric calcination at 1450°C for 12h. was used for the fabrication of SiO_2 doped YAG and Nd:YAG ceramics. The morphological features of the optimum powder are shown in Fig. 5.1.

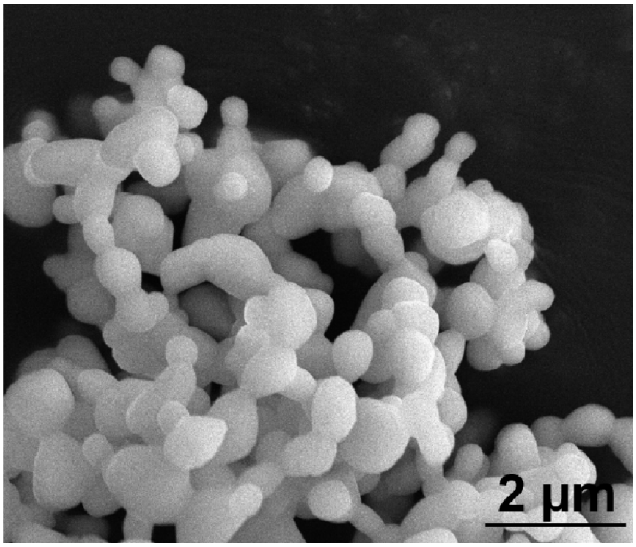

Figure 5.1: FESEM image representing morphology of the optimized YAG nanopowder with an average particle size of ~0.7 µm.

5.2.2 Green Forming and Sintering

5.2.2A Fabrication of SiO_2 doped YAG Ceramics

SiO_2 doped YAG green compacts containing 0, 1000, and 2000 ppm of SiO_2 were prepared by thoroughly mixing the optimized YAG nanopowder with binder (PVA, 3 wt.%) and Tetraethyl orthosilicate (TEOS) in an agate mortar and dried at 70°C followed by uniaxially pressing the mix at 400 MPa and sintering at 1700°C for 2 h. in air atmosphere. The process flowchart is represented in Fig. 5.2a. Tetra ethyl orthosilicate (TEOS) was used as the SiO_2 source and it was added in stoichiometric proportions in order to obtain the required concentration of SiO_2 (0-2000 ppm) in YAG ceramics.

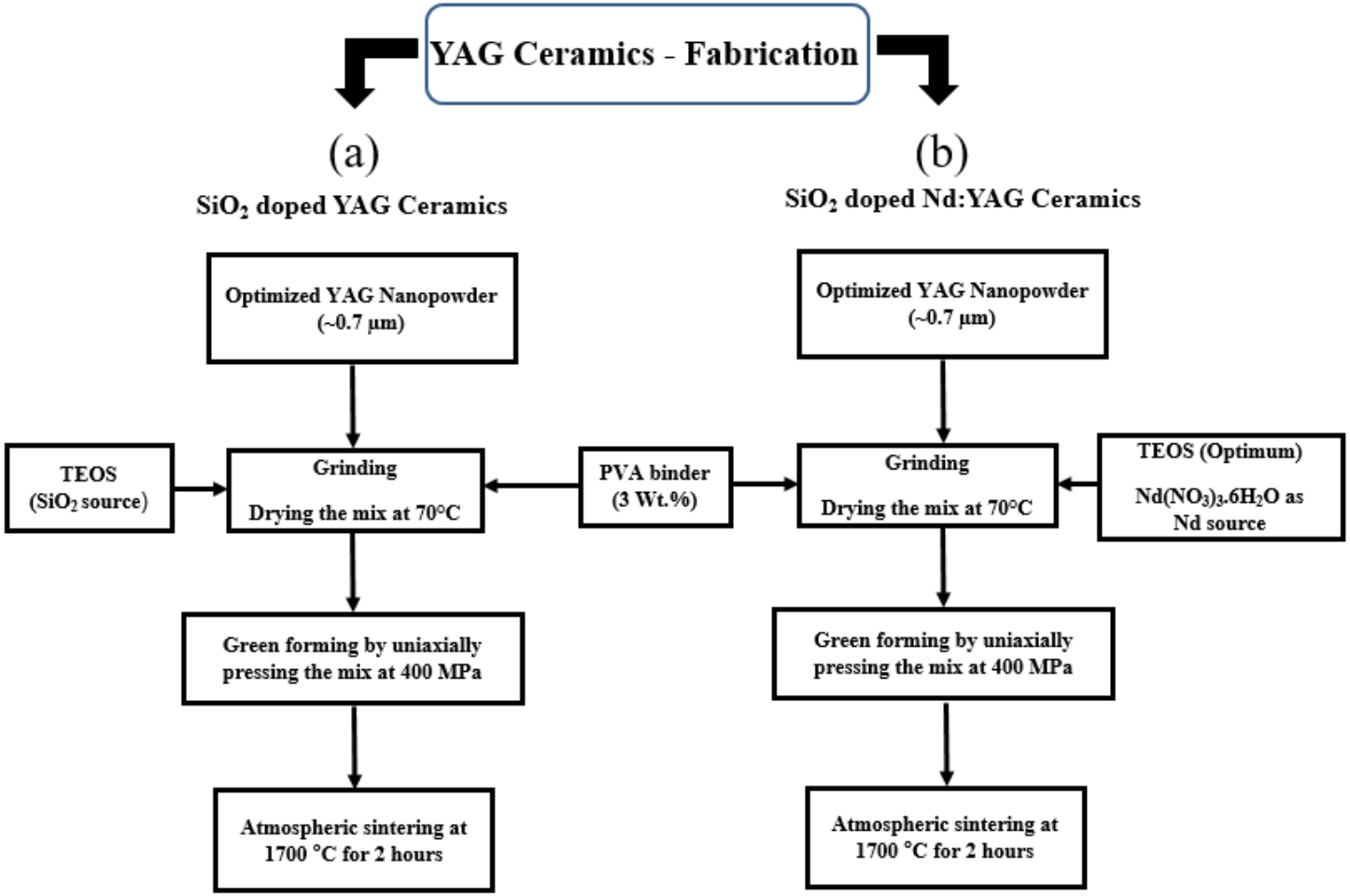

Figure 5.2: Process flow chart illustrating fabrication of (a) SiO_2 doped YAG ceramics and (b) SiO_2 doped Nd:YAG ceramics.

Further, the optimum SiO_2 concentration was chosen based on the obtained sintering study and used for the fabrication of Nd:YAG ceramics.

5.2.2B Fabrication of SiO_2 doped Nd:YAG Ceramics

SiO_2 doped Nd:YAG green compacts containing 0, 0.5, 1.0, 1.5, and 2.0 at.% of Nd were prepared by thoroughly wet mixing the optimized YAG nanopowder with binder (PVA, 3 wt.%), TEOS, and Neodymium nitrate hexahydrate ($Nd(NO_3)_3.6H_2O$) in an agate mortar and drying the mix in oven at 70°C followed by uniaxially pressing the mix at 400 MPa and sintering at 1700°C for 2 h. in air atmosphere. Tetraethyl orthosilicate (TEOS) was used as the SiO_2 source, Neodymium nitrate hexahydrate was used as the Nd source and they were added in stoichiometric proportions in order to obtain the required concentration of SiO_2 (1000 ppm) and Nd (0-1.5 at.%) in YAG ceramics. Further, the optimum concentration of Nd was selected and evaluated the mechanical, thermal, and optical properties of the optimized Nd:YAG ceramics.

5.2.3 Physical Characteristics of the Green and Sintered Ceramics

The green density, shrinkage, sintered density, and porosity of the SiO_2 doped YAG and Nd:YAG ceramics were determined according the similar methodology reported in Chapter 4 at section 4.2.3. However, theoretical density of the silica doped Nd:YAG (ρ) ceramics was calculated according to the following expression [29].

$$\rho = \frac{(\text{Effective number of atoms per unit cell x atomic weight})}{(\text{Lattice parameter})^3} \quad \ldots\ldots\ldots (5.1)$$

5.2.4 Microstructural Characterization

Microstructural features and distribution of SiO_2 and Nd in sintered YAG ceramics were evaluated by using field emission scanning electron microscopy (FESEM, NOVA NANOSEM FEI 450, Netherland). For microstructural characterization, the sintered

specimens were ground sequentially on SiC abrasive pads having grit sizes of 800, 1000 and 1200 μm. These samples were then polished with 1 μm diamond paste to get a mirror finish. Further, the polished specimens were cleaned with acetone and thermally etched at 1550 °C for 30 minutes to reveal the grain boundaries. The average grain size was measured from several hundred grains. The EDX analysis has been performed to study the distribution of SiO_2 and Nd in the sintered YAG ceramics.

5.2.5 Phase Analysis by XRD

X-ray diffraction (Rigaku (Japan) Ultima-IV X-Ray Diffractometer) measurements were performed at room temperature using nickel filtered Cu Kα radiation (1.5418 °A) as a source to investigate the phase, crystal structure, and lattice parameter of the SiO_2 doped YAG and Nd:YAG sintered discs. The scattering angle (2θ) for all data ranged from 20° to 50° with 0.05° step size at a scanning rate of 20° per minute. The obtained experimental XRD results were analysed with the standard X-ray powder diffraction database (JCPDS – Joint Committee on Powder Diffraction Standards) to investigate the phase purity.

5.2.6 Mechanical, Thermal, and Optical Properties Evaluation

5.2.6A Hardness Measurement

Hardness is nothing but a characteristic of a material which can be defined as the resistance to indentation. The hardness of the materials were determined by measuring diagonal lengths of the indentation produced under the given load by a diamond indenter. For hardness measurement, specimens were primarily ground with SiC abrasive pads having grit sizes of 800, 1000 and 1200 μm. These samples were then polished with 1 μm diamond paste to get a mirror finish. The polished flawless specimens were cleaned ultrasonically in acetone and thermally etched at 1550°C for 30 min in air. Hardness of the optimized Nd:YAG specimens were then determined by Vicker's hardness method using a Vickers Semi- Micro Hardness Tester (Leco, Japan), under load of 20 N for 15 seconds. The Vicker's hardness (H_V) values were determined by using the following equation:

$$H_V = \frac{1.8544\,P}{d^2} \qquad \ldots\ldots\ldots\ldots\ldots\ldots (5.2)$$

Where,

P = Applied load (N)

d = Mean diagonal length (mm), obtained as the average of the two diagonal lengths.

5.2.6B Flexural Strength Measurement

The flexural strength or bend strength is one of the crucial design aspects of structural ceramics, and it can be defined as the ability of a material (either bar or slab) to resist failure under bending stress. In this, a bar specimen is placed on two parallel supporting pins and the middle portion of the specimen is subjected to load with the aid of a loading pin, until the specimen fractures. The flexural strength of the samples can be calculated from the fracture load and the dimensions of the test samples.

The flexural strength of optimized Nd:YAG ceramics (3 mm x 4 mm x 35 mm) was determined by performing the standard 3-point bending test in a universal testing machine (Instron Universal Testing Machine Model No.1195) with a span length and cross head speed of 30 mm and 0.5 mm/min, respectively. The edges were polished prior to the examination. The following expression was used to determine the flexure strength (σ)

$$\sigma = \frac{3LP}{2bd^2} \qquad \ldots\ldots\ldots\ldots\ldots\ldots\ldots\ldots\ldots (5.3)$$

Where, L = length of the specimen (mm), P = Fracture load (N), b = width of the specimen (mm), and d = thickness of the specimen (mm).

5.2.6C Linear Thermal Expansion Coefficient Measurement

Thermal expansion coefficient measurements of the optimized Nd:YAG sintered ceramics were conducted using a dilatometer (Netzsch DIL 402C) in the temperature range of 30°C to 1000°C at a heating rate of 5°C/min, and the sample dimension used was 3 mm x 4 mm x 15 mm.

5.2.6D Thermal Shock Resistance Parameter Measurement

Thermal shock resistance refers to the ability of a material to resist failure under thermal stresses. Two different thermal shock resistance parameters (R_1 and R_2) of the optimized Nd:YAG ceramics (3 mm x 4 mm x 35 mm) were determined in the temperature range of room temperature to 1000°C by using the following expressions [27].

$$R_1 = \frac{\sigma(1-\nu)}{\alpha E} \qquad \ldots\ldots\ldots (5.4)$$

$$R_2 = \frac{\sigma(1-\nu)k}{\alpha E} \qquad \ldots\ldots\ldots (5.5)$$

Where,

R_1 = Resistance to fracture initiation under maximum ΔT allowable for steady state heat flow,
R_2 = Resistance to fracture initiation under maximum heat flux allowable for steady state flow,
σ = Flexural strength of the thermal shocked specimen, ~187 MPa.
ν = Poission's ratio.
α = Coefficient of thermal expansion, 9.124 x 10^{-6}/°C.
k = Thermal conductivity, 10.7 W/m.K. [27]
E= Modulus of elasticity, 280 GPa [27]

Modulus of elasticity (E) and thermal conductivity (k) of highly dense Nd:YAG ceramics reported in literature [27] were considered as the representative values to determine thermal shock resistance parameters.

5.2.6E Optical Transmittance Measurement

The optical transmission for a laser proficiency material is very much crucial because the lasing action takes place in the infrared range (1064 nm) whereas optical energy absorption occurs in the visible region (532 nm). For transmittance measurements, the optimized Nd:YAG specimens were ground to 1.9 mm thickness with SiC abrasive pads having grit sizes of 800, 1000 and 1200 μm, followed by polishing both of the surfaces

using 1 μm diamond paste to get a mirror finish. The mirror - polished specimens were ultrasonically cleaned and thermally etched at 1550°C for 30 min. The optical transmittance tests were performed on both mirror polished surfaces using a UV-VIS-NIR spectrophotometer (Cary 5000, Varian lnc. US) in the range of 200-1100 nm. The in-line transmittance of the optimized specimen was determined from the spectrophotometric data by plotting the in-line transmittance as a function of wavelength of the radiation [21].

5.3 Results and Discussions

5.3.1 Optimization of SiO_2 Concentration in the SiO_2 doped YAG Ceramics

Fig. 5.3 shows the XRD pattern of 0, 1000, and 2000 ppm SiO_2 doped YAG ceramics sintered at 1700°C for 2 h. as a function of SiO_2 concentration. The YAG ceramics containing 0 ppm SiO_2 represent strong cubic diffraction pattern of pure garnet phase (JCPDS 82-0575).

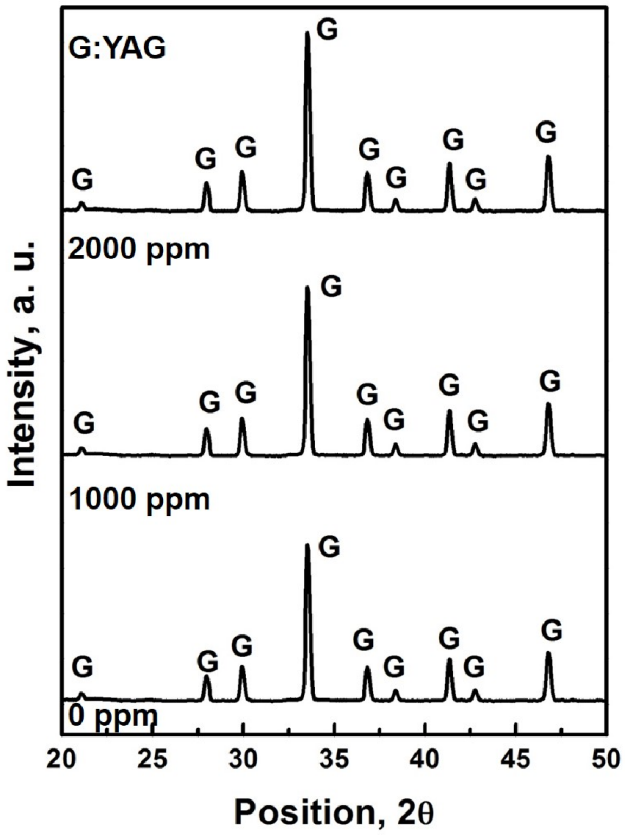

Figure 5.3: XRD patterns of the SiO_2 doped YAG ceramics sintered at 1700°C for 2h. The SiO_2 concentrations are in the range of 0 – 2000 ppm.

The XRD observations clearly revealed that there are no other SiO_2 rich secondary phases detected with the further increase of SiO_2 concentration to 1000 and 2000 ppm in YAG ceramics, respectively. These results are in agreement with observations of Stevenson et al. [30].

Fig. 5.4 presents the densification and grain growth behaviour in 0, 1000, and 2000 ppm SiO_2 doped YAG ceramics sintered at 1700°C for 2 h. as a function of SiO_2 concentration.

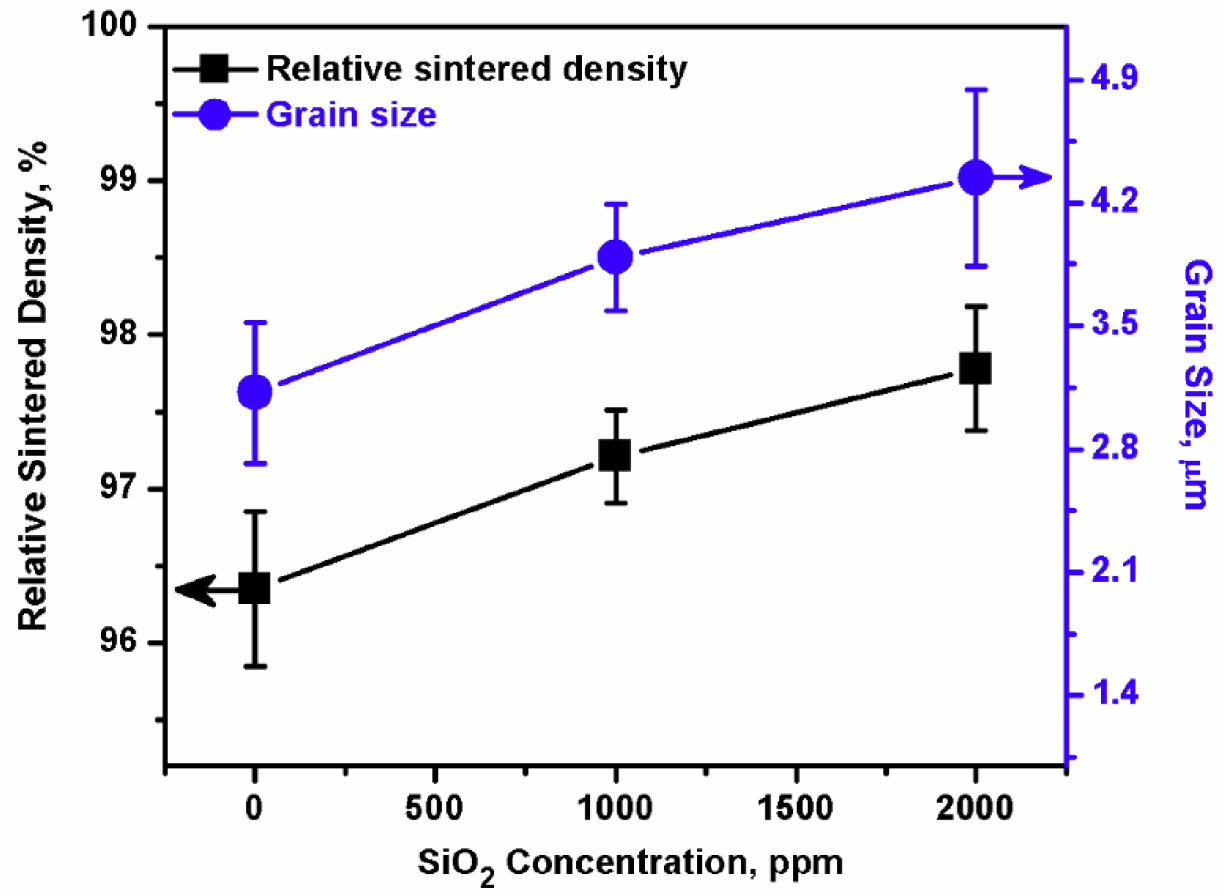

Figure 5.4: Effect of SiO_2 concentration on the densification and grain growth behaviour of YAG ceramics sintered at 1700°C for 2h.

The sintered density and grain size increases with the increase of SiO_2 concentration. A linear raise in density plateau is noticed with increasing SiO_2 concentration to 1000 ppm and later it follows a nearly steady slope. However, no such behaviour is observed in

grain growth trend with respect to SiO_2 concentration. In this, the increase in density and grain size with the increase of SiO_2 concentration is primarily ascribed to the liquid phase sintering kinetics actuated by the formation of eutectic liquid by silica with YAG [23]. These results are explained in details at a later section (5.3.3). The relative sintered density and grain size of the 1000 ppm SiO_2 doped YAG ceramics are found to be 97.2% and 3.9 µm, respectively.

Fig. 5.5 shows the linear and volume shrinkage behaviour in 0, 1000, and 2000 ppm SiO_2 doped YAG ceramics sintered at 1700°C for 2h. as a function of SiO_2 concentration. It is noticed that the percent linear and volume shrinkages tend to increase with increasing SiO_2 concentration but an accelerated shrinkage behaviour is observed in between 0 and 1000 ppm SiO_2. The rise in shrinkage trend with increasing SiO_2 concentration is primarily attributed to enhanced flux of the matter transport triggered under liquid phase sintered condition [31].

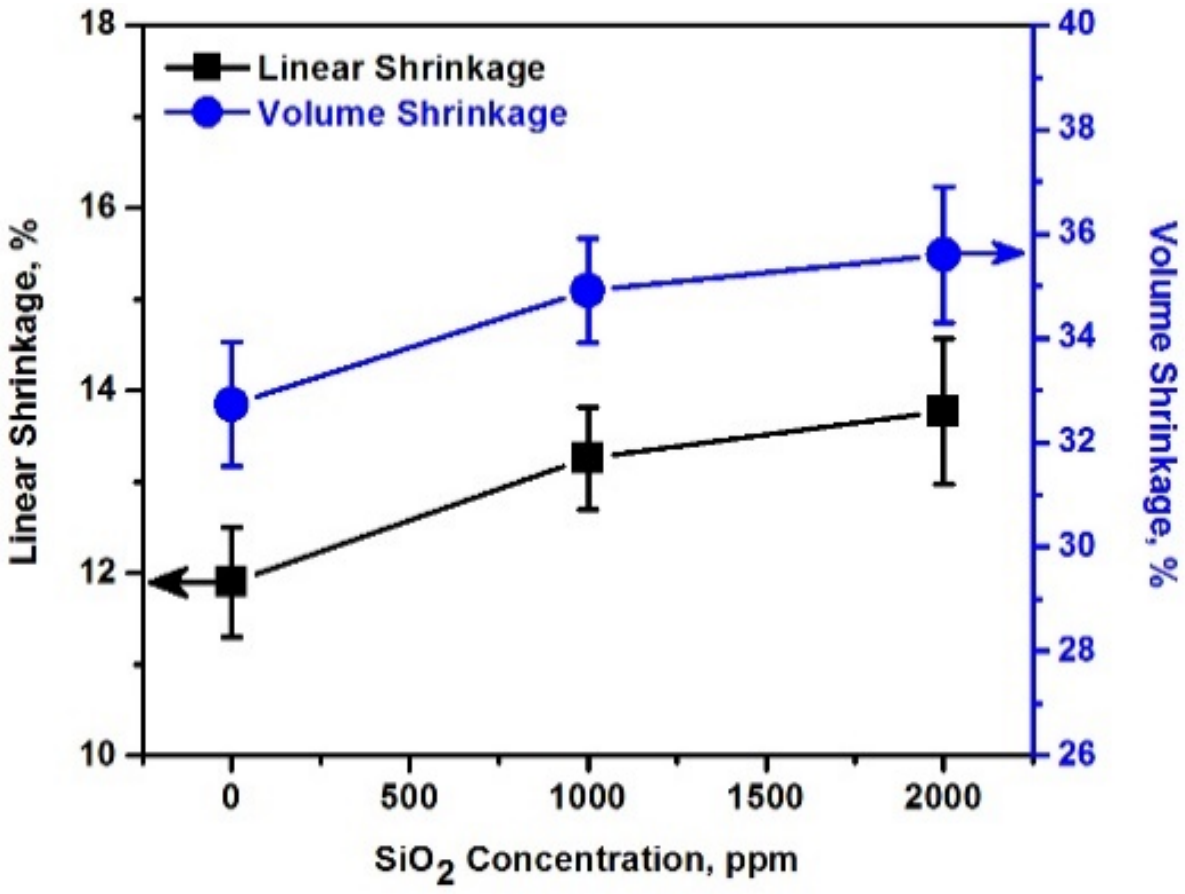

Figure 5.5: Influence of SiO_2 concentration on the shrinkage behaviour of YAG ceramics sintered at 1700°C for 2h.

The increase in density (Fig. 5.4) with increasing silica concentration confirms the above obtained shrinkage results. The linear and volume shrinkages in 1000 ppm SiO_2 doped YAG ceramics are found to be ~ 13% and ~ 35%, respectively.

Fig.5.6 illustrates the change of percent true porosity in 0, 1000, and 2000 ppm SiO_2 doped YAG ceramics sintered at 1700°C for 2 h. as a function of SiO_2 concentration.

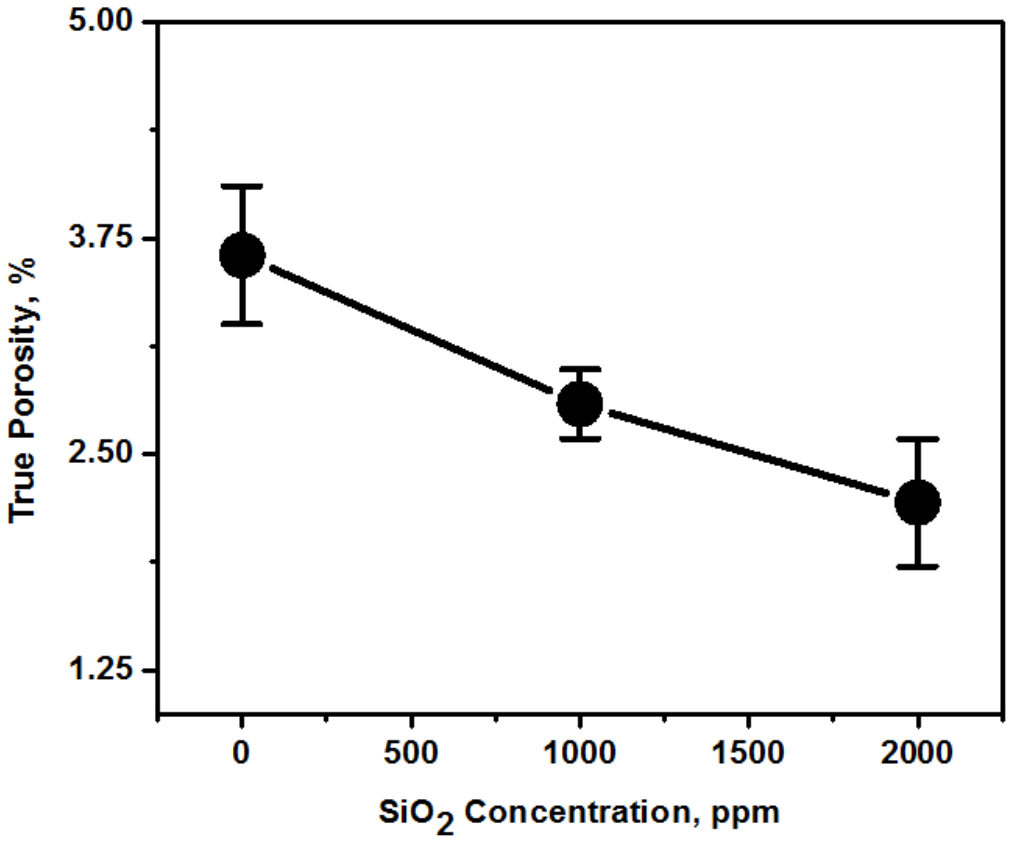

Figure 5.6: Effect of SiO_2 concentration on the percent true porosity of YAG ceramics sintered at 1700°C for 2h.

It is observed that the pore volume generation is reduced with the addition of SiO_2. The increase in density and shrinkage of YAG ceramics as a function of SiO_2 concentration supports the above stated porosity results. The percent true porosity in 1000 ppm SiO_2 doped YAG ceramics is found to be ~2.8%.

Fig. 5.7 presents FESEM microstructures of the 0, 1000, and 2000 ppm of SiO_2 doped YAG ceramics sintered at 1700°C for 2 h. The grain sizes of 0 ppm SiO_2 (Fig. 5.7a), 1000 ppm SiO_2 (Fig. 5.7b), and 2000 ppm SiO_2 (Fig. 5.7c) doped YAG ceramics are 3.1

μm, 3.9 μm, and 4.3 μm, respectively. The microstructural observations clearly demonstrate that the grain size increases with increasing SiO_2 concentration.

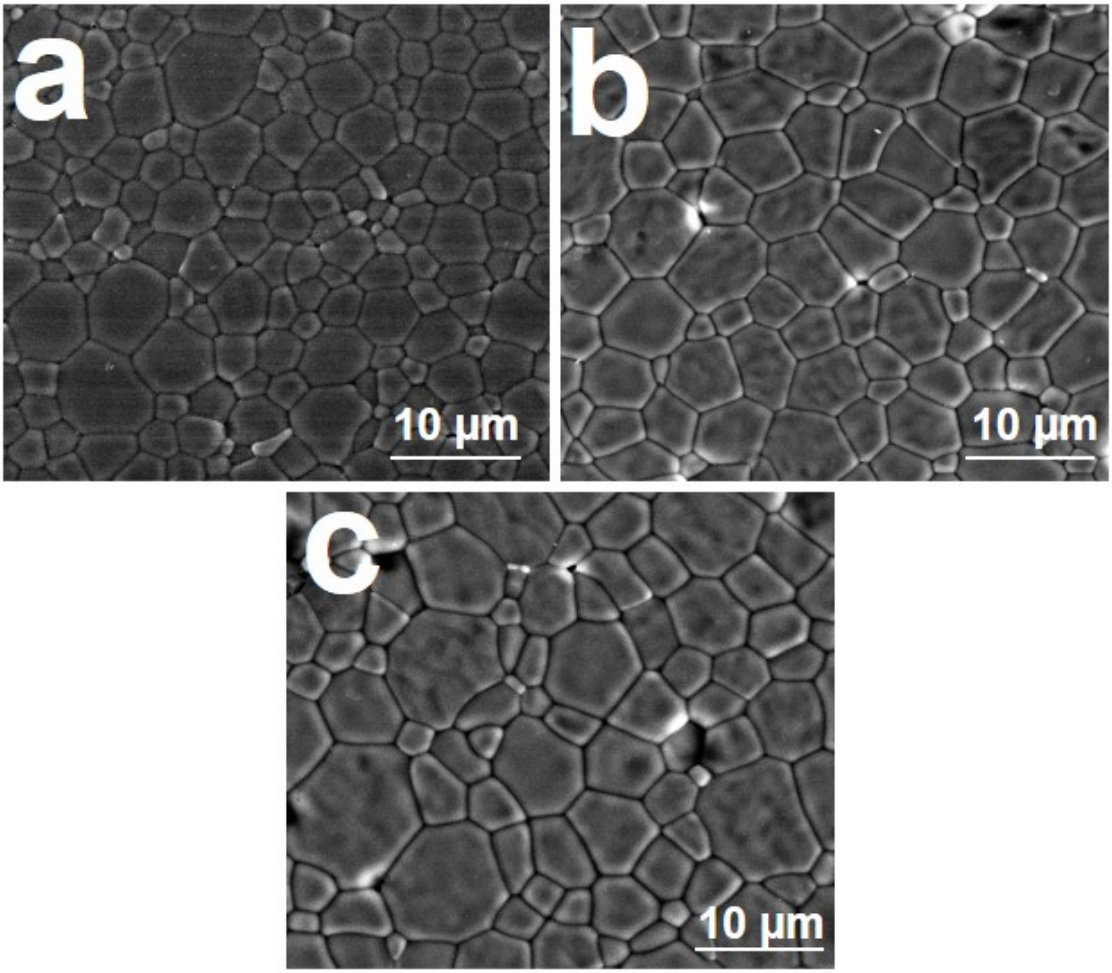

Figure 5.7: FESEM microstructures of the (a) 0 ppm, (b) 1000 ppm, and (c) 2000 ppm SiO_2 doped YAG ceramics sintered at 1700°C for 2h.

Based on the above experimental results, it is clearly understood that the SiO_2 doped YAG ceramics containing 1000 ppm SiO_2 enables to obtain relatively higher sintered density and a finer grain size of ~97.2% and ~3.9 μm, respectively. So, the optimum SiO_2 concentration is chosen as 1000 ppm in the perspective of high sintered density with fine grain microstructure.

5.3.2 Optimization of Nd Concentration in the Optimum Silica doped

Nd:YAG ceramics

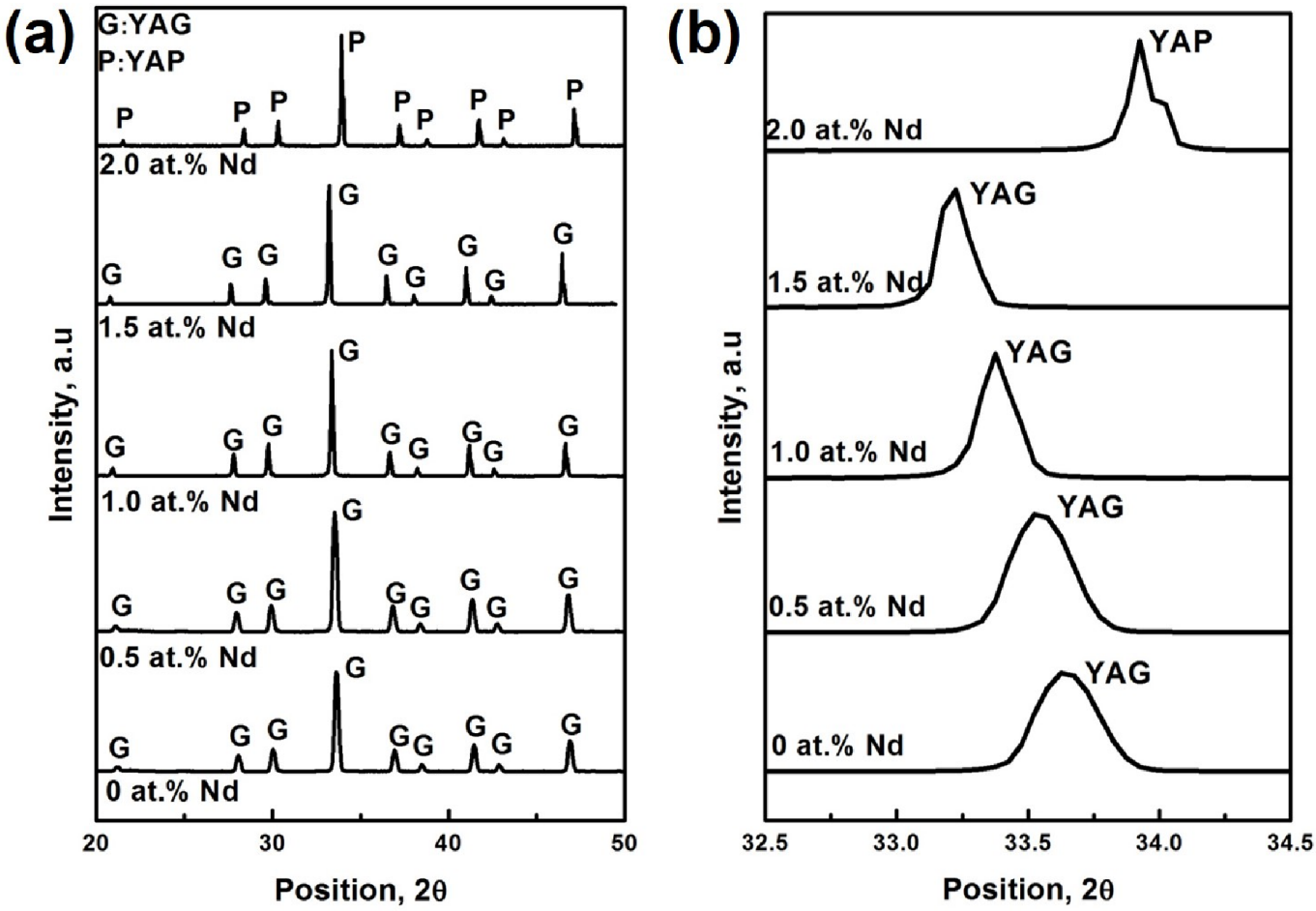

Figure 5.8: (a) XRD patterns indicating the phase structures of the optimum SiO_2 (1000 ppm) doped Nd:YAG ceramics sintered at 1700°C for 2h. The Nd concentration is in the range of 0-2 at.%. (b) Shift in the peak position with the increase of Nd concentration to 1.5 at.% suggests that the increase of lattice parameter due to substitution of host Y^{+3} ion sites with optically active Nd^{+3} ions.

Fig. 5.8a presents the XRD spectra of optimum SiO_2 (1000 ppm) doped Nd:YAG ceramics sintered at 1700°C for 2h. as a function of Nd concentration (0-2 at.%). The optimum SiO_2 doped YAG (0 at.% Nd) ceramics represent strong cubic diffraction pattern of garnet composition (JCPDS 82-0575). The XRD observations clearly revealed that there are no other intermediate phases rich in either SiO_2 or Nd detected with the increase of Nd concentration to 1.5 at.%. A complete reversible phase transition of garnet to perovskite composition (JCPDS 34-0368) is noticed with the further increase of Nd

concentration to 2 at.%. This kind of transition has also reported by Hreniak [32] and Marezio [33], however, the critical factors involved in driving such kind of reaction is still under investigation. The lattice parameter of optimum SiO_2 doped YAG ceramics (0 at.% Nd) is found to be 12.008°A. The increase in lattice parameter to 12.010°A, 12.016°A, and 12.026°A is observed (Fig. 5.8b) with subsequent increase in Nd concentration to 0.5, 1.0, and 1.5 at.%, respectively, which clearly reflects the partial substitution of Y^{+3} ion sites (r = 1.02 °A) with optically active Nd^{+3} ion (r = 1.12 °A) in the host lattice. Lattice parameter calculations were performed using XRD measurements [34].

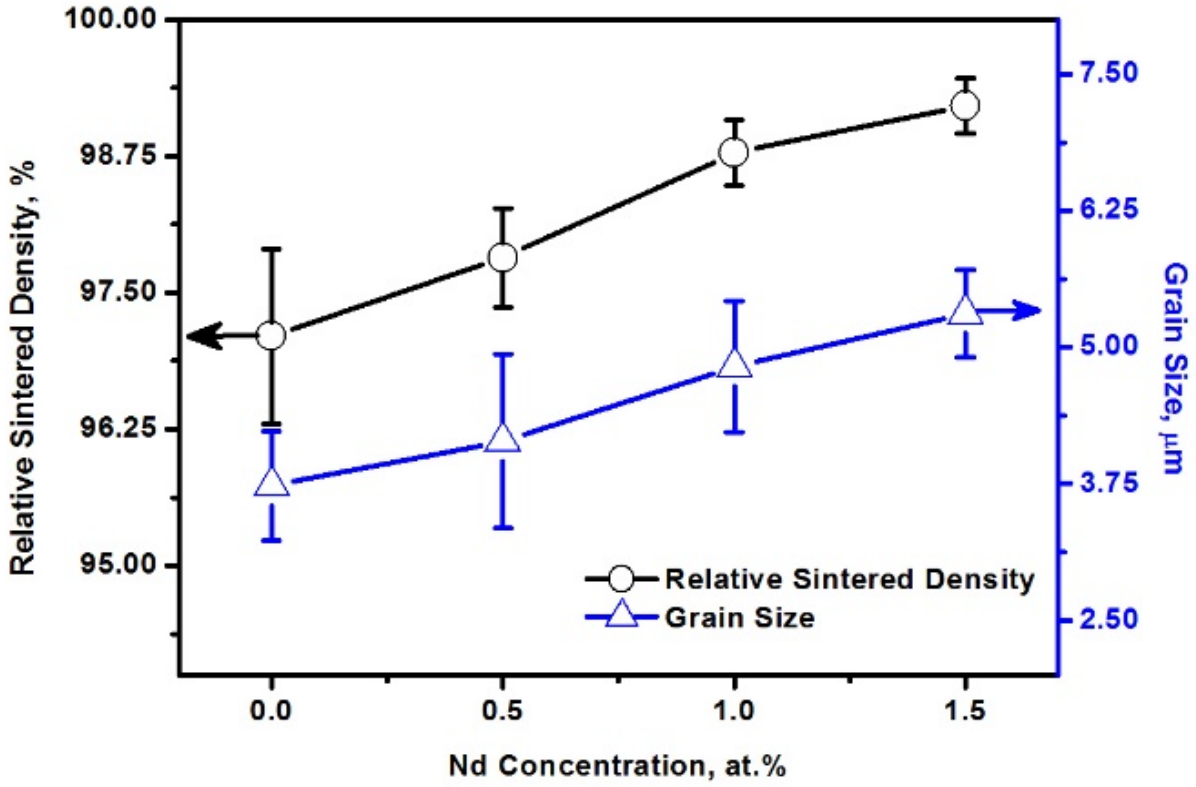

Figure 5.9: Effect of Nd concentration on the densification and grain growth behaviour of optimum SiO_2 doped Nd:YAG ceramics sintered at 1700°C for 2 h. in air.

Fig. 5.9 shows the densification and grain growth behaviour in optimum SiO_2 doped Nd:YAG ceramics sintered at 1700°C for 2 h. as a function of Nd concentration (0-1.5 at.%). The sintered density and grain size trend steadily increases with increasing Nd concentration. The rise in density and grain size trends as a function of Nd concentration is mainly ascribed to the enhanced liquid phase sintering condition [31, 35]. This is

engendered by the formation of eutectic liquid by SiO_2 with Nd_2O_3 [24]. However, these results are discussed comprehensively in the forthcoming section (5.3.3). The relative sintered density and grain size of the optimum SiO_2 doped 1.5 at.% Nd:YAG ceramics are observed to be ~99.2% and 5.3 μm, respectively.

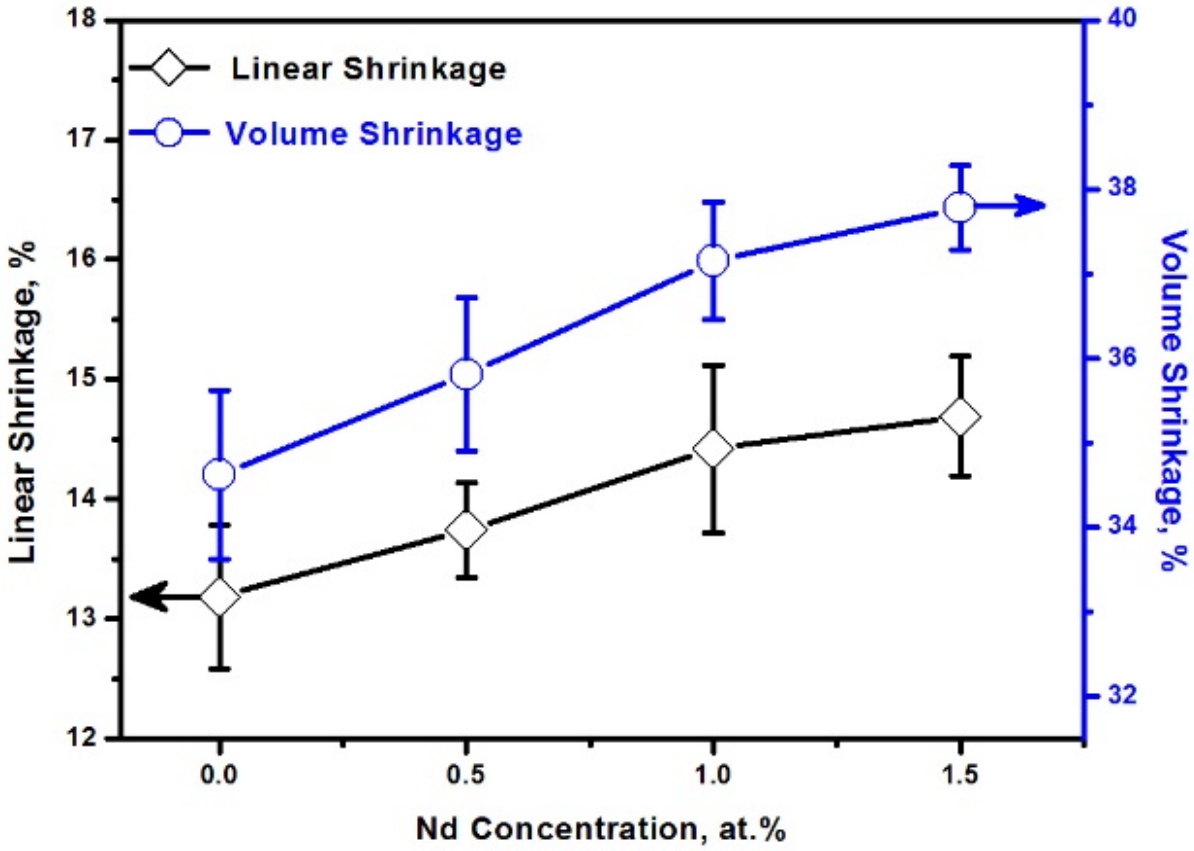

Figure 5.10: Influence of Nd concentration on the shrinkage nature of optimum SiO_2 doped Nd:YAG ceramics sintered at 1700°C.

Fig. 5.10 illustrates the linear and volume shrinkage behaviour in optimum SiO_2 doped Nd:YAG ceramics sintered at 1700°C for 2h. as a function of Nd concentration (0-1.5 at.%). It is noticed that the percent linear and volume shrinkages tend to increase with the increase of Nd concentration to 1.5 at.%. The increase in shrinkage trend as a function of Nd concentration is primarily due to dominant particle diffusion kinetics actuated under enhanced liquid phase sintering condition [31, 35]. The linear and volume shrinkages in optimum SiO_2 doped 1.5 at.% Nd:YAG ceramics are found to be ~14.7% and ~37.8%, respectively.

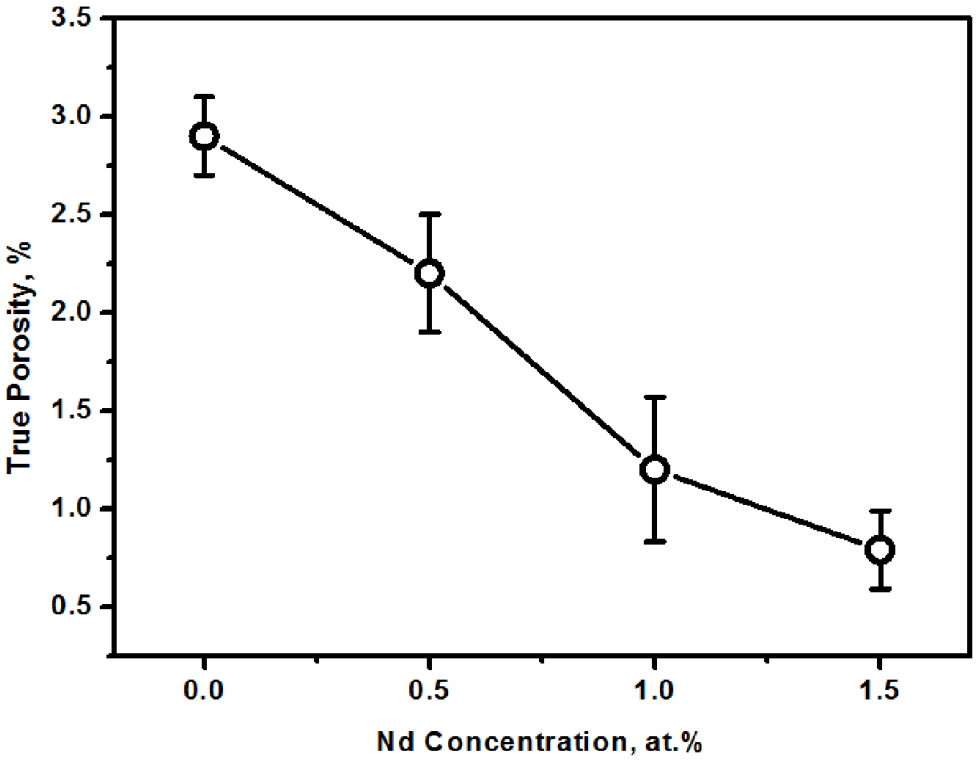

Figure 5.11: Effect of Nd concentration on the percent true porosity of optimum SiO_2 doped Nd:YAG ceramics.

Fig. 5.11 illustrates the change of percent true porosity in optimum SiO_2 doped Nd:YAG ceramics sintered at 1700°C for 2h. as a function of Nd concentration (0-1.5 at.% Nd). It is observed that porosity decreases with the increase of Nd concentration to 1.5 at.%. The rise in density and shrinkage trends of silica doped YAG ceramics as a function of Nd concentration confirms the above obtained porosity results. The percent true porosity in optimum silica doped 1.5 at.% Nd:YAG ceramics is found to be ~0.8%.

Fig. 5.12 shows the SEM microstructures of the optimum SiO_2 doped Nd:YAG ceramics sintered at 1700°C for 2h. as a function of Nd concentration (0-1.5 at.% Nd). The microstructural development in 0 at.% Nd (Fig. 5.12a), 0.5 at.% Nd (Fig. 5.12b), 1.0 at.% Nd (Fig. 5.12c), and 1.5 at.% Nd (Fig. 5.12d) containing SiO_2 doped Nd:YAG ceramics at this sintering temperature suggests that the tendency of dense packing of grains and grain growth increases with the increase of Nd concentration.

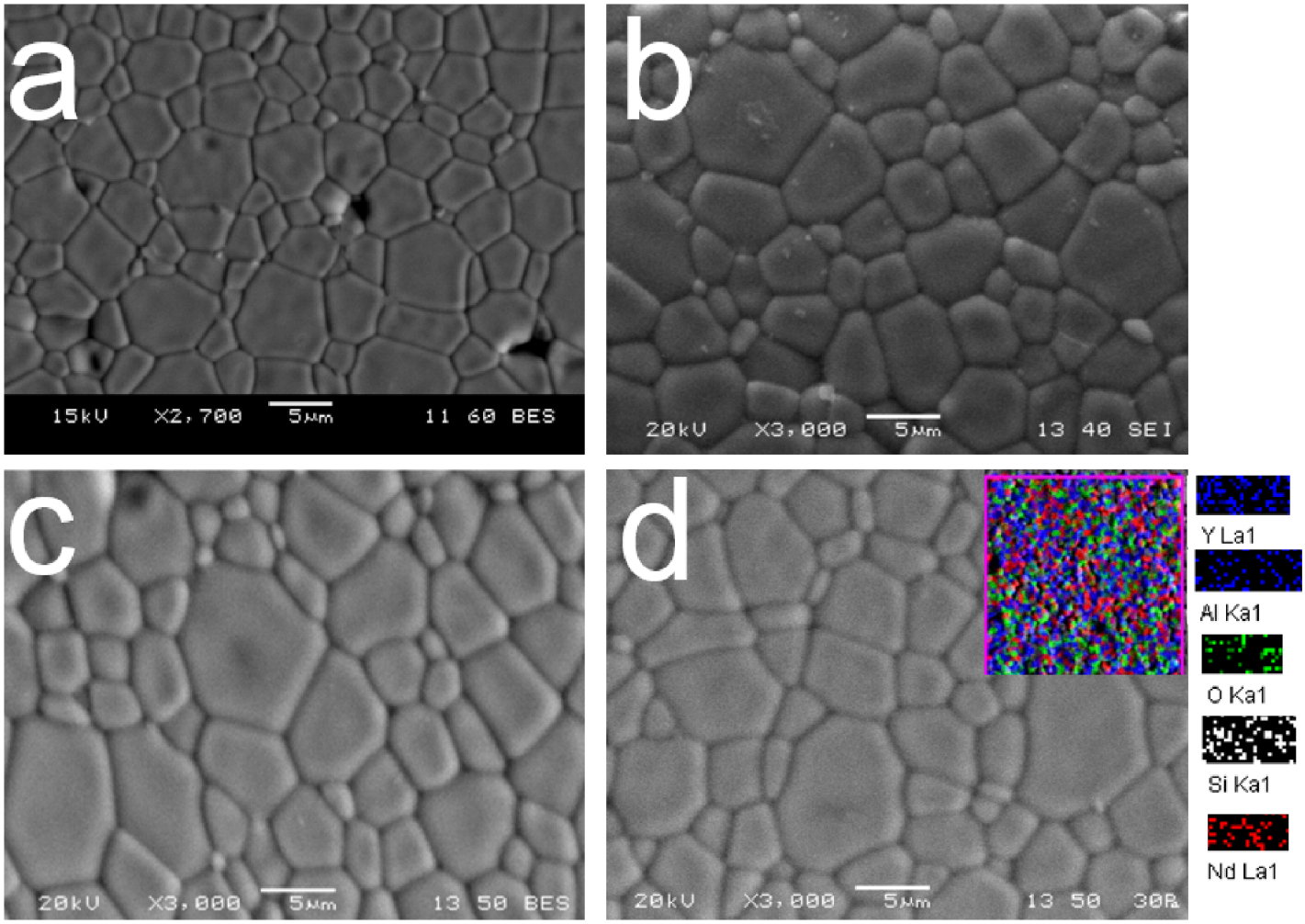

Figure 5.12: SEM sintered micrographs of the optimum SiO_2 doped Nd:YAG cermaics containing (a) 0 at.%, (b) 0.5 at.% (c) 1.0 at.%, and (d) 1.5 at.% Nd. The sintering conditions and atmosphere is 1700°C for 2 h. and air, respectively. EDX results indicating the homogenous distribution of SiO_2 and Nd in the YAG matrix.

In consideration of the above experimental results, it is clearly evidenced that the optimum SiO_2 (1000 ppm) doped Nd:YAG ceramics containing 1.5 at.% Nd enables to obtain the highest sintered density i.e., ~ 99.2% in this study. So, the optimum Nd concentration is chosen as 1.5 at. % in the perspective of highest sintered density as well as optically active ion (Nd^{+3}) concentration even though the sintered microstructure is slightly coarse grained in nature. Therefore, the ~99.2% dense 1000 ppm SiO_2 doped 1.5 at. % Nd:YAG ceramics are considered as optimized Nd:YAG ceramics.

5.3.3 The Role of SiO_2 in the Sintering Behaviour of YAG and Nd:YAG Ceramics

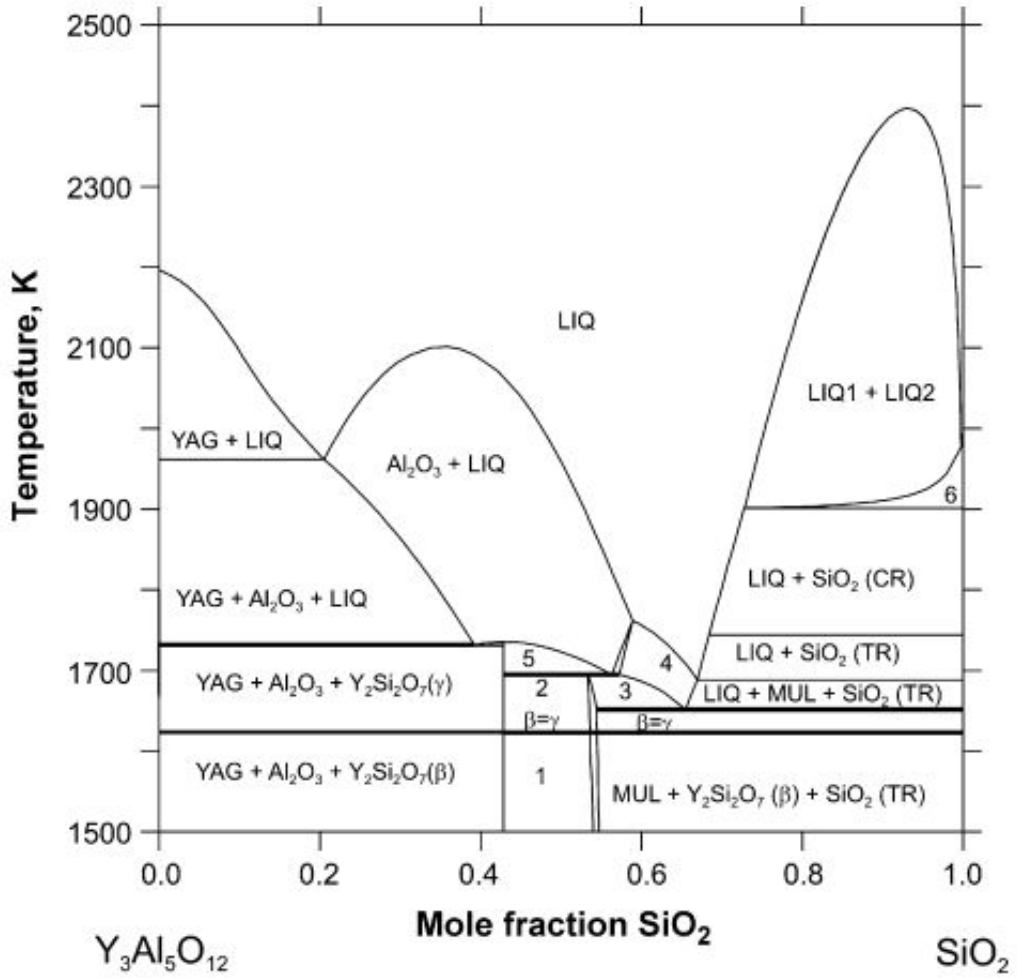

Figure 5.13: YAG – SiO_2 phase diagram [36].

The sintering study of SiO_2 doped YAG ceramics clearly demonstrate that the sintered density and grain size increases with the increase of SiO_2 concentration ranging from 0 ppm to 2000 ppm. Fig. 5.13 presents the binary phase diagram of the $Y_3Al_5O_{12}$-SiO_2 system. It shows the formation of a eutectic liquid with chemical composition ($Y_2Si_2O_7$) at a temperature above 1400°C (1673 K) due to solid-solid reaction between silica and YAG particles [25]. So that, it can be understood that the faster densification and grain growth kinetics in SiO_2 doped YAG ceramics with increasing SiO_2 concentration is a result of enhanced liquid phase sintering [23]. The increase in shrinkage rate with the increase of SiO_2 concentration confirms the above stated experimental observations.

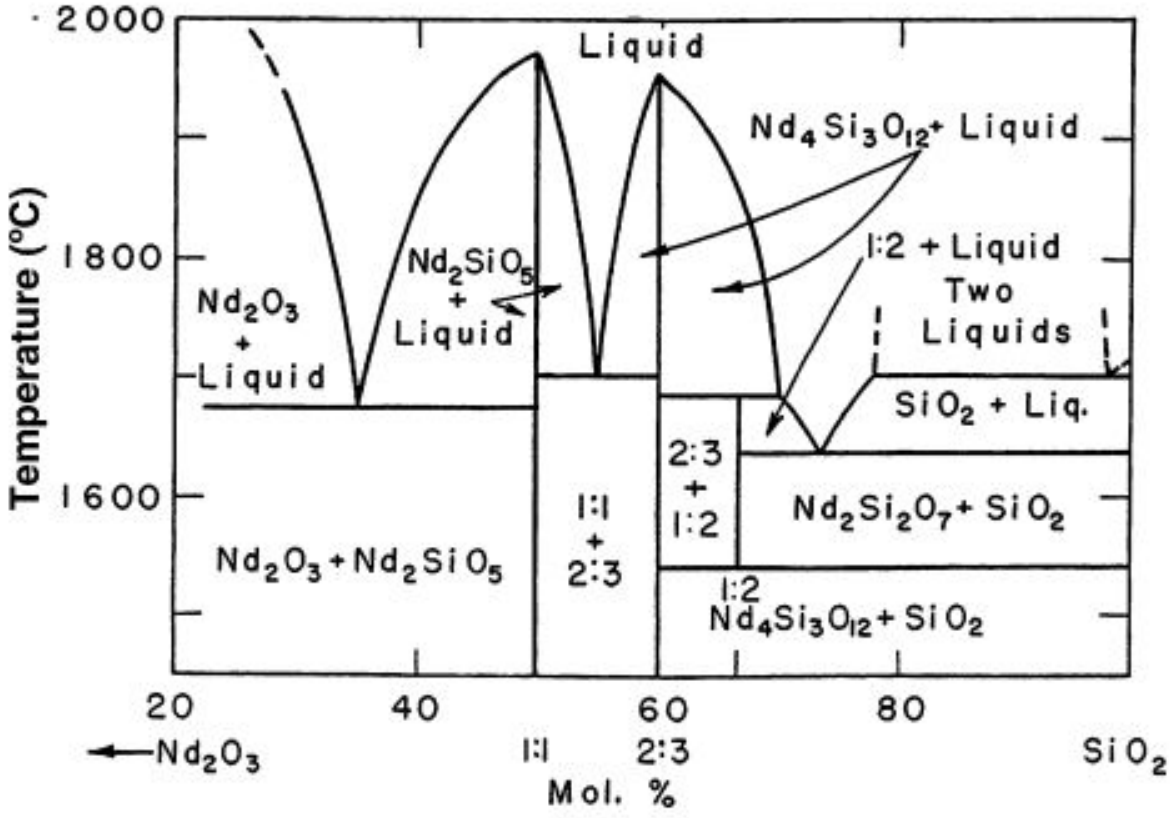

Figure 5.14: SiO_2 – Nd_2O_3 phase diagram [37].

However, in a similar fashion, the sintered density and grain size of optimum SiO_2 doped Nd:YAG ceramics increases with increasing Nd concentration. The densification and grain growth kinetics are observed to be slightly faster in SiO_2 doped Nd:YAG compared to YAG ceramics. Fig. 5.14 presents the binary phase diagram of Nd_2O_3-SiO_2 system. A liquid phase is formed by Nd_2O_3 with SiO_2 at a temperature around 1700°C. So, the faster densification kinetics in SiO_2 doped Nd:YAG ceramics is because of the enhanced liquid phase sintering ensured by the presence of additional amount of liquid phase compared to SiO_2 doped YAG ceramics [24-25]. The higher shrinkage rate in SiO_2 doped Nd:YAG ceramics compared to the SiO_2 doped YAG ceramics supports the above obtained experimental results. However, quicker grain growth kinetics in this system is mainly attributed to the increased grain boundary mobility actuated by the increase in grain boundary diffusion coefficients of Y^{+3} and Nd^{+3} under enhanced liquid phase sintering condition [26, 30].

The obtained experimental results regarding densification and grain growth behaviour in SiO_2 doped YAG and Nd:YAG systems are well in agreement with the observations of Kottachawana and Ikesue [23-24]. The enhanced grain growth in both systems supports the absence of secondary phases rich in SiO_2, as evidenced from the XRD observations.

5.3.4 Mechanical, Thermal, and Optical Property Evaluation

Table 5.1 summarizes the different mechanical, thermal, and optical properties of the optimized Nd:YAG ceramics (~99.2% dense 1000 ppm SiO_2 doped 1.5 at.% Nd:YAG) in the current study and ceramic obtained in literature.

Table 5.1: Mechanical, Thermal, and Optical Properties of the Optimized Nd:YAG Ceramics

Property	Nd: YAG Ceramic in the Current Study	Nd: YAG Ceramic in the Literature
Mechanical Property		
Vickers Hardness	~13.1 GPa	12.8 GPa (CIP 250 MPa and Vacuum Sintering at 1720°C under 10^{-3} Pa) [21]
Flexural Strength	~202 MPa	234 MPa [28]
Thermal Property		
Linear Thermal Expansion Coefficient (in the range of 30°C-1000°C)	~9.124x10^{-6} /°C	8.173x10^{-6} /°C (CIP 250 MPa and Vacuum Sintering at 1720°C under 10^{-3} Pa) [21]
Thermal Shock Resistance Parameters	R1= ~51 °C	120 °C [27]
	R2= ~548 W/m	1290 W/m [27]
Optical Property		
In-line Transmittance	20% in the visible region	------

The mechanical properties of the Nd doped YAG ceramics that include Vickers hardness and flexural strength are 13.1 GPa and 202 MPa, respectively. The Vickers hardness (13.1 GPa) is slightly higher than the value of Nd:YAG ceramics reported by J. Li et al. [21]. The increase in hardness is primarily attributed to the finer grain size (~5.3 µm) of the optimized ceramics compared to the Nd:YAG ceramics (~7 µm) in literature. The flexural strength (~202 MPa) of the optimized ceramics is observed to be in the comparable range of value reported for Nd:YAG ceramics (~234 MPa) [28]. However, the reduction in flexural strength is mainly attributed to relatively lower sintered density (~99.2%) although the grain sizes are in comparable range with the one in reported literature. The thermal properties of the optimized ceramics in terms of average linear

thermal expansion coefficient is 9.124 x 10^{-6} /°C in the temperature range of 30°C to 1000°C and thermal shock resistance parameters R_1 and R_2 are 51°C and 548 W/m, respectively, at 1000°C. It can be observed that the linear thermal expansion coefficient (9.124 x 10^{-6} /°C) measured for the optimized ceramics is in proximity to the value reported in the literature [21]. The calculated thermal shock resistance parameters (R_1 = 51°C and R_2 = 548 W/m) for optimized ceramics are lower compared to the values reported for the Nd:YAG ceramic in literature [27]. The reduction in thermal shock resistance is presumably due to lower density and higher grain size compared to the literature. The in-line transmittance of the optimized Nd:YAG ceramics is nearly ~20%, however, till date no investigation has been made on transparency of pressureless sintered discs.

Over all, the mechanical properties are nearly similar to those reported in the literature. However, optical transparency and thermal properties that demands more improvement for qualifying as a desired SSL host material.

5.4 Conclusions

Based on the above experimental results and theoretical observations the following conclusions have been drawn:

(i) Near to pore-free and highly dense 99.2% optimum SiO_2 doped 1.5 at.% Nd:YAG ceramics with ~5.3 μm grain size were fabricated by careful optimization of SiO_2 and Nd concentration and pressureless sintering at 1700˚C for 2 h.

(ii) The optimum SiO_2 and Nd concentration have been found to be 1000 ppm and 1.5 at. %, respectively, in the fabricated highly dense ceramics.

(iii) The densification and grain growth rate of SiO_2 doped YAG ceramics increase with increasing SiO_2 concentration due to the formation of eutectic liquid phase that accelerates the particulate diffusion kinetics.

(iv) The enhanced densification and grain growth rates of SiO_2 doped Nd:YAG compared to YAG ceramics with increasing SiO_2 concentration was most likely due to the increased liquid phase content by the formation of additional eutectic liquid phase with SiO_2 by Nd_2O_3.

(v) The different properties of the optimized Nd:YAG ceramics were found as;

a) Mechanical properties that include Vicker's hardness and flexural strength were obtained as 13.1 GPa and 202 MPa, respectively.
b) Thermal properties that include two different thermal shock resistance parameters and average thermal expansion coefficient from 30˚C to 1000˚C were determined to be ~51°C, ~548 W/m, and ~9.124x 10^{-6} $°C^{-1}$, respectively.
c) The in-line transmittance was found to be 20% in the visible region. No literature reports are available for transparency measurements of pressureless sintered discs, however, need to be improved in a higher level to qualify the desired criterion of a laser host material.

References

1. T. Taira, Ceramic YAG lasers, Comptes Rendus Physique 8 (2007) 138-152.
2. A. Ikesue, Y. L. Aung, Ceramic laser materials, Nature photonics 2 (2008) 721-727.
3. A. Ikesue, T.Kinoshita, Fabrication and optical properties of high performance polycrystalline Nd:YAG ceramics for solid-state lasers, J. Am. Ceram. Soc., 78 (1995) 1033-1040.
4. N. Uehara, K. Ueda, Ultra-stabilized by laser-diode pumped Nd:YAG lasers, Rev. Lasers Eng., 21 (1993) 590-600.
5. G. With De, H. J. A. Van Dijk, Translucent $Y_3Al_5O_{12}$ ceramics, Mater. Res. Bull., 19 (1984) 1669-1674.
6. A. Ikesue, I. Furusato, and K. Kamata, Fabrication Of Polycrystalline, Transparent YAG Ceramics By A Solid-State Reaction Method, J. Am. Ceram. Soc. 78 (1995) 225-228.
7. K. Ueda, J. F. Bisson, H. Yagi, K. Takaichi, A. Shirakawa, T. Yanagitani, and A. A. Kaminskii, Scalable Ceramic Lasers, Laser Physics, 15 (2005) 927–938.
8. J. Lu, M. Prabhu, J. Song, C. Li, J. Xu, K. Ueda, A. A. Kaminskii, H. Yagi and T.Yanagitani, Optical Properties and Highly Efficient Laser Oscillation of Nd:YAG Ceramics, Appl. Phys. B, 71 (2000) 469-473.
9. J. Lu, J. Song, M. Prabhu, J. Xu, K. Ueda, H. Yagi, T. Yanagitani and A. Kudryashov, High-Power Nd:$Y_3Al_5O_{12}$ Ceramic Laser, Jpn. J. Appl. Phys., 39 (2000) 1048-1050.
10. A. Ikesue, Polycrystalline Nd:YAG Ceramics Lasers, Opt. Mater., 19 (2002) 183-187.
11. Y. Zhang, H. Yu, Synthesis of YAG powders by the co-precipitaton method, Ceram. Int., 35 (2009) 2077-2081.
12. A. Ikesue, I Furussato, K. Kamata, Fabrication of polycrystalline, transparent YAG ceramics by a solid-state reaction method, J. Am. Ceram. Soc., 78 (1995) 225-228.
13. N. Frage, V. Kasiyan, A. Rothman, M.P. Dariel , Effect of the spark plasma sintering parameters and LiF doping on the mechanical properties and the transparency of polycrystalline Nd-YAG, Ceram. Int., 38 (2012) 5513-5519.
14. A. Krell, J. Klimke, T. Hutzler, Transparent compact ceramics: Inherent physical issues, Opt. Mater., 41 (2013) 20-54.
15. J. Lu, M. Prabhu, J. Song, C. Li, J. Xu, K. Ueda, A. A. Kaminskii, H. Yagi and T.Yanagitani, Optical Properties and Highly Efficient Laser Oscillation of Nd:YAG Ceramics, Appl. Phys. B, 71 (2000) 469-473.
16. S. Bhattacharyya, T. K. Mukhopadhyay, K. Dana, S. Ghatak, Pressureless reaction sintering of yttrium aluminium garnet (YAG) from powder precursor in the hydroxyhydrogel form, Ceram. Int., 37 (2011) 3463-3468.
17. B. Liu, J. Li, R. Yavetskiy, M. Ivanov, Y. Zeng, T. Xie, Fabrication of YAG Transparent Ceramics using Carbonate Precipitated Yttria Powder. J. Eur. Ceram. Soc., 35 (2015) 2379-2390.
18. M. Suarez, A. Fernandez, J.L. Menéndez, M. Nygren, R. Torrecillas, Z. Zhao, Hot Isostatic Pressing of Optically Active Nd:YAG Powders Doped by a Colloidal Processing Route. J. Eur. Ceram. Soc., 30 (2010) 1489–1494.
19. H.Yihua, J. D. Zhang, J. Qingling, Z. HUANG, Sintering of transparent Nd: YAG ceramics in oxygen atmosphere. J. Rare. Earth., 31 (2003) 153-157.
20. W. Zhang, T.C. Lu, N. Wei, Y.L. Shi, B.Y. Ma, H. Luo, Co-precipitation synthesis and vacuum sintering of Nd:YAG powders for transparent ceramics, Mater. Res. Bull., 70 (2015) 365-372
21. J. Li, Y.S. Wu, Y. B. Pan, Fabrication, microstructure and properties of highly transparent Nd:YAG laser ceramics, Opt. Mater., 31 (2008) 6-17.
22. S. Kochawattana, A. Stevenson, S. H. Lee, M. Ramirez, V. Gopalan, J. Dumm, V. K. Castillo, G. J. Quarles, G. L. Messing., Sintering and grain growth in SiO_2 doped Nd:YAG. J. Eur. Ceram. Soc., 28 (2008) 1527 – 1534.

23. S. Kochawattana, Phase formation and sintering of YAG Ceramics, The Pennsylvania State University, 2008.
24. A. Ikesue and K. Kamata, Role of Si on Nd solid-solution of YAG ceramics, J. Jpn.Ceram. Soc.,103 (1995) 489-493.
25. R. Boulesteix, A. Maître, J.-F. Baumard, C. Sallé, and Y. Rabinovitch, Mechanism of the liquid-phase sintering for Nd:YAG ceramics, Opt. Mater., 31 (2009) 711-715.
26. R. Boulesteix, A. Maître, J.-F. Baumard, Y. Rabinovitch, C. Sallé, S. Weber, and M. Kilo, The effect of silica doping on neodymium diffusion in yttrium aluminum garnet ceramics: implications for sintering mechanisms, J. Eur. Ceram. Soc., 29 (2009) 2517-2526.
27. D. L. Kim, B. T. Kim, Fracture characteristics of ceramic Nd: YAG, Optics Express, 22 (2014) 11331-11339.
28. T.I . Mah, T.A. Parthasarathi, D.L. Lee, Polycrystalline YAG; structural or functional?, J. Ceram. Process. Res., 5 (2004) 369-379.
29. W. Koechner, M. Bass, Solid-state lasers: a graduate text, Springer, New York, 2003.
30. A. J. Stevenson, X. Li, M. A. Martinez, J. M. Anderson, D. L. Suchy, G. L. Messing, Effect of SiO_2 on densification and microstructure development in Nd: YAG transparent ceramics, J. Am. Ceram. Soc., 94(2005) 1380-1387.
31. Randall M. German, Liquid Phase Sintering, Springer, New York, 1985.
32. D. Hreniak, G. Stanislaw, L. Witold, S. Wiesław, P. Mazur, R. Fedyk. High-pressure induced structural decomposition of RE-doped YAG nanoceramics, Solid state phenomena, 106 (2005) 17-22.
33. M. Marezio, J. P. Remeika, A. Jayaraman, High-pressure decomposition of synthetic garnets, J. Chem. Phys., 45 (1966) 1821-1824.
34. C. Suryanarayana, M. Grant Norton, X-ray diffraction: A Practical Approach, Plenum Press, New York, 1998.
35. M. N. Rahaman, Ceramic processing and sintering, Marcel Dekker, New York, 1995.
36. O. Fabrichnaya, H.J. Seifert, R. Weiland, T. Ludwig, F. Aldinger, A. Navrotsky, Phase equilibria and thermodynamics in the Y_2O_3-Al_2O_3-SiO_2 system Z. Metallkd., 92 (2001) 1083–1097.

Chapter 6
Summary and Future Scope

6.1 Summary

6.1.1 Co-Precipitation Synthesis of YAG Nanoparticles

The synthesis of YAG nanopowder via co-precipitation, physio-chemical characterization and phase formation mechanism of the precipitated precursor were explored. The YAG nanopowder was synthesized by reverse strike precipitation of $Al(NO_3)_3.9H_2O$, $Y(NO_3)_3.6H_2O$, NH_4HCO_3 at pH ~ 8 and calcination temperature of 900°C. Thermal analysis (DSC-TG) observations revealed that the precursor was crystallized to YAP and YAG compositions at 820°C and 910°C, respectively. XRD results showed that the onset of crystallization started at a calcination temperature of 750°C by transforming the amorphous precursor to YAP and YAG phases and complete transformation to YAG composition at 900°C. FESEM morphology of the YAG nanopowder obtained at 900°C displayed relatively discrete and nearly spherical shaped particles with an average particle size of ~40 nm.

In co-precipitation synthesis, it was observed that the phase formation procedure of amorphous precursor to YAG composition was not actually a solid state reaction between Y_2O_3 and Al_2O_3. The plausible path developed for the formation mechanism as revealed from DSC-TG, XRD and TEM observations that the amorphous precursor was transformed to Y-Al-O system by releasing all the decomposable matter at a calcination temperature of 600°C. Further, crystallization of the Y-Al-O system to YAP and YAG phases at 750°C was observed followed by growth of YAG phase and reduction in YAP content under subsequent calcination to 850°C, and complete transition to YAG composition was reached at 900°C. The growth of YAG phase compared to YAP at 850°C suggests that the system tends to transform towards YAG composition and establishes YAG as more thermodynamically stable than YAP. This phenomenon follows the Ostwald's 'Rule of Stages' where as an amorphous precursor of highest free energy

transforms to a most stable crystalline state of lowest free energy via metastable intermediate phases.

Hence, the experimental evidences disclosed a fact that the amorphous precursor prepared via co-precipitation synthesis was completely transformed into the most thermodynamically stable crystalline phase YAG via a metastable intermediate crystalline YAP.

6.1.2 Nanoparticle Coarsening Effect on Sintered Density and Microstructural Development of YAG.

The influence of particle calcination temperature and time on coarsening kinetics of YAG nanoparticles and their sintering behaviour was studied as a function of particle size and green state of compacted specimens.

YAG nanoparticles (~40 nm) were calcined in the temperature range of 900°C-1550°C for 1, 6, and 12 h. in order to understand the influence of particle calcination temperature and time on their coarsening behaviour and green forming. The average particle size was found to be increased with the increase of calcination temperature and time, however, a significant increase in the particle size was noticed above 1150°C. Calcination time was found to have a profound influence on the particle coarsening relatively at higher temperatures since coarsening kinetics are critically influenced by the temperature. The highest average particle size (~1 μm) was obtained by the powders calcined at 1550°C for 12 h. in this study. The increase in green density as obtained from the calcined particles was primarily due to the formation of densely packed structures in the green state with wider sized fractions triggered by the breaking down of agglomerated powders that produced during calcination. The powders which were calcined above 1150°C compacted to a minimum of 50% green density and the highest (i.e. 66%) was obtained by the powders calcined at 1550°C for 12 h.

The sintering behavior of the selected YAG ceramics at 1700°C for 2 h. prepared from the powders calcined at 1350°C, 1450°C, and 1550°C for 12h. constituting particle sizes and green densities of (~0.3 μm, ~55%), (~.7 μm, ~60%), and (~1 μm, 66%), respectively, was studied to optimize the particle size based on their sintered density and

microstructural evolution. YAG ceramics fabricated from the powders calcined at 1450°C for 12 h. were sintered to highest density (~96.1%) than those fabricated from the powders calcined at 1550°C for 12 h. (~92%). The increment in grain size is because of the increasing particle size with the rise in particle calcination temperature. The fall in shrinkage trend was primarily due to the reduced particulate diffusion kinetics triggered from the coarsening of particles with increasing calcination temperature and the highest percent apparent porosity (~3%) was obtained for the YAG ceramics fabricated from the powders calcined at 1550°C for 12h. The FESEM microstructures that exhibit finer sized grains with more number of pores, densely packed grains with minimal porosity, and large or crack like voids in between relatively denser regions were obtained for the specimens fabricated from the powders calcined at 1350°C, 1450°C, and 1550°C for 12 h. respectively. The appearance of crack like voids is signature of the sintering behaviour of hard agglomerated powder. Based on the theories of sintering, the powder compacts with finer particle size (~0.3 μm, 1350°C/12 h.) should have the highest densification rate or the one with the highest green density (~66%, 1550/12 h.) can have the greater sintering potential to attain highest sintered density. In this case, however, the powder compacts (1450°C/12 h.) with an average particle size (~0.7 μm) and green density (~ 60%) have attained the highest sintered density emphasizing the significance of particle packing on the densification behaviour. The presence of hard agglomerates in the green state (1550°C/12 h.) reduced the sintering potential by triggering differential densification results in lowest sintered density (~92%). Summarizing that, particle calcination temperature has profound effect on coarsening kinetics, green forming, and sintering behaviour. The optimum particle size was chosen as ~0.7 μm (1450°C/12 h) based on the sintered density (~96.1%) and microstructural features.

6.1.3 Optimization and Properties of Silica doped Nd:YAG Ceramics

The fabrication of ~99.2% dense 1000 ppm SiO_2 doped 1.5 at.% Nd:YAG ceramics by careful optimization of SiO_2 and Nd concentration, the role of SiO_2 in densification behaviour and microstructural development of YAG and Nd:YAG systems, and properties of the optimized ceramics were demonstrated in detail. SiO_2 was added in different proportions in the range of 0-2000 ppm to the optimized powder (~0.7 μm) in order to understand the influence of SiO_2 concentration on the sintering behavior of YAG

ceramics. The sintered density, grain size, and shrinkage of SiO_2 doped YAG ceramics has increased with the increase of SiO_2 concentration when sintered at 1700°C. The enhanced densification and grain growth rate with increasing concentration were attributed to the formation of a plausible eutectic liquid phase by SiO_2 with YAG at a temperature above 1400°C, hence, it was a result of liquid phase sintering. The SiO_2 doped YAG ceramics containing 1000 ppm SiO_2 attained a higher sintered density and finer grain size of ~97.2 % and 3.9 μm, respectively. So, the optimum SiO_2 concentration was selected as 1000 ppm in the perspective of high sintered density with fine grained microstructure.

Nd was added in different proportions in the range of 0-2 at.% to the optimized SiO_2 doped YAG powder (1000 ppm, ~0.7 μm) in order to fabricate highly dense Nd:YAG ceramics by understanding the influence of Nd concentration on phase transition and densification behaviour of SiO_2 doped YAG ceramics. The XRD observations clearly revealed that YAG was the only phase detected with the increase of Nd concentration to 1.5 at.%. A complete reversible phase transition of garnet to perovskite composition was noticed with further increase of Nd content to 2 at%, hence, Nd content in YAG ceramics was limited to 1.5 at.%. The increase in lattice parameter of SiO_2 doped YAG ceramics containing 0 at. % Nd to 1.5 at.% Nd content confirmed the partial substitution of Y^{+3} ion sites with optically active Nd^{+3} ions in the host lattice. The sintered density, grain size, and shrinkage rate of optimum SiO_2 doped Nd:YAG ceramics increased with the increment of Nd concentration to 1.5 at.%. The enhanced densification and grain growth kinetics in SiO_2 doped Nd:YAG ceramics compared to SiO_2 doped YAG ceramics were attributed to the formation of liquid phase by Nd_2O_3 with SiO_2 which yields an additional amount of liquid phase at the prevailing sintering conditions. Hence, the faster sintering kinetics in SiO_2 doped Nd:YAG ceramics was a result of enhanced liquid phase sintering action compared to SiO_2 doped YAG ceramics. The 1000 ppm SiO_2 doped Nd:YAG ceramics containing 1.5 at.% Nd obtained a higher sintered density and grain size of ~99.2% and 5.3 μm, respectively. Hence, the optimum Nd concentration was selected as 1.5 at.% in the perspective of highest sintered density as well as optically active ion (Nd^{+3}) concentration. Therefore, the optimum concentrations of SiO_2 and Nd were 1000 ppm and 1.5 at.%, and the optimized ceramics were designated as ~99.2% dense 1000

ppm SiO_2 doped 1.5 at.% Nd:YAG ceramics. The mechanical properties of the optimized YAG ceramics that include Vickers hardness and flexural strength were 13.1 GPa and 202 MPa, respectively. The thermal properties including average linear thermal expansion coefficient from 30°C to 1000°C was 9.124 x 10^{-6} /°C and thermal shock resistance parameters, R_1 and R_2, at 1000°C were 51°C and 548 W/m, respectively. The in-line transmittance was ~20% in the visible region.

6.2 Future Scope

- To fabricate highly dense (>99.9%) optimized Nd:YAG ceramics with finer grain sizes (<5 μm) by further enhancement of densification and microstructural control through modulation of sintering parameters like time, temperature, and atmosphere.
- To improve the optical transmittance of optimized Nd:YAG ceramics close to the ideal value (i.e. 84%) in visible (532 nm) as well as infrared regions (1064 nm) by controlling the scattering centers.
- To study and improve different mechanical and thermal properties of the optimized Nd:YAG ceramics as a function of grain size.
- To investigate the laser performance of optimized Nd:YAG ceramics under continuous and pulse operation mode as a function of grain size.

Curriculum Vitae

Name: Katakam Sarath Chandra
Permanent Add: B-11-386/2, House Thota,
Butchi Reddy Palem, Nellore, Andhra Pradesh-524305
Ph: +91-7077946668
E-mail: ssarath89@gmail.com

Date of Birth: 18th February, 1989

Academic Credentials

- M. Tech (R) in Ceramic Engineering, National Institute of Technology Rourkela, 2016 - till date.
- B.Tech in Ceramic Technology, Andhra University College of Engineering, Andhra University, 2011.

Research Interest: Sintering, Advanced Ceramics.

Publications

1. K.V.Ramesh, **K.Sarath Chandra**, M.S.N. Murty, C.Bhaskara Sarma, Parametric effects of a helicoidal tape promoter on gas and liquid holdups of a three-phase fluidized bed, The IUP Journal of Chemical Engineering, 1 (2009) 18-35.
2. **K. Sarath Chandra**, K.V.Ramesh, Refractories in Indian Steel Industry: Past and Present Scenario, Global Journal Engineering and applied sciences, 1 (2011) 50-52.
3. Y.V.S.S.S.Kiran, P.U.R.Vital ,**K.Sarath Chandra**, M.S.N.Murty, K.V.Ramesh, "Water flow split in commercial T-junctions with outlet ends open to atmosphere", Chemical Technology an Indian Journal (TSI) , 9 (2014) 205-211.
4. K. Ashok Kumar, **K. Sarath Chandra**, T. Bhargavi, K.V. Ramesh, Flow regime mapping of liquid-solid inclined fluidized beds, International Journal of Engineering and Applied Sciences, 3 (2016) 56-57.